AD-A173 879 A FUSION BREEDER REACTOR BASED ON A CATALYZED D-D SPHERICAL TORUS(U) ARMY MILITARY PERSONNEL CENTER ALEXANDRIA VA K L WRISLEY 08 AUG 86 1/2

UNCLASSIFIED F/G 18/1 NL

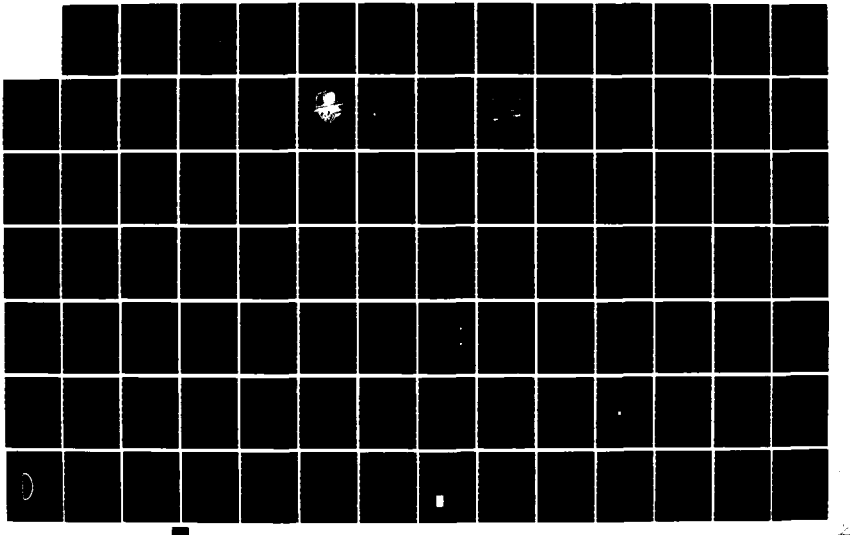

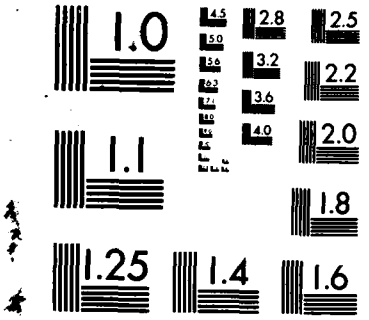

(2)

A FUSION BREEDER REACTOR BASED ON A CATALYZED D-D SPHERICAL TORUS

Kenneth L. Wrisley, Jr., O-3
HQDA, MILPERCEN (DAPC-OPA-E)
200 Stovall Street
Alexandria, VA 22332

FINAL REPORT, 8 August 1986

A thesis submitted to Rensselaer Polytechnic Institute, Troy, New York, in partial fulfillment of the requirements for the degree of Mater of Science.

REPORT DOCUMENTATION PAGE

READ INSTRUCTIONS BEFORE COMPLETING FORM

1. REPORT NUMBER
2. GOVT ACCESSION NO.
3. RECIPIENT'S CATALOG NUMBER

4. TITLE (and Subtitle)

A FUSION BREEDER REACTOR BASED ON A CATALYZED D-D SPHERICAL TORUS

5. TYPE OF REPORT & PERIOD COVERED

Final Report, 8 August 1986

6. PERFORMING ORG. REPORT NUMBER

7. AUTHOR(s)

Kenneth L. Wrisley, Jr.

8. CONTRACT OR GRANT NUMBER(s)

9. PERFORMING ORGANIZATION NAME AND ADDRESS

Student, HQDA, MILPERCEN (DAPC-OPA-E)
200 Stovall Street
Alexandria, Virginia 22332

10. PROGRAM ELEMENT, PROJECT, TASK AREA & WORK UNIT NUMBERS

11. CONTROLLING OFFICE NAME AND ADDRESS

HQDA, MILPERCEN (DAPC-OPA-E)
200 Stovall Street
Alexandria, VA 22332

12. REPORT DATE

8 August 1986

13. NUMBER OF PAGES

169

14. MONITORING AGENCY NAME & ADDRESS (if different from Controlling Office)

15. SECURITY CLASS. (of this report)

UNCLASSIFIED

15a. DECLASSIFICATION/DOWNGRADING SCHEDULE

16. DISTRIBUTION STATEMENT (of this Report)

Approved for public release; distribution unlimited.

17. DISTRIBUTION STATEMENT (of the abstract entered in Block 20, if different from Report)

18. SUPPLEMENTARY NOTES

Thesis submitted to Rensselaer Polytechnic Institute, Troy, New York in partial fulfillment of the requirements for the degree of Master of Science

19. KEY WORDS (Continue on reverse side if necessary and identify by block number)

Fusion; Deuterium-Deuterium Fuel Cycle; Fusion-Fission Breeder Reactor; Spherical Torus; Aqueous Self-Cooled Blanket Concept; Fissile Breeding

20. ABSTRACT (Continue on reverse side if necessary and identify by block number)

One of the potentially attractive applications of nuclear fusion is to breed fissile fuel for use in fission reactors. This thesis examines a novel non-power producing fusion reactor based on the spherical torus concept with a catalyzed deuterium-deuterium fuel cycle and aqueous self-cooled blanket for use as a fissile breeder.

(continued on back)

20. continued

The breeding of fissile fuel is accomplished by dissolving a uranium salt, uranyl nitrite, in heavy water which flows through the first wall and blanket providing both cooling and fissile breeding. The need for tritium breeding is eliminated by the use of a catalyzed D-D fuel cycle.

Analysis of this novel reactor concept indicates a fissile breeding ratio of 1.34 [Pu-239/source neutron] using a 15 [cm] beryllium moderator and 7 mol% uranyl nitrite in the heavy water. A typical reactor using this blanket can produce more than 8000 [kg/yr] of plutonium at a cost of less than $40 per gram. This indicates the potential for a reactor which can provided fissile fuel at, or below, its current mined cost.

A FUSION BREEDER REACTOR BASED ON A CATALYZED D-D SPHERICAL TORUS

by

Kenneth L. Wrisley

A Thesis Submitted to the Graduate

Faculty of Rensselaer Polytechnic Institute

in Partial Fulfillment of the

Requirements for the Degree of

MASTER OF SCIENCE

Approved:

Dr. Don Steiner
Thesis Advisor

Rensselaer Polytechnic Institute
Troy, New York

August 1986

TABLE OF CONTENTS

LIST OF FIGURES.....v

LIST OF TABLES.....vi

ACKNOWLEDGMENTS.....vii

ABSTRACT.....viii

1. INTRODUCTION.....1
   1.1. Previous Concepts.....2
      1.1.1. Fuel Cycles.....3
      1.1.2. Confinement Schemes.....3
      1.1.3. Blanket Concepts.....4
         Molten-Salt Fueled D-D Hybrid 4
         Helium-Cooled Molten-Salt Fusion Breeder .6
         Liquid-Metal-Cooled Tandem Mirror Fission-Suppressed Fusion Breeder .9
   1.2. Summary of Systems.....9
      1.2.1. Catalyzed D-D Fuel Cycle.....11
         Neutron Output.....11
         Critical Issues.....12
      1.2.2. Spherical Torus Reactor Concept Conc.13
      1.2.3. Aqueous Self-Cooled Blanket..15
   1.3. Scope and Method of Analysis.....16

2. DETERMINATION OF PLASMA REACTION RATES...19
   2.1. Profiles and Power Density.....19
   2.2. Modeling of the Spherical Torus Behavior.....23
      2.2.1. Paramagnetism.....25
      2.2.2. Total Average Density.....27
   2.3. Steady State Densities.....28
   2.4. Benchmark of the Code.....31
   2.5. Typical Results and Examples.....32
   2.6. Conclusions.....35

3. PLASMA POWER BALANCE.....36
   3.1. Auxiliary Power.....37
   3.2. Radiation Losses.....38

3.3. Transport Losses.....40
3.3.1. Scaling Laws.....41
Ion Confinement.....41
Electron Confinement.....42
3.4. Typical Results and Examples.....46
3.5. Concluding Remarks.....49

4. REACTOR POWER BALANCE.....50
4.1. Toroidal Field Coils.....52
4.2. Poloidal Field (PF) Components.....57
4.3. Current Drive.....58
4.4. Superconducting Options.....62
4.5. Analysis of Results.....62
4.6. Conclusions.....65

5. IMPURITY CONTROL.....66
5.1. Limiter.....66
5.1.1. Material Selection.....69
5.1.2. Design Issues.....71
5.2. Divertor.....71
5.2.1. Design Issues.....75
5.3. Conclusions.....75

6. FIRST WALL, BLANKET, SHIELD.....77
6.1. Design.....78
6.2. Neutronics.....81
6.3. Conclusions.....87

7. COST ANALYSIS.....88
7.1. Power Flow.....88
7.2. Reactor Costing.....92
7.3. Cost of Fuel.....95
7.4. Typical Results and Examples.....97
7.5. Conclusions.....99

8. RESULTS AND COMPARISON WITH PREVIOUS WORK ...100
8.1. Presentation of Results.....100
8.2. Comparison with Previous Designs...102

9. CONCLUSIONS.....105
9.1. Catalyzed D-D Fuel Cycle.....105
9.2. Spherical Torus Reactor Design.....107
9.3. Aqueous Self-Cooled Blanket.....108

10. REFERENCES.....110

APPENDICES

A. Results of Design Space Analysis.....112
A.1. Glossary of Terms.....112
A.2. Tables of Results.....115

B. PARAMETRIC SYSTEMS CODE.....143
B.1. Code Listing.....144

LIST OF FIGURES

1-1: One module of a helium-cooled molten-....7
salt blanket
1-2: Cross section along the axis of one 8
segment of the helium-cooled molten-
salt blanket
1-3: Reference liquid-metal-cooled, fission-.10
suppressed tandem mirror hybrid
1-4: Conceptual Spherical Torus Reactor.....14
Design

2-1: Geometry of plasma model.....21
2-2: Variations of R, a, κ, B_{t_0}, and f_α 24
2-3: Reaction rate $\langle\sigma v\rangle$ [m^3/s] versus T.....29

3-1: Fraction of cyclotron radiation lost ...39
from the plasma versus T
3-2: Effects of temperature on the plasma ...46
power gain
3-3: Effect of temperature on the fusion.....47
and auxiliary power

4-1: Magnet system design cross section.....51

5-1: Detail of limiter system.....68
5-2: Overview of reactor illustrating 72
divertor system
5-3: Cross section of poloidal divertor.....73

6-1: Top view of first wall and blanket.....79
6-2: Blanket and shield positions.....80
6-3: Model of reactor for neutronics 83
analysis
6-4: Fissile breeding and fissioning.....85
versus moderator thickness
6-5: Fissile breeding and fissioning 86
versus uranium concentration
7-1: Diagram of the power flow for a hybrid..90
breeder

LIST OF TABLES

1-1: Comparison of Previous Hybrid Reactor Designs ...5

2-1: WILDCAT Reference Parameters.....33
2-2: Benchmark Results - Steady State Particle Densities 33
2-3: Plasma Parameter Design Space.....34

3-1: Typical Results for Power Balance 48

4-1: Reactor Power Balance Results.....64

5-1: Candidate Structural Materials.....70
5-2: Divertor Design Parameters.....74

6-1: Solubilities of Selected Uranium and Thorium Salts 79
6-2: Candidate Shielding Materials.....81
6-3: Breeding and Competing Reactions.....82
6-4: Neutronics Analysis.....84

7-1: Definition of Economics and Power Flow .89
7-2: Spherical Torus Hybrid Breeder Cost Analysis.....93
7-3: Cost of Fuel Account Analysis 96
7-4: Typical Results of Cost Analysis.....98

8-1: Criteria and Common Parameters.....101
8-2: Basic Parameters for the Reference Desgin 102
8-3: Comparison of the D-D Spherical Torus Hybrid Breeder to Previous Concepts .103
A-1: Glossary of Terms - Plasma Parameters..113
A-2: Glossary of Terms - Plasma Power Balance 114
A-3: Glossary of Terms - Reactor Power Balance 114
A-4: Glossary of Terms - Cost Analysis.....115
A-5: Results - Plasma Parameters.....116
A-6: Results - Plasma Power Balance.....128
A-7: Results - Reactor Power Balance.....134
A-8: Results - Cost Analysis.....137

ACKNOWLEDGMENTS

I would like to thank the following people for their assistance and support: William Duggan, Georgios Varsamis, Dan Herbison, and William Kelleher for their technical assistance; Charles Butkus for computer support and assistance in computer program development; Dee Ann Wrisley for typing and editing support; and special thanks to Dr. Don Steiner for his guidance, direction, and patience in this endeavor. Finally, I wish to thank the United States Army, and indirectly the United States Taxpayer, for their funding of this endeavor.

ABSTRACT

One of the potentially attractive applications of nuclear fusion is to breed fissile fuel for use in fission reactors. This thesis examines a novel non-power producing fusion reactor based on the spherical torus concept with a catalyzed deuterium-deuterium fuel cycle and aqueous self-cooled blanket for use as a fissile breeder.

The breeding of fissile fuel is accomplished by dissolving a uranium salt, uranyl nitrite, in heavy water which flows through the first wall and blanket providing both cooling and fissile breeding. The need for tritium breeding is eliminated by the use of a catalyzed D-D fuel cycle.

Analysis of this novel reactor concept indicates a fissile breeding ratio of 1.34 [Pu^{239}/source neutron] using a 15 [cm] beryllium moderator and 7 mol% uranyl nitrite in the heavy water. A typical reactor using this blanket can produce more than 8000 [kg/yr] of plutonium at a cost of about $52 per gram. This indicates the potential for a reactor which can provide fissile fuel at, or below, its current mined cost.

1. INTRODUCTION

There are only a few energy sources that can be considered inexhaustible in the practical sense. Included in these are solar, nuclear fusion, and nuclear fission given the technology to convert the vast resources of fertile isotopes to fissile isotopes. The Liquid Metal Fast Breeder Reactor (LMFBR) is one possibility for such technology. The fusion-fission hybrid breeder is another possibility with higher performance potential but also with a higher technological risk. It is the purpose of this thesis to examine a fusion-fission hybrid breeder based on three unique and potentially beneficial concepts: the spherical torus, the catalyzed deuterium-deuterium fuel cycle, and the aqueous self-cooled blanket.

This study differs from previous studies in that: (1) a deuterium fuel cycle is used to eliminate the need to breed tritium; (2) a compact tokamak (spherical torus) is used as a confinement scheme; (3) and an aqueous self-cooled blanket is utilized to provide neutron moderation, to suppress fissioning, and to ease removal and processing of the fissile material. Additionally, uranium (U^{238}) will be the fertile material employed and a denatured uranium-plutonium

light-water reactor fuel cycle will be considered in the analysis.

An overview of previous work, as well as a summary of the deuterium-deuterium fuel cycle, the spherical torus, and the aqueous self-cooled blanket, will be provided in this chapter. The scope and methods of analysis will then be defined and a brief synopsis of the remainder of the paper will be provided.

1.1. Previous Concepts

Prior to describing the reactor concept proposed here, it is beneficial to review some of the previously proposed hybrid designs. Each of the designs illustrated has its own advantages and disadvantages as a fissile fuel and power producer. Two of the illustrated designs proposed by Lawrence Livermore National Laboratory (LLNL) are current designs and continue to be studied and upgraded. The remainder are conceptual designs with only limited analysis having been performed. The differences among the previous concepts and that proposed here will be examined on the basis of three major features: fuel cycle; reactor embodiment or confinement scheme; and blanket design or

concept. It is worth noting that the design proposed here is the only one which does not generate electricity.

1.1.1. Fuel Cycles

Of the three designs examined in review of previous concepts [1,2,3], all except the Molten-Salt Fueled D-D Hybrid proposed by Oak Ridge National Laboratory (ORNL) [1] use a deuterium-tritium (D-T) fuel cycle and must, therefore, breed tritium. The Molten-Salt D-D Hybrid utilizes a semi-catalyzed deuterium-deuterium fuel cycle where the tritium and helium-3 produced are allowed to remain in the plasma, but are not purposely recycled back into the plasma. This differs from the design proposed here where all of the tritium and 90% of the helium-3 are recycled back into the plasma.

1.1.2. Confinement Schemes

Just as most of the current designs utilize the D-T fuel cycle, most of these designs consider some form of tandem mirror as the plasma confinement scheme. The Molten-Salt Fueled D-D Hybrid [1] does not specifically

describe any confinement scheme, but does utilize the cost model from WILDCAT, which is based on tokamak confinement.

1.1.3. Blanket Concepts

The blanket concept for each of the reactor designs are given in detail in the following subsections, and the concepts are compared in Table 1-1. All reactors assume a thorium-uranium breeding cycle, whereas the design presented herein uses a uranium-plutonium breeding cycle to capitalize on the higher solubility of uranium salts. Comparison of the two breeding cycles is given in Chapter 6.

Molten-Salt Fueled D-D Hybrid [7]

The molten-salt fueled D-D hybrid blanket is composed of a molten fluoride salt, 71 mol% NaF, 2 mol% BeF_2, 27 mol% ThF_4, flowing through a stainless steel structure and out to a reprocessing station. The major cooling and heat removal are accomplished by a 2.5 [cm] water cooled first wall, with the remainder of the heat removal being accomplished by heat exchange with the molten salt. Lithium is not required in this system

Table 1-1: Comparison of Previous Hybrid Reactor Designs

	Helium-Cooled Molten Salt Fusion Breeder [2]	Liquid-Metal-Cooled Fission-Suppressed Fusion Breeder [3]	Molten-Salt-Fueled D-D Hybrid Reactor [1]
P_{fusion} [MW]	3000	2600	1986
$P_{electric}$ [MWe]	1380	1990	926
$P_{wall\ load}$ [MW/m^2]	2	1.7	not given
Tritium Breeding Ratio, T [#/neutron]	1.0	1.06	N/A
Fissile Breeding Ratio, F [#/neutron]	0.6	0.84	0.7
Blanket Multiplication, M [E_{blnkt}/E_n]	1.6	2.4	1.5
Fissile Production [kg/yr] @ 80% Capacity	6380	6660	6808
Blanket Coolant	He	Li (liquid)	water
Structure	SS-316	SS-316	SS-316
Neutron Multiplier	Be Pebbles	Be Spheres	Be (in breeder)
Breeder	Molten Salt: LiF 70 mol% BeF_2 12 mol% ThF_4 18 mol%	Th (metal)	Molten Salt: NaF 71 mol% BeF_2 2 mol% ThF_4 27 mol%
Total Cost [M$] (Direct & Indirect)	4,867	6,300	11,400

because the deuterium-deuterium fuel cycle does not necessitate tritium breeding.

Helium-Cooled Molten-Salt Fusion Breeder [2]

The helium-cooled molten-salt fusion breeder is currently under investigation by R. W. Moir and associates at Lawrence Livermore National Laboratory. The breeding material utilized is a mixture of 70 mol% LiF, 12 mol% BeF_2 and 18 mol% ThF_4. This molten salt breeding material is circulated through the blanket to an online processing system where the tritium and uranium are removed (see Figures 1-1 and 1-2).

Fission is suppressed by using beryllium spheres as a neutron multiplier (Figure 1-2) and minimizing the fissile content in the blanket. The beryllium spheres are approximately 1 cm in diameter and flow through the blanket. A yearly replacement rate of about 20% is used to prevent swelling and cracking. The entire blanket is cooled with high pressure (5 [MPa]) helium.

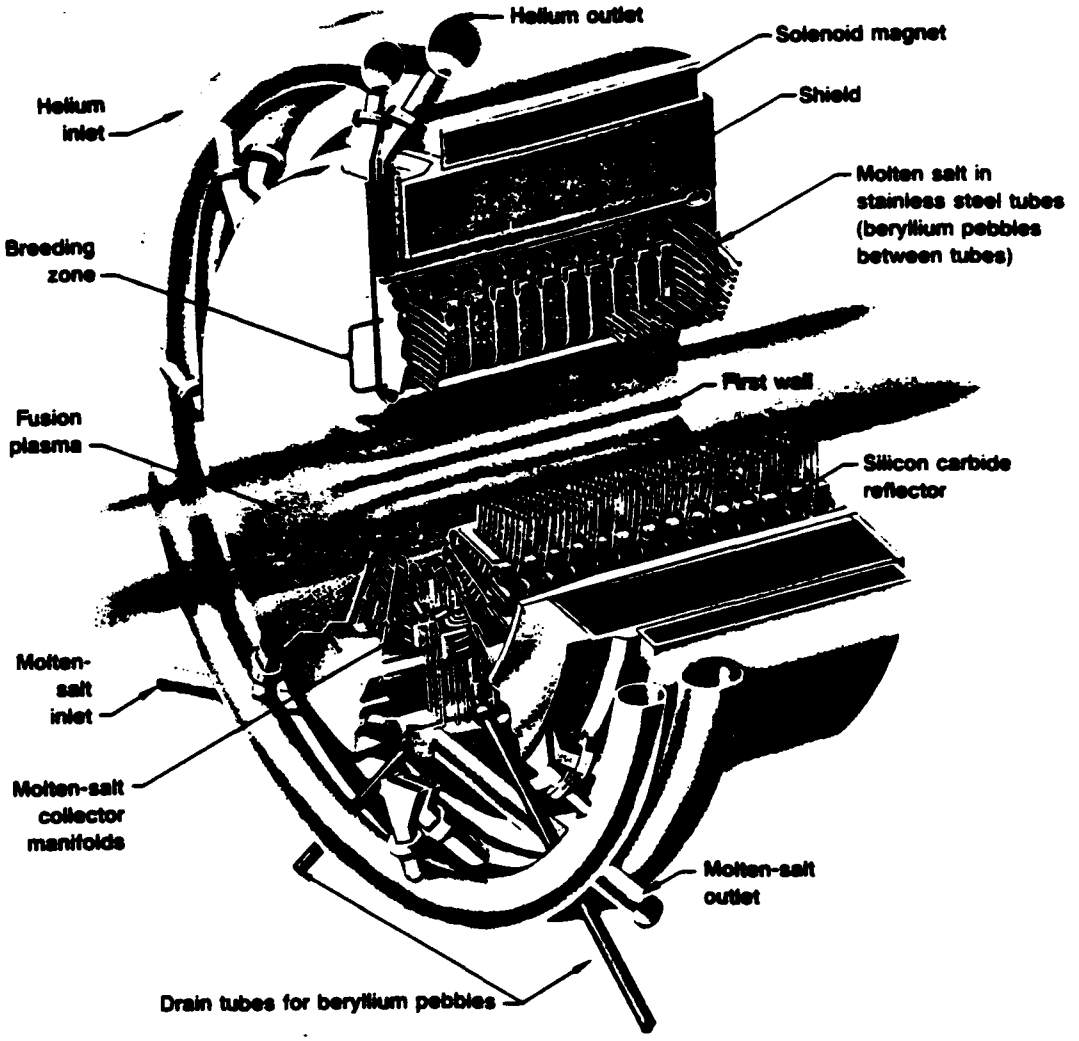

Figure 1-1: One module of a helium-cooled molten-salt blanket. Helium under 5-MPa pressure flows from the rear most ring header to the apex of each pod, then radially outward through the blanket to the forward ring header, and thence to heat exchangers for generating electricity [2].

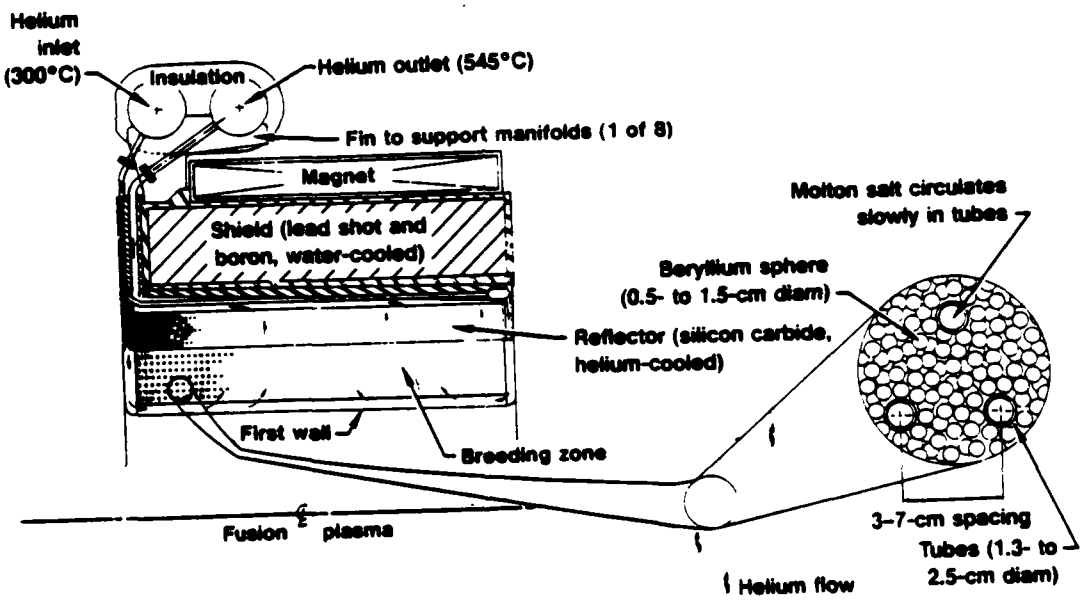

Figure 1-2: Cross section along the axis of one segment of a helium-cooled molten-salt blanket, showing arrangement of helium flow and of beryllium spheres and tubing for the molten salts [2].

Liquid-Metal-Cooled Tandem-Mirror Fission-Suppressed Fusion Breeder [3]

The liquid-metal-cooled tandem-mirror fission-suppressed fusion breeder, also proposed by Lawrence Livermore National Laboratory, is shown in Figure 1-3. It uses liquid lithium as coolant and tritium breeding material. Uranium is bred from thorium in the form of snap rings on 3 [cm] diameter beryllium spheres. The total volume of thorium on each sphere is 15 vol%. The spheres circulate through the blanket and out to a pool prior to reprocessing. The thorium snap rings are then removed and the uranium extracted. Swelling of the beryllium is expected to be around 0.3% [Δ V/V] over the operating cycle.

1.2. Summary of Systems

The systems used in the D-D Spherical Torus Hybrid Breeder will be examined and compared to those of the designs presented in the previous section. This examination will be divided into the areas of the deuterium-deuterium fuel cycle, the spherical torus, and the aqueous self-cooled blanket. In each case, the benefits of using such a system will be presented.

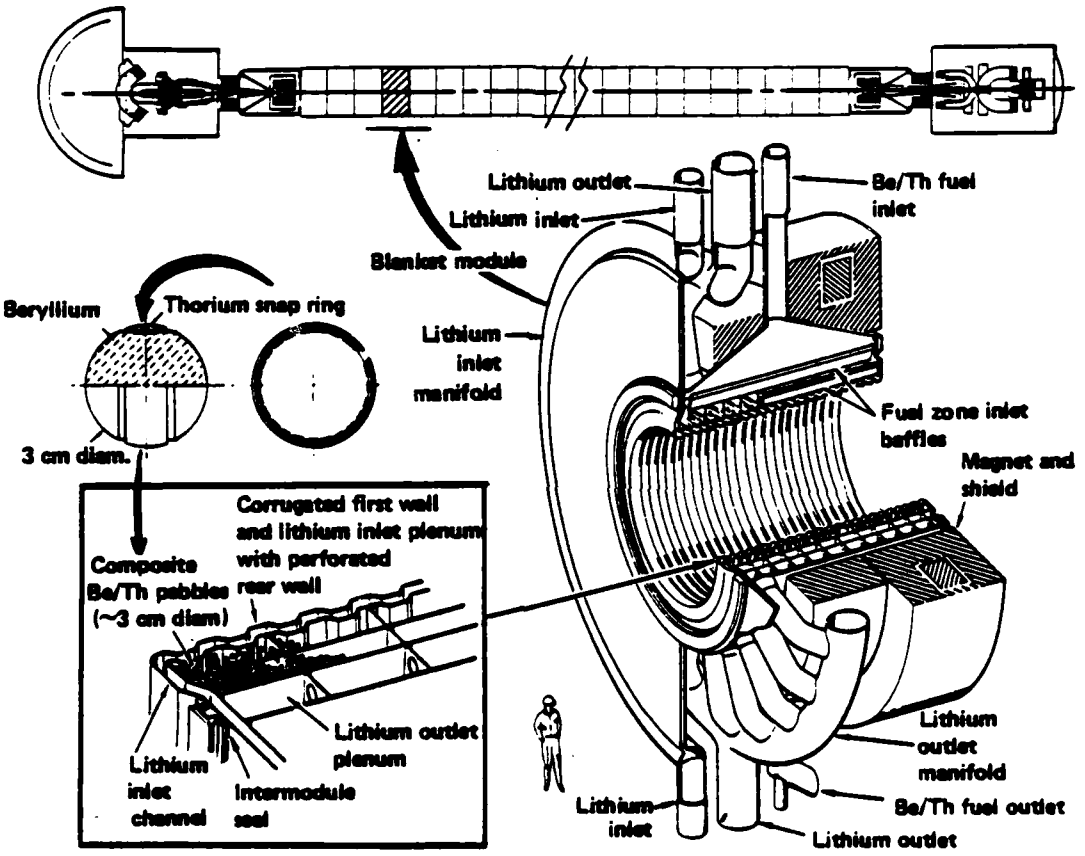

Figure 1-3: Reference liquid-metal-cooled, fission-suppressed, tandem-mirror fusion-hybrid blanket features direct cooling of a bed of beryllium-thorium pebbles [3].

1.2.1. Catalyzed D-D Fuel Cycle

The catalyzed deuterium-deuterium fuel cycle utilizes only deuterium, ^{2}H, as the input fuel, thereby eliminating the requirements for tritium breeding. The tritium and helium-3 produced by the deuterium-deuterium reactions are recycled into the reaction chamber and also react with deuterium.

This fuel cycle has the advantages of an almost unlimited supply of fuel, no requirement for tritium breeding, and a lower neutron wall loading than the deuterium-tritium fuel cycle. Disadvantages to this fuel cycle include: maintaining the plasma at a higher relative temperature (30 [keV] versus 10 [keV] for a D-T plasma); a lower power output than a D-T system for a given reactor size and magnetic field; and the addition of hydrogen, $^{1}H_{1}$, removal requirements in the exhaust and impurity control system. It is hoped that a higher neutron density (fluence) can therefore be obtained, thereby increasing fissile production.

Neutron Output

The neutrons produced by the D-D reaction are born with an average energy of 2.45 [MeV], those from the D-

T reaction at 14.1 [MeV], and those from the T-T reaction at 5.04 [MeV] each. All neutrons will need to be thermalized in the first wall/moderator region of the blanket to increase the conversion efficiency and decrease the fission rate.

Critical Issues

If the D-D fuel cycle is to be employed rather than the D-T fuel cycle, the confinement and plasma heating requirements will be more stringent. Comparing the Wildcat [4] and Starfire [5] values for $\langle n\tau_E \rangle$, 2.7 x 10^{21} [s/m^3] and 2.9 x 10^{20} [s/m^3] respectively, it can be seen that the D-D system requires an order of magnitude better confinement than the D-T system. These values are based on an operating temperature of about 30 [keV] for the D-D system, which appears to be optimum from power balance calculations.

The higher operating temperature necessitates high efficiency plasma heating systems, as well as good confinement. Additional requirements for efficient impurity control are also necessary to minimize the radiated energy.

1.2.2. Spherical Torus Reactor Concept

The fusion core adopted for this study is based on a concept proposed by Y-K. M. Peng [6]. Figure 1-4 illustrates the cross-sectional design of a proposed spherical torus, including placement of the toroidal and poloidal field coils. The concept utilizes a small aspect ratio torus and normal toroidal field coils to achieve a compact reactor. Compactness is enhanced by leaving only a cooled normal conductor in the center of the device to carry current for the toroidal field coils. The result is a device with a very low aspect ratio, normally between 1.5 and 2.0, high beta, and relatively low field requirements. The device does not employ an ohmic-heating solenoid, therefore requiring non-inductive current drive techniques. Generally, a simple set of dipole coils is employed for the poloidal field system and a natural plasma elongation as indicated by MHD analysis [7], is assumed.

The spherical torus offers several potential advantages for the catalyzed D-D hybrid system. Because of its small size and low aspect ratio, the neutron flux at first wall is much higher than that of a conventional tokamak of equivalent total power. This

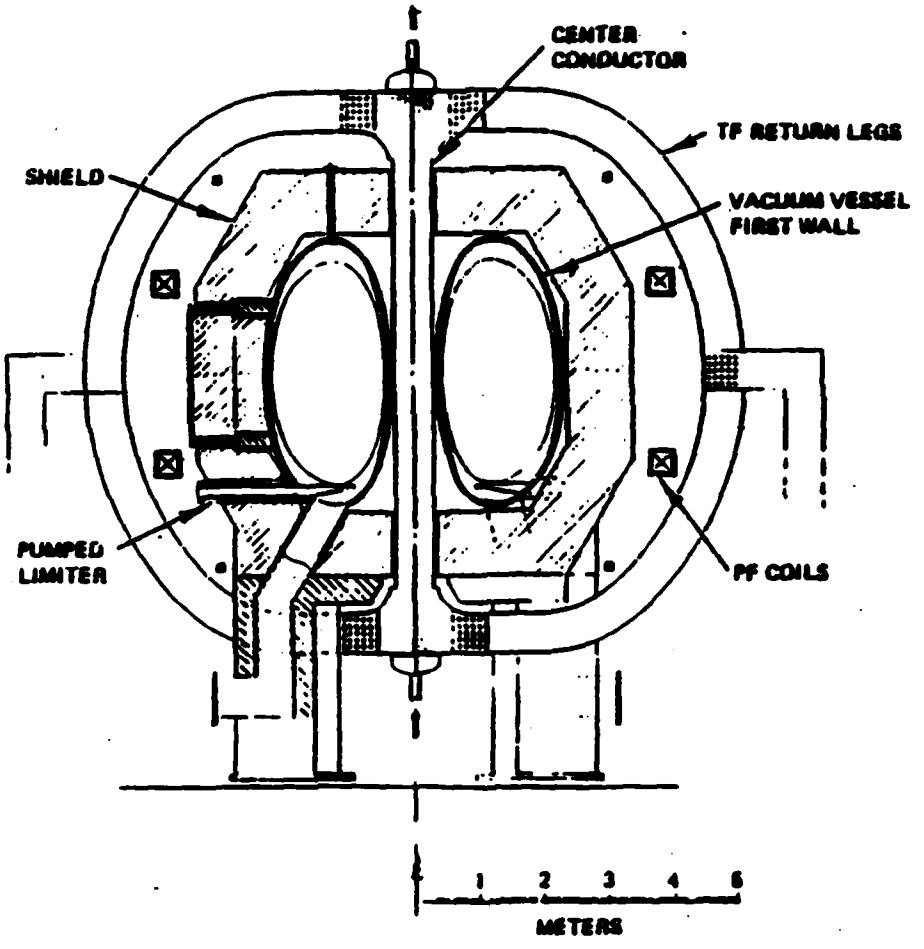

Figure 1-4: Conceptual Spherical Torus Reactor Design [6].

offers the potential of more cost effective breeding in the blanket due to the need for less inventory of fertile material and less overall structure. This should lead to a lower cost per fissile atom and, therefore, a lower cost of electricity for the total system. This will be further investigated later in this study.

The magnet requirements are reduced in the spherical torus due to compact size and the paramagnetic effect. This lowers cost in terms of reduced resistive losses and capital expenditure for the coils and power supplies, assuming resistive coils are used.

1.2.3. Aqueous Self-Cooled Blanket

The blanket adopted for this study was proposed by D. Steiner and associates at Rensselaer Polytechnic Institute [8]. The concept is unique in that the breeding and coolant functions of the blanket are combined into one single component. Breeding is achieved by neutron interactions with compounds dissolved in the coolant. Neutron multiplication is provided by the first wall and blanket structural materials and by the heavy water coolant.

Due to the elimination of additional neutron multipliers in the blanket, structural materials with low neutron absorption must be chosen. Zircaloy was chosen as the structural material because of its low absorption cross-section and extensive fission reactor database.

By employing the aqueous self-cooled blanket concept, the amount of structural material in the blanket can be reduced to approximately 5%. A simplified on-line plutonium extraction process can be employed because the uranium is already in aqueous solution.

1.3. Scope and Method of Analysis

The basic systems of the proposed fusion hybrid breeder reactor were evaluated during this research. The evaluation included modeling of the plasma and reaction rates; plasma power balance and particle confinement; magnet systems design, materials, and power losses; impurity control; first wall, blanket, and shield design and neutronic analysis; and reactor cost and cost of the bred fissile material.

Plasma modeling and reaction rate determination is

detailed in Chapter 2. A parametric design space study was conducted limiting the plasma current and minimum fusion power. The computer code listed in Appendix B was used for this part of the study.

The plasma power balance for the design space determined above was calculated using the methods given in Chapter 3. A particular particle confinement scaling was not used, rather, a comparison of presently available scalings was conducted.

Design and losses of the toroidal field, poloidal field, and current drive systems is elucidated in Chapter 4. Detailed loss and design analysis is performed for the normal coil option, but a superconducting option is also considered in a brief and qualitative manner. The physics of the oscillating field current drive is given briefly and the resultant equations for power requirements stated.

Impurity control options are considered qualitatively in Chapter 5. Limiter and divertor systems for the spherical torus are considered and then compared. A detailed analysis of both options is being conducted independently of this study and additional consideration of impurity control is beyond this study's scope.

Blanket design and neutronics were given detailed analysis, which is presented in Chapter 6. Neutronics analysis was performed using the discrete neutron transport code ONEDANT [9] on the Magnetic Fusion Engineering (MFE) Computer System. Stress analysis of the first wall and blanket was considered beyond the scope of this study and not performed here. Lifetime analysis of the first wall blanket shield (FBS) module was based on previous work done for WILDCAT and other studies.

Cost analysis is based on the cost model [10] used in the reversed field pinch compact reactor (RFPCR/TITAN) study with fissile costing based on methods used in the previous design studies indicated in the previous subsection. The equations used and power flow model considered are given in Chapter 7.

In Chapter 8, the results of this design study are presented and compared with those of the previous studies. Conclusions and future work required are summarized in Chapter 9.

2. DETERMINATION OF PLASMA REACTION RATES

The steady-state reaction rates for the catalyzed deuterium-deuterium (D-D) fuel cycle in the spherical torus will be derived in this chapter. To accomplish this, the particle and temperature profiles will be developed, as well as an expression for the power density. Then, the total average particle density and plasma beta for the spherical torus will be determined. Additionally, the topic of paramagnetism will be discussed.

With this background, the reactions of interest will be presented, the rate equations will be developed, and finally the steady state densities for these equations will be determined. These equations are then benchmarked against the results presented in WILDCAT [4] and parametric design space results from this study are presented.

2.1. Profiles and Power Density

Based on the approaches used by STARFIRE [5], a commercial D-T tokamak study, and WILDCAT [4], a commercial D-D tokamak study, a cylindrical profile model was assumed for the temperature and particle profiles. This yields the following equations as a function of r,

the distance from the center of the plasma:

$$n(r) = \bar{n}\ (1 + \alpha_n)[1 - (r/\tilde{a})^2] \qquad [2.1.1]$$

$$T(r) = \bar{T}\ (1 + \alpha_T)[1 - (r/\tilde{a})^2] \qquad [2.1.2]$$

where,

$$\bar{n} = \int_V n(\rho)\ dV/V \qquad [2.1.3]$$

$$\bar{T} = \int_V T(\rho)\ dV/V \qquad [2.1.4]$$

and $\bar{n}$ is the average particle density, $\bar{T}$ is the average plasma temperature, α_n and α_T are constants to be determined by experimental or theoretical means, and $\tilde{a}$ is the effective minor radius, given by:

$$\tilde{a} = [a\cos(\theta + d\sin\theta) + \kappa\, a \sin\theta]^{0.5}\, d\theta \qquad [2.1.5]$$

where a is the minor radius and θ is the angle between r and the midplane of the plasma, as illustrated in Figure 2-1. For this analysis, the values chosen in WILDCAT [4],

$$\alpha_n = \alpha_T = 0.7$$

are used. Average particle densities and temperatures are found by integrating the profiles over the volume of the plasma.

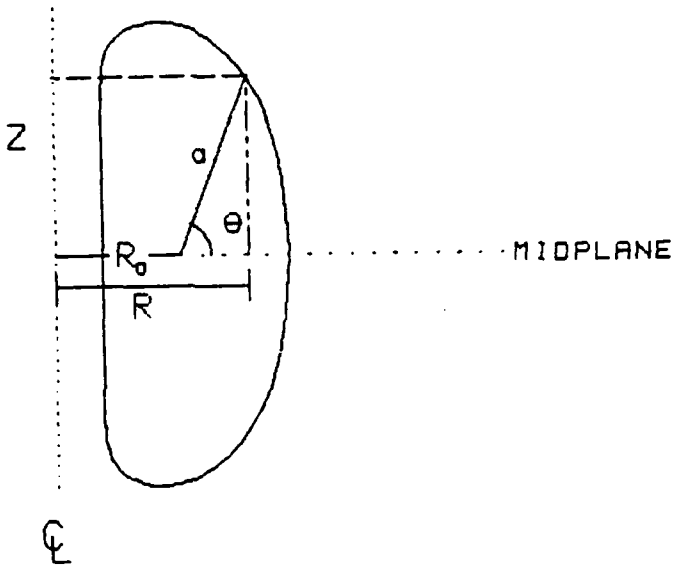

Figure 2-1: Geometry of plasma model.

The plasma boundary can be defined by:

$$R = R_o + a\cos(\theta + d\sin\theta) \qquad [2.1.6]$$

$$Z = \kappa a \sin\theta \qquad [2.1.7]$$

where R_o is the major radius, a is the minor radius, κ is the elongation, and d is the D-shapeness, which is assumed to be the same as WILDCAT. The plasma volume is then given by:

$$V = \int_v dV = 4\pi\kappa \int_v [R + \rho\cos(\theta + d\sin\theta)] * [\cos(\theta + d\sin\theta)\ \rho\cos\theta(\rho\sin(\theta + d\sin\theta)]d\rho d\theta \qquad [2.1.8]$$

where ρ is the radial distance from the center of the plasma.

From Dolan [11], the following expression for the reaction rate parameter $\langle\sigma v\rangle$ is obtained:

$$\langle\sigma v\rangle = 10^{-6} \exp[a_1 T^{-r} + a_2 + a_3 T + a_4 T^3 + a_5 T^4] \quad [2.1.9]$$

where r, and a_1 through a_5 are constants dependent on the reaction species.

As will be shown in the next subsection, profile factors for each reaction must be determined. These profile factors are defined by:

$$f_p^i = \frac{\int_V n_i^2 \langle\sigma v\rangle^i \, dV}{n_i^2 \langle\sigma v\rangle^i_{@T} \, V} \quad [2.1.10]$$

The fusion power for each reaction is then given by:

$$P_i = n_1 n_2 \langle\sigma v\rangle^i_{@T} E_f^i f_p^i V \quad [2.1.11]$$

where i is the reaction, $\langle\sigma v\rangle^i_{@T}$ is the reaction rate parameter at the average plasma temperature, n_1 and n_2 are the volume average particle densities and, in cases where the reacting particles are identical $n_1 = n_2/2$; E_f is the energy released per event in [MJ]; and V is the plasma volume. The total fusion power is just the sum of the individual powers.

2.2. Modeling of the Spherical Torus Behavior

Plasma elongation, κ, as previously stated, is assumed to occur naturally in the spherical torus, with no need for additional shaping fields. Based on free-boundary MHD equilibrium calculations, Peng and Strickler [7] report κ as a function of aspect ratio, $A = R/a$. These calculations are shown graphically in figure 2-2 and have been fitted by the following relation:

$$\kappa = 2.277 - 0.1949\ A,$$

which is valid over the range $1.4 \leq A \leq 3.0$.

The equilibrium toroidal plasma current is approximated by the formula [6]:

$$I_p\ [MA] = \frac{5a\ B_{t_o}\ C_I\ (1+\kappa)^2}{2\ q_o\ (1-\epsilon)^2} \qquad [2.2.1]$$

where B_{t_o} is the vacuum toroidal field on axis, $\epsilon = 1/A$, q_o is the safety factor on axis, and $C_I = 1.22 - 0.68\epsilon$.

The beta limit is based on experimental indications [7] and is approximated by:

$$\beta_c = \frac{0.033\ I_o\ [MA]}{a\ [m]\ B_t\ [T]} \qquad [2.2.2]$$

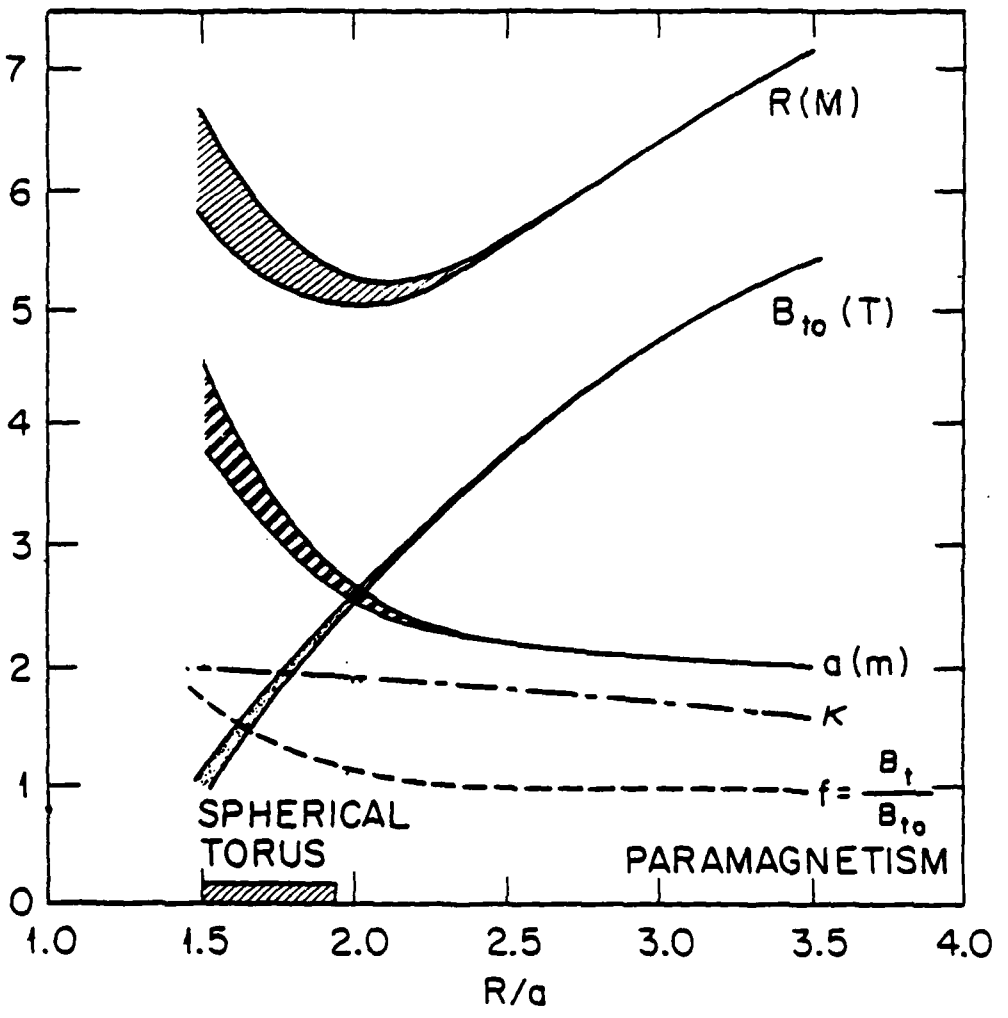

Figure 2-2: Variations of R, a, κ, B_{to}, and paramagnetism for a 2000 [MW(t)] Tokamak restricted by Troyon limit [7].

and by definition is:

$$\beta = \frac{2\mu_o \langle p \rangle}{B_t} \qquad [2.2.3]$$

where $\langle p \rangle$ is the plasma pressure, and a is the plasma minor radius.

2.2.1. Paramagnetism

The vacuum toroidal field in the presence of the plasma can be either diminished (diamagnetism), or enhanced (paramagnetism). Paramagnetism occurs when the magnetic field associated with the poloidal component of the plasma current is in the same direction as the applied toroidal field. Due to the small aspect ratio and highly pitched magnetic field of the spherical torus, its equilibria exhibit a high degree of paramagnetism. Figure 2-2 shows the calculated paramagnetism factor, $f_o = B_t/B_{to}$, as a function of the aspect ratio.

The impact of strong paramagnetism on the plasma pressure balance is uncertain because equation 2.2.2 is based on empirical data and theoretical situations for which B_t differed little from B_{to}. This leads to a range of possibilities as to where B_t should be used as opposed to B_{to}.

Rewriting equation 2.2.2 and 2.2.3 indicating the field in 2.2.2 as B_1 and in 2.1.3 as B_2, and combining equations, we obtain the plasma pressure, $\langle p \rangle$, in the form:

$$\langle p \rangle = \frac{\beta_t B_2^2}{2\mu_o} = \frac{0.033\ B_2^2\ I_a}{2\mu_o\ a\ B_1} \qquad [2.2.4]$$

The anticipated effect of paramagnetism differs depending on what B_1 and B_2 are assumed to be. The four possible cases are given below:

1. $B_1 = B_2 = B_{to}$,

then $\langle p \rangle \propto I_p B_{to}/a$, this is the standard case;

2. $B_1 = B_2 = B_t$,

then $\langle p \rangle \propto I_p f_a B_{to}/a$;

3. $B_1 = B_{to}$ and $B_2 = B_t$,

then $\langle p \rangle \propto I_p f_a^2 B_{to}/a$;

4. $B_1 = B_t$ and $B_2 = B_{to}$,

then $\langle p \rangle \propto I_p B_{to}/a f_a$.

In our analysis of the plasma parameters we will use case 2, $B_1 = B_2 = B_t$, which represents a moderately optimistic case. For this study the following curve fit to the results of Figure 2-2 was used for the

paramagnetism factor f_m:

$$f_m = -19.297 - 111.69\ A + 406.53\ A^2 - 477.56\ A^3 + 265.6\ A^4 - 71.93\ A^5 + 7.66\ A^6 \qquad [2.2.5]$$

This fit is valid over the range $1.4 \leq A \leq 2.3$.

2.2.2. Total Average Density

The total volume average density is calculated using the volume average pressure and the volume average temperature. The maximum value of the volume average pressure is given by equation 4.1.2 with $B_2 = B_{t_0} f_m$:

$$\langle nT \rangle = \frac{\beta_c\ f_m^2\ B_{t_0}^2}{2\mu_0} \qquad [2.2.6]$$

where n is the total plasma density. In the calculation procedure, B_{t_0}, β_c, and f_m are specified. Using the profile equations, $\langle nT \rangle$ can also be written as:

$$\langle nT \rangle = \frac{\int_V n(r)\ T(r)\ dV}{V} \qquad [2.2.7]$$

Thus, the total volume average density, $\bar{n}$, is given by:

$$n_{TOTAL} = \frac{\langle \sigma v \rangle_{\sigma T}\ V}{[1+\alpha_n][1+\alpha_T]T \int [1-(\rho/a)^2]^{\alpha_n+\alpha_T}\ dV} \qquad [2.2.8]$$

where T, the average plasma temperature, is specified. For convenience in further equations, the average density will be written as n, omitting the bar.

2.3. Steady State Densities

The reactions occurring in the catalyzed D-D fuel cycle are given in equations 2.3.1 through 2.3.5 along with the energy produced by each reaction [11].

$$D + D \rightarrow {}^3He + n + 3.27 \qquad [2.3.1]$$

$$D + D \rightarrow T + p + 4.03 \qquad [2.3.2]$$

$$D + T \rightarrow {}^4He + n + 17.59 \qquad [2.3.3]$$

$$D + {}^3He \rightarrow {}^4He + p + 18.3 \qquad [2.3.4]$$

$$T + T \rightarrow {}^4He + n + n + 11.3 \qquad [2.3.5]$$

The cross sections for the above reactions are shown in Figure 2-3 over the temperature range of interest in this study.

The rate equations for these reactions are given below. All densities are volume average densities.

$$\frac{dn_T}{dt} = \frac{n_D^2}{2} f_{DDT}\langle\sigma v\rangle_{DDT} - n_T n_D f_{DT}\langle\sigma v\rangle_{DT} - \frac{n_T^2}{2} f_{TT}\langle\sigma v\rangle_{TT} \qquad [2.3.6]$$

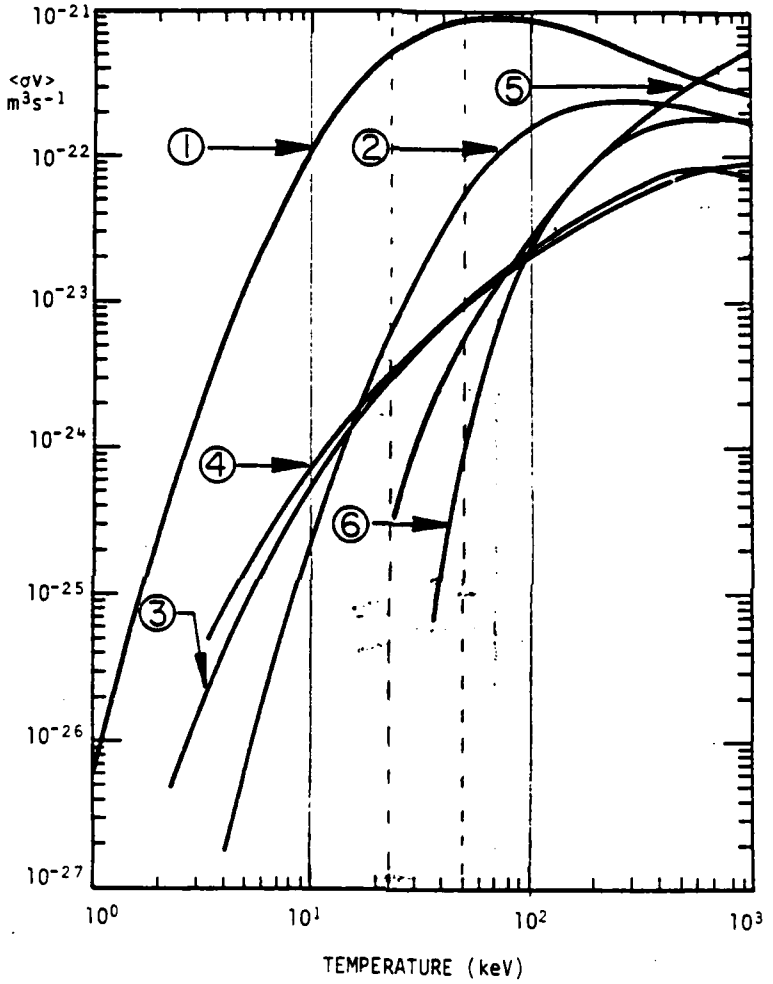

Figure 2-3: Reaction rate $\langle\sigma v\rangle$ [m^3/s] versus temperature [keV] for the reactions of interest [11]. (1) D+T -> n+^{4}He, (2) D+^{3}He->H+^{4}He, (3) D+D->H+T, (4) T+T->^{4}He+2n, (5) T+^{3}He->(various products), (6) H+^{11}B->3(^{4}He). The curve for D+D->^{3}He+n is about the same as curve (3).

$$\frac{dn_3}{dt} = \frac{n_D^2}{2} f_{DD3}\langle\sigma v\rangle_{DD3} - n_D n_3 f_{D3}\langle\sigma v\rangle_{D3} - n_3 R_3 \qquad [2.3.7]$$

$$\frac{dn_\alpha}{dt} = n_D n_3 f_{D3}\langle\sigma v\rangle_{D3} + n_D n_T f_{DT}\langle\sigma v\rangle_{DT} + \frac{n_T^2}{2} f_{TT}\langle\sigma v\rangle_{TT} - R_\alpha n_\alpha \qquad [2.3.8]$$

$$\frac{dn_p}{dt} = \frac{n_D^2}{2} f_{DDT}\langle\sigma v\rangle_{DDT} + n_D n_3 f_{D3}\langle\sigma v\rangle_{D3} - n_p R_p \qquad [2.3.9]$$

where R_i is the removal coefficient of species i, given by:

$$R_i = \frac{\text{number of i particles removed per unit time}}{\text{number of i particles present}}.$$

The steady state density of each species is then determined by setting the rate equations equal to zero. The following results are obtained:

$$\frac{n_T}{n_D} = \frac{f_{DDT}\langle\sigma v\rangle_{DDT}}{2f_{DT}\langle\sigma v\rangle_{DT} + (n_T/n_D) f_{TT}\langle\sigma v\rangle_{TT} + 2R_T/n_D} \qquad [2.3.10]$$

$$\frac{n_3}{n_D} = \frac{f_{DD3}\langle\sigma v\rangle_{DD3}}{2f_{D3}\langle\sigma v\rangle_{D3} + 2R_T/n_D} \qquad [2.3.11]$$

$$\frac{n_\alpha}{n_D} = \frac{n_3 f_{D3}\langle\sigma v\rangle_{D3} + n_T f_{DT}\langle\sigma v\rangle_{DT} + (n_T^2/2n_D) f_{TT}\langle\sigma v\rangle_{TT}}{R_\alpha} \qquad [2.3.12]$$

$$\frac{n_a}{n_p} = \frac{n_p f_T \tau \langle \sigma v \rangle_{pT} + 2 n_a f_{aa} \langle \sigma v \rangle_{aa}}{2 R_p} \qquad [2.3.13]$$

To calculate n_p we invoke charge balance and equation 2.2.8 for the total density to obtain:

$$n_p = \frac{n_{TOTAL}}{2 + 2\left(\frac{n_T}{n_p} + \frac{n_a}{n_p}\right) + 3\left(\frac{n_3}{n_p} + \frac{n_4}{n_p}\right) + \Sigma_i (Z_i + 1)} \qquad [2.3.14]$$

where z_i and n_i are the charge and density of impurity species assumed to be present in the plasma. The total average particle density is determined as previously described and then n_p is determined by iteration of equations 2.3.10 - 2.3.14.

2.4. Benchmark of the Code

It is desirable to assess the validity of the methods and equations used in the code prior to its application. To this end, the code (see Appendix B) was benchmarked against the WILDCAT [4] parameters, Table 2-1. The results of this benchmark are given in Table 2-2.

It appears that the code accurately reproduces the WILDCAT results. The difference in densities for Helium 4 are noted but should have little effect on the performance and reliability of the code.

Table 2-1: WILDCAT Reference Parameters

Major Radius, R [m]	8.58
Aspect Ratio, A	3.25
Peak Toroidal Field, B_{TFC} [T]	14.35
Number of TF Coils	12
Plasma Beta, β	0.11
Plasma Current, I_p	29.9
Temperature [keV]	
Average Electron	30
Average Ion	32
Average Densities [m^{-3}]	
Proton	1.2×10^{19}
Deuterium	1.7×10^{20}
Tritium	8.2×10^{17}
Helium 3	1.9×10^{19}
Helium 4	5.0×10^{18}
Electron	2.5×10^{20}

Table 2-2: Benchmark Results - Steady State Particle Densities

PARTICLE	WILDCAT	CODE
D	1.7×10^{20}	1.7×10^{20}
T	8.2×10^{17}	8.2×10^{17}
3He	1.9×10^{19}	1.9×10^{19}
4He	5.0×10^{18}	5.4×10^{18}
p	1.2×10^{19}	1.2×10^{19}
e	2.5×10^{20}	2.5×10^{20}

2.5. Typical Results and Examples

Typical results of the plasma parameter design space analysis are shown in Table 2-3. The parameters listed in the table are the major radius (R), minor radius (r), aspect ratio (A), plasma elongation (K), magnetic field on axis (B_t), plasma beta, plasma current (I_p), fusion power (P_{fus}), and total density (n_{tot}). The numbers given in the left-hand column are reference numbers and apply to the same cases throughout the thesis and Appendix A. It is interesting to note that in all cases where the aspect ratio was below 1.9, either the plasma current was higher than technologically reasonable (>75 [MA]) or the fusion power was lower than economically beneficial (<600 [MW]). Cases meeting the criteria were found with aspect ratios between 1.9 and 2.3 and major radii between 5.0 and 8.0. All results given here are for an average temperature of 30 [keV].

Table 2-3: Plasma Parameter Design Space

#	R [m]	a [m]	A	kappa	Bt [T]	beta	Ip [MA]	P fusion [MW]	n tot [m-3]	V [m3]
101	7.5	3.3	2.3	1.8	7.0	0.1	63.1	1139	1.53E+20	2803
102	7.0	3.0	2.3	1.8	7.0	0.1	58.9	926	1.53E+20	2279
103	6.5	2.8	2.3	1.8	7.0	0.1	54.7	742	1.53E+20	1825
104	8.0	3.5	2.3	1.8	6.5	0.1	62.5	1026	1.32E+20	3401
105	7.5	3.3	2.3	1.8	6.5	0.1	58.6	846	1.32E+20	2803
106	7.0	3.0	2.3	1.8	6.5	0.1	54.7	687	1.32E+20	2279
107	7.5	3.4	2.2	1.8	6.5	0.1	67.1	1203	1.50E+20	3093
108	7.0	3.2	2.2	1.8	6.5	0.1	62.6	978	1.50E+20	2515
109	6.5	3.0	2.2	1.8	6.5	0.1	58.1	783	1.50E+20	2013
110	6.0	2.7	2.2	1.8	6.5	0.1	53.6	616	1.50E+20	1584
111	6.5	3.1	2.1	1.9	6.5	0.1	67.1	1185	1.74E+20	2231
112	6.0	2.9	2.1	1.9	6.5	0.1	62.0	932	1.74E+20	1754
113	5.5	2.6	2.1	1.9	6.5	0.1	56.8	718	1.74E+20	1351
114	8.0	3.5	2.3	1.8	6.0	0.1	57.7	744	1.12E+20	3401
115	8.0	3.6	2.2	1.8	6.0	0.1	66.0	1058	1.28E+20	3754
116	7.5	3.4	2.2	1.8	6.0	0.1	61.9	872	1.28E+20	3093
117	7.0	3.2	2.2	1.8	6.0	0.1	57.8	709	1.28E+20	2515
118	7.0	3.3	2.1	1.9	6.0	0.1	66.7	1072	1.49E+20	2786
119	6.5	3.1	2.1	1.9	6.0	0.1	62.0	858	1.49E+20	2231
120	6.0	2.9	2.1	1.9	6.0	0.1	57.2	675	1.49E+20	1754
121	6.0	3.0	2.0	1.9	6.0	0.1	66.9	1021	1.73E+20	1952
122	5.5	2.8	2.0	1.9	6.0	0.1	61.3	786	1.73E+20	1504
123	8.0	3.6	2.2	1.8	5.5	0.1	60.5	746	1.07E+20	3754
124	8.0	3.8	2.1	1.9	5.5	0.1	69.9	1128	1.25E+20	4158
125	7.5	3.6	2.1	1.9	5.5	0.1	65.6	929	1.25E+20	3426
126	7.0	3.3	2.1	1.9	5.5	0.1	61.2	755	1.25E+20	2786
127	6.5	3.1	2.1	1.9	5.5	0.1	56.8	605	1.25E+20	2231
128	6.5	3.3	2.0	1.9	5.5	0.1	66.4	914	1.46E+20	2482
129	6.0	3.0	2.0	1.9	5.5	0.1	61.3	719	1.46E+20	1952
130	5.5	2.9	1.9	1.9	5.5	0.1	66.7	859	1.71E+20	1681
131	5.0	2.6	1.9	1.9	5.5	0.1	60.7	646	1.71E+20	1263

2.6. Conclusions

The steady-state reaction rates for a catalyzed D-D Spherical Torus reactor have been developed and verified against reported values. A reactor design space has been found in the compact spherical torus regime with acceptable plasma currents and fusion power. The issues of magnet requirements, current drive, and plasma temperature maintenance must still be addressed before this design space can be considered viable. These issues will be addressed in subsequent chapters.

3. PLASMA POWER BALANCE

It is necessary to address the plasma power balance, in other words, the plasma energy losses and gains, in order to determine an operating temperature and the requirements for additional plasma heating. Additionally, the amount of energy transported from the plasma by charged particles is important when considering the impurity control system.

In steady-state a simple power balance for self-sustaining plasma is obtained from:

$$P^{cp}_{fus} + P_{aux} = P_{loss} = P_{rad} + P_{tr}$$

where P^{cp}_{fus} is the fusion power of the charged daughter products (which can be calculated using the procedure outlined in the previous chapter), P_{aux} is the auxiliary heating power, P_{tr} is the transport loss associated with the charged particles leaving the plasma, and P_{rad} is the power lost to the first wall due to all types of radiation.

In this chapter the terms of the power balance will be examined in detail. Various confinement scaling laws will also be examined and, finally, the results of this analysis will be presented.

3.1. Auxiliary Power

The auxiliary power is the additional power required to sustain the plasma temperature at steady-state. This power can be provided by a number of different sources: current drive power, resistive losses in the plasma, and additional power injected into the plasma. In using the power balance equation for figures of merit the auxiliary power will be separated into the following,

$$P_{aux} = P_{add} + P_{\Omega} + f_{CD}P_{CD} \qquad [3.1.1]$$

where P_{add} is the additional power required to maintain the plasma temperature, P_{Ω} is the power due to resistive losses in the plasma, f_{CD} is the fraction of current drive power remaining in the plasma, and P_{CD} is the power required to drive the plasma current, as described in a subsequent section of this thesis. The fraction of current drive power remaining in the plasma, f_{CD}, is assumed to be approximately unity for the oscillating field current drive and this value will be used throughout the remainder of this paper.

The plasma energy gain factor, Q, is defined as:

$$Q = \frac{P_{fusion}}{P_{aux}} \qquad [3.1.2]$$

This Q will be used as a figure of merit in this study to determine the desired operating temperature and also to compare the various scaling laws. A large value of Q is desired because this minimizes the power that must be added to the plasma.

3.2. Radiation Losses

The radiation losses from the plasma are associated with the electrons and are due mainly to two types of radiation: bremmstrahlung and cyclotron. Losses due to bremmstrahlung radiation are given by:

$$P_{brem} = 5.35\times10^{-43}\ n_e^2\ Z_{eff}\ T_e^{0.5}\ V \qquad [3.2.1]$$

where n_e and T_e are the electron density and temperature, respectively, and Z_{eff} is the effective plasma charge given by:

$$Z_{eff} = \sum_i \frac{n_i Z_i^2}{n_e}.$$

Power losses from the plasma due to cyclotron radiation are given by [11]:

$$P_{cyc} = 6.21\times10^{-23}\ K_c\ n_e\ T_e\ B_{te}^2\ V\ \left[1+\frac{T_e}{146}+\ldots\right] \qquad [3.2.2]$$

where n_e and T_e are the electron density and temperature,

$B_{\circ}$ is the magnetic field on axis, and K_c is the fraction of cyclotron radiation absorbed in the first wall, assuming a cylindrical plasma profile. The factor K_c is a function of $T_{\circ}$ and the "plasma depth", D, given by:

$$D = \frac{2\, n_{\circ}\, \hat{a}}{B^{1.8}\, \eta^{0.5}\, (1-\beta)^{0.75}}$$

where $\hat{a}$ is the effective plasma radius,

$$\hat{a} = a[1+\kappa^2]^{\frac{1}{2}} / 2$$

and η is the electrical resistivity of the first wall.

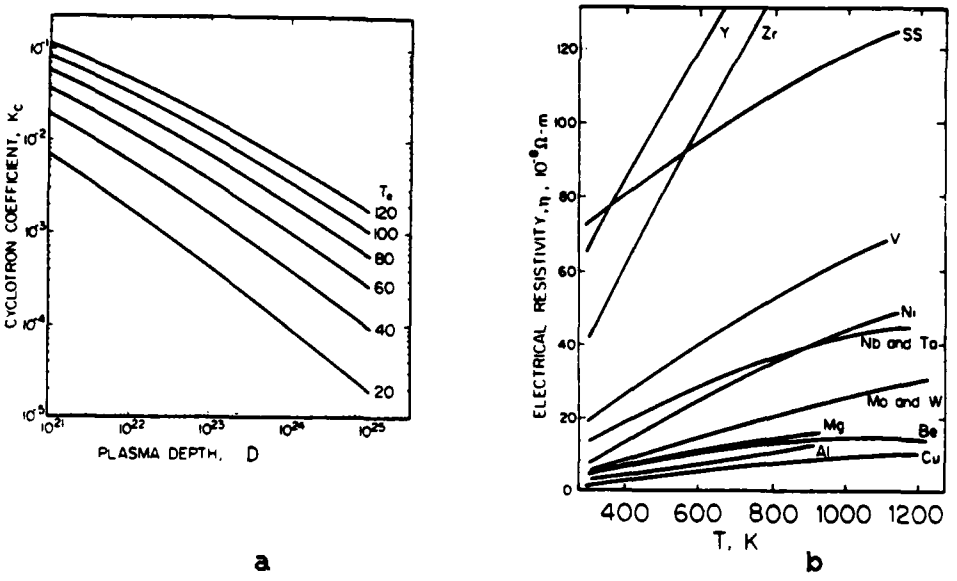

Figure 3-1: Fraction of cyclotron radiation lost from the plasma(a), as a function of temperature and plasma depth, and electrical resistivities(b) for various metals as a function of first wall temperature [11].

Values for K_ϵ and n are shown in Figures 3-1a and 3-1b respectively.

3.3. Transport Losses

Transport losses from the plasma can be written based on the global energy confinement time as:

$$P_{tr} = \int \frac{3}{2} \frac{n_i k T_i + n_e k T_e}{\tau_E} dV = \frac{3}{2} \frac{\langle nkT \rangle (1 + T_e/T_i)}{\tau_E} \star V \quad [3.3.1]$$

which can be rewritten using the plasma pressure balance as:

$$P_{tr} = \frac{3}{2} \frac{\beta_\epsilon (f_e B_{t0})^2}{2\mu_0 \tau_E} \star V \quad [3.3.2]$$

where τ_E is the global energy confinement time. For this part of the study an elliptical plasma cross section is used to simplify calculations. This results in a global confinement time given by:

$$\tau_E = \frac{3}{8} \frac{\tilde{a}^2}{\chi_E} \quad [3.3.3]$$

where χ_E is the total effective diffusivity, and $\tilde{a}$ is the effective plasma size,

$$\tilde{a}^2 = a^2 [2K^2/(1+K^2)].$$

The total effective diffusivity is defined as [12]

$$\chi_e = (\chi_i + \chi_e \frac{T_e}{T_i})[\frac{2}{1 + T_e/T_i}] \qquad [3.3.4]$$

where χ_e and χ_i are the electron and ion thermal diffusivities given by the various scaling laws.

3.3.1. Scaling Laws

Ion Confinement

In nearly all current tokamak experiments the observed ion confinement time is generally consistent with the predictions of neoclassical theory for the entire range of ion collisionality. The magnitude of the transport rates are within a factor of one to four of the neoclassical value with the mean being about two. The ion thermal diffusivity can thus be written

$$\chi_i = f_i \chi_i^{CH} \qquad [3.3.5]$$

where f_i is the enhancement factor, and χ_i^{CH} is the neoclassical ion thermal diffusivity as described by Chang and Hinton [13]. The neoclassical ion thermal diffusivity for low collisionality is given by:

$$\chi_i^{CH} = 6.5 \times 10^{-22}\ K_2^2\ A^{1.5}\ \frac{n_e Z_{eff}}{T_i^{0.5}}\ \frac{q^2}{B_\theta^2}\ (\frac{2}{1+K^2})\ [m^2/s] \qquad [3.3.6]$$

where

$$K_2^* = (0.66 + 1.88\ A^{-0.5} - 1.54\ A^{-1}) * (1 + 1.5\ A^{-2})$$

accounts for the effect of finite aspect ratio.

To be absolutely correct a term for the ripple should be added to equation 3.3.6 if the magnitude of the toroidal ripple is large, i.e. >1-2% at the plasma edge. The ripple contribution to the ion diffusivity is of the form

$$\chi_i^{ripple} \approx \delta^{1.5}\ T_i^{3.5},$$

where δ is the magnitude of the field ripple (peak to average). For the design space of interest in this study ripple losses are assumed to be small and have been neglected.

Electron Confinement

Various empirical and semi-empirical scaling laws for the electron confinement time or thermal diffusivity have been proposed for tokamak plasmas with ohmic and strong auxiliary auxiliary heating. Results from almost all of the experiments conducted indicate that the confinement properties of ohmically heated plasmas are

degraded when auxiliary heating is applied. The auxiliary heated regime has further been shown to have two confinement modes; an L-mode which is characterized by very poor confinement, and an H-mode with confinement being about twice that of L-mode. The mode in which the plasma operates (H- or L-) is a complex function of geometry, type and amount of auxiliary heating, and plasma and impurity density [14] and as such is beyond the scope of this thesis. In this study it will be assumed that conditions can be created such that auxiliary heated plasmas can be modeled using H-mode scalings.

In ohmically heated plasmas the neo-alcator scaling has been shown to provide a reasonable fit to all available tokamak data [15]. The expression for the thermal diffusivity is

$$\chi_{e.} = 4.68\times10^{20} \frac{\tilde{a}}{n_{.} R^2 q} \qquad [3.3.7]$$

where $\tilde{a}$ is the effective plasma radius as previously defined, R is the major radius, and q is the safety factor at the plasma edge.

Another scaling law for ohmically heated plasmas was proposed by Pfeiffer and Waltz [16] an can be expressed

as

$$\chi_{e,o}^{PM} = 5.95 \times 10^{19} \frac{a^{1.02}}{n_o^{0.9} R^{1.63} Z_{eff}^{0.23}}. \qquad [3.3.8]$$

This scaling is very close to Neo-Alcator in non-ignited devices, but extrapolates to ignited devices with a much different result.

While the confinement data for ohmic heated plasmas is fairly large, the data base for auxiliary heated plasmas is much smaller, with most of the data being for neutral beam heating. The scaling studies that have been carried out are mostly fits to individual sets of data and may not be valid when extrapolated to the devices under consideration in this study.

The scaling presented by Garbunov, Mirnov, and Strelkow, commonly called modified-GMS or Mirnov scaling, is one exception to this. A simplified form of this H-mode scaling is given by

$$\chi_{e,o}^{GMS} = 0.96 \frac{a}{I_p} \qquad [3.3.9]$$

where I_p is the plasma current [MA]. Confinement improves with plasma current and GMS scaling thus predicts favorable confinement at low aspect ratio.

Goldston and Kaye [17] presented another empirical

neutral beam scaling, the H-mode form of which is given by

$$\chi_{E,o}^{KG} = 150 \frac{\beta^{0.76} B_{t,o}^{1.73} T^{0.62} a^{2.38} \kappa^{0.71}}{I_p^{2.98} A^{2.55}} \qquad [3.2.10]$$

where T is the average electron temperature in keV, I_p is the plasma current [MA], $B_{t,o}$ is the toroidal field on axis [T], a is the plasma minor radius [m], κ is the elongation, and A is the aspect ratio.

The ASDEX group presented a semi-empirical scaling based on their auxiliary heated confinement data in H-mode. This is given as

$$\chi_{E,o}^{ASDEX} = 5.93 \frac{a^2}{I_p R A_i^{0.5}} \qquad [3.2.11]$$

where A_i is the effective atomic mass number of the ions.

Without further study and a large data base on compact high current reactors, one scaling law cannot be chosen over another. We will therefore endeavor to compare the effects of the various scalings on the parameters of interest rather than judging the merits of the confinement scalings.

3.4. Typical Results and Examples

The effects of temperature and the various scaling laws on the plasma power gain, Q, and the required auxiliary power are shown in Figures 3-2 and 3-3. These figures are for a fixed aspect ratio, major radius, and magnetic field. The wide variational effects of the confinement scalings can also be readily seen from the figures.

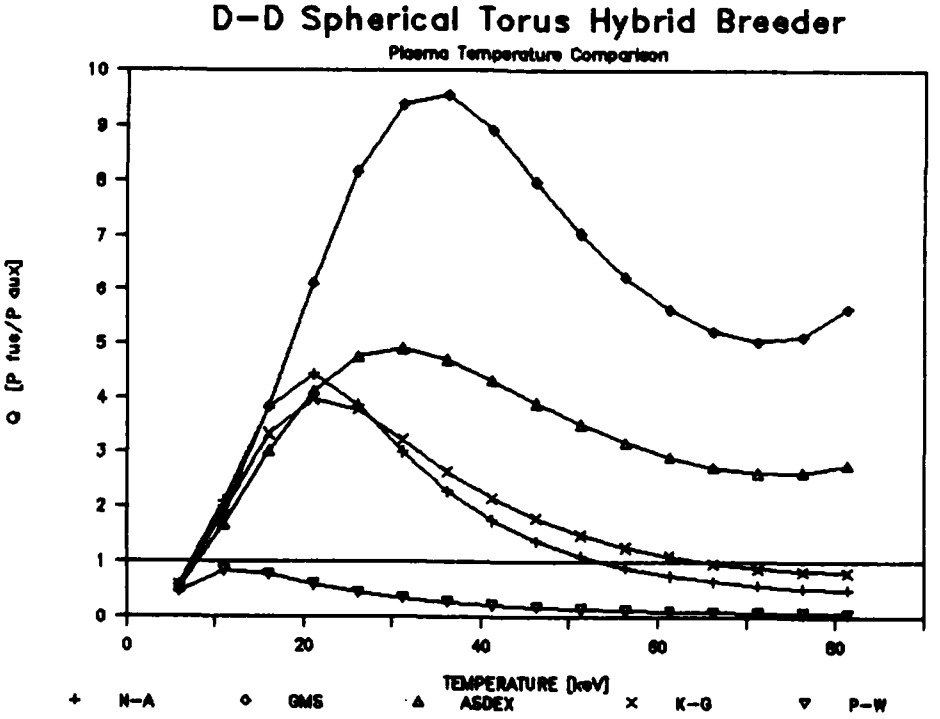

Figure 3-2: Effects of temperature on the plasma power gain for various particle confinement scaling laws.

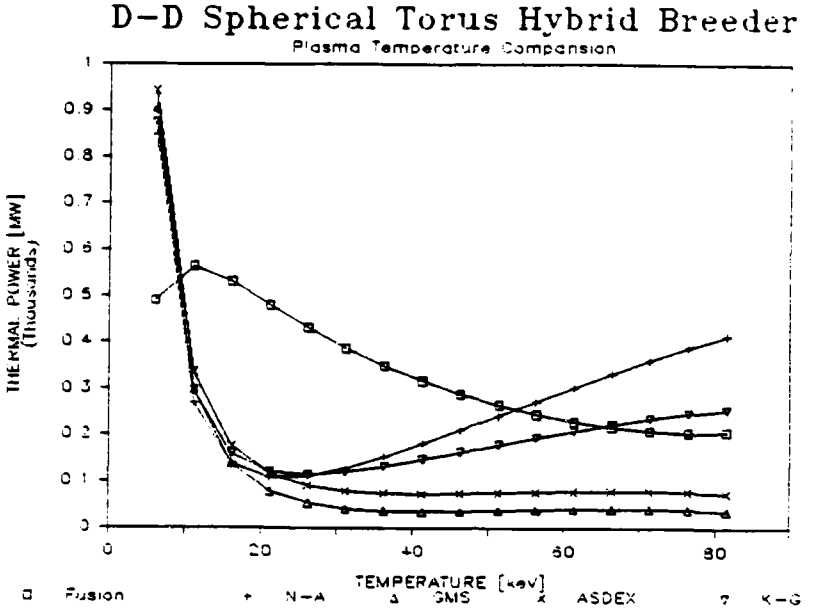

Figure 3-3: Effect of temperature on the fusion power and auxiliary power for various particle confinement scalings.

Typical results of the charged particle power, bremmstrahlung losses, auxiliary power, plasma gain, energy confinement time, and transport power for the various scaling laws are given in Table 3-1. A temperature of 30 [keV] is used throughout the table. Negative numbers in the table for P_{aux} indicate that no auxiliary power is needed to sustain the plasma, i.e. the fusion power is greater than the power loss from the plasma. In the calculation of P_{aux}, however, the presence of impurity ions has not been considered.

Table 3-1: Typical Results for Power Balance Calculations

#	neo-ALCATOR P aux [MW]	neo-ALCATOR Q plasma [P o/P i]	Pfeiffer-Waltz P aux [MW]	Pfeiffer-Waltz Q plasma [P o/P i]	GMS (Mirnov) P aux [MW]	GMS (Mirnov) Q plasma [P o/P i]	ASDEX P aux [MW]	ASDEX Q plasma [P o/P i]	Goldston-Kaye P aux [MW]	Goldston-Kaye Q plasma [P o/P i]
101	-92.1	-15.2	707.3	2.0	41.4	33.9	-45.1	-31.1	142.4	9.9
102	-52.6	-21.7	722.6	1.6	49.4	23.1	-16.1	-70.9	149.5	7.6
103	-18.4	-49.6	731.6	1.3	54.2	16.8	7.5	121.1	152.2	6.0
104	-68.3	-18.5	741.3	1.7	79.0	16.0	-22.8	-55.4	178.3	7.1
105	-35.4	-29.5	751.4	1.4	80.6	12.9	0.3	3295.5	179.7	5.8
106	-6.6	-127.9	756.3	1.1	80.1	10.6	19.3	44.0	177.8	4.8
107	-97.4	-15.2	749.0	2.0	33.6	44.0	-53.7	-27.6	127.4	11.6
108	-55.7	-21.6	765.1	1.6	43.4	27.8	-22.7	-53.0	136.9	8.8
109	-19.7	-48.9	774.4	1.3	49.6	19.4	2.6	373.9	141.8	6.8
110	11.0	68.8	777.1	1.0	52.8	14.4	22.6	33.5	142.5	5.3
111	-90.8	-16.0	767.8	1.9	-6.1	-237.2	-58.3	-25.0	78.0	18.7
112	-43.1	-26.6	785.3	1.5	10.8	106.3	-22.6	-50.7	94.1	12.2
113	-2.9	-299.8	793.7	1.1	22.7	38.9	5.6	157.0	103.8	8.5
114	-15.0	-61.1	780.7	1.2	112.3	8.2	18.3	50.0	209.9	4.4
115	-67.5	-19.3	788.6	1.7	76.0	17.2	-26.3	-49.7	167.6	7.8
116	-33.6	-32.0	798.3	1.4	78.3	13.7	-2.3	-463.7	170.4	6.3

#	P brem [MW]	P part [MW]	neo-ALCATOR Tau e [s]	neo-ALCATOR P tr [MW]	Pfeiffer-Walt Tau e [s]	Pfeiffer-Walt P tr [MW]	GMS (Mirnov) Tau e [s]	GMS (Mirnov) P tr [MW]	ASDEX Tau e [s]	ASDEX P tr [MW]	Goldston-Kaye Tau e [s]	Goldston-Kaye P tr [MW]
101	198.0	414.1	60.3	124.0	8.1	923.4	29.1	257.5	43.7	171.0	20.9	358.6
102	161.0	336.7	49.4	123.2	6.8	898.4	27.0	225.2	38.1	159.6	18.7	325.3
103	128.9	269.6	39.8	122.3	5.6	872.3	25.0	194.9	32.9	148.2	16.6	292.9
104	178.1	369.4	63.6	123.0	8.4	932.6	29.0	270.3	46.5	168.5	21.2	369.7
105	146.8	304.4	52.8	122.3	7.1	909.0	27.1	238.3	40.8	157.9	19.1	337.4
106	119.3	247.5	43.2	121.5	5.9	884.4	25.2	208.3	35.6	147.4	17.1	306.0
107	209.1	436.8	62.0	130.3	8.3	976.6	30.9	261.3	46.4	174.0	22.8	355.0
108	170.0	355.1	50.8	129.4	6.9	950.2	28.8	228.5	40.4	162.4	20.4	322.0
109	136.1	284.3	40.9	128.5	5.7	922.6	26.6	197.8	34.9	150.8	18.1	290.0
110	107.1	223.6	32.4	127.6	4.6	893.7	24.4	169.4	29.7	139.2	16.0	259.0
111	206.2	434.8	49.4	137.8	6.8	996.4	30.6	222.5	39.9	170.3	22.2	306.6
112	162.2	342.0	39.1	136.7	5.5	965.1	28.1	190.6	34.0	157.2	19.5	273.9
113	124.9	263.4	30.4	135.6	4.4	932.3	25.6	161.2	28.6	144.1	17.0	242.3
114	129.0	265.3	55.0	121.3	7.3	917.0	26.8	248.6	43.1	154.7	19.3	346.2
115	183.7	380.2	64.7	129.1	8.5	985.2	30.7	272.5	49.1	170.3	22.9	364.2
116	151.3	313.3	53.6	128.3	7.2	960.2	28.7	240.3	43.1	159.6	20.7	332.4

3.5. Concluding Remarks

The equations governing the plasma power balance have been derived and the effects of temperature on the power requirements determined. An optimum operating temperature of 30 [keV] has been chosen based on the effects of plasma gain. A design space exists where plasmas close to ignition have been found.

The required auxiliary heating calculated in this study assumes no impurity ions are present in the plasma, which invariably will not be the case. Additionally, assuming unity for the fraction of current drive power remaining in the plasma is overly optimistic. It is apparent that confinement scaling on the order of Mirnov or ASDEX scaling is desired; however, this question will only be answered by experimentation and careful data analysis.

4. REACTOR POWER BALANCE

The reactor power balance will be considered in this chapter as it pertains to losses in the poloidal and toroidal field coils and the current drive system. Due to the necessity to maintain high plasma densities and large plasma currents, a considerable amount of power is required by the current drive and the toroidal and poloidal field coils. It is necessary to determine the losses in these systems in order to evaluate the power and coolant requirements for these systems.

The magnet systems for the D-D Spherical Torus Hybrid Breeder are first considered to be normal resistive copper coils with water coolant. A packing fraction of 90% is assumed for both poloidal and toroidal field coils. Figure 4-1 illustrates the basic design and positions of the toroidal and poloidal field coils. An important issue in this analysis is whether the coil losses can be kept low enough to be economically and technologically feasible.

This chapter is divided into analyses of the major systems: toroidal field (TF) coils, poloidal field (PF) coils, and current drive. Superconducting poloidal and poloidal/toroidal options are then considered as well.

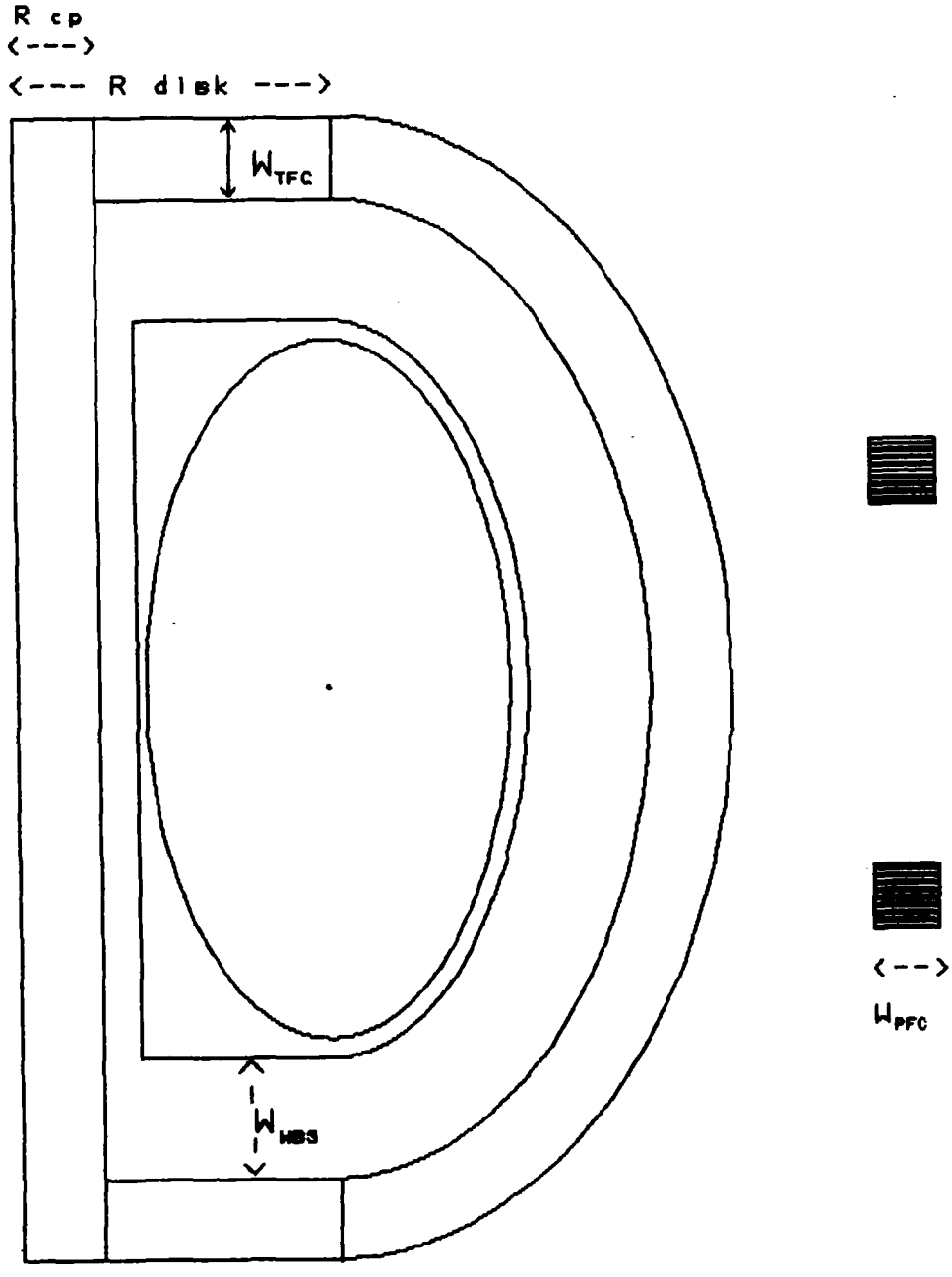

Figure 4-1: Magnet system design cross section.

An analysis of results and conclusions about the TF and PF systems closes the chapter.

4.1. Toroidal Field Coils

In this design the center conductor post carries the entire current, I_o, required to produce the toroidal magnetic field. In each toroidal field coil (TFC) return leg, a power supply drives the necessary current given by I_o/N; this total current meets at the center conductor post which carries the total current which is then again distributed to each TFC return leg as I_o/N. The endplate conductors allow for more contact area at the endplate-to-TFC-return-leg junction by virtue of the larger circumference. This in turn allows a larger number of TFC return legs, N, and reduced cost of the TFC return leg conductors, since additional machining of the return legs (ie. flaring the ends) is not required. An additional advantage of increasing N is increased plasma stability due to minimized toroidal ripple.

For the toroidal geometry, it is known that:

$$B_T = \frac{\mu_o I_o}{2\pi R}$$

and therefore:

$$I_o = \frac{2\pi R B_T}{\mu_o} \qquad [4.1.1]$$

In order to determine the viability of normal coils, an analysis of the resistive losses in the TFC return legs is now undertaken. The resistance of each return leg, R_o^{TFC}, is given by:

$$R_o^{TFC} = \frac{\rho_{Cu} l_{TFC}}{A_{TFC}} \qquad [4.1.2]$$

with ρ_{Cu} being the resistivity of copper; the length of the TFC return leg being:

$$l_{TFC} = \pi \left[\frac{a_1^2 + b_1^2}{2}\right]^{\frac{1}{2}} \qquad [4.1.3]$$

where

$$a_1 = Ka + 0.1a + W_{MBS} + W_{TFC} \qquad [4.1.4]$$

and

$$b_1 = a + 0.1a + W_{MBS} + W_{TFC} \qquad [4.1.5]$$

and

$$A_{TFC} = W_{TFC}^2 \qquad [4.1.6]$$

with W_{MBS} and W_{TFC} being the thickness of the outer

first wall, blanket, and shield, and the thickness of the toroidal field coils, respectively.

Since each TFC return leg carries I_o/N, the resistive losses in each leg are given by:

$$P_Q^{TFC}(\text{one leg}) = (\frac{I_o}{N})^2 R_Q^{TFC} \qquad [4.1.7]$$

for a total loss in N legs of:

$$P_Q^{TFC} = \frac{I_o^2}{N} R_Q^{TFC} \qquad [4.1.8]$$

For resistive losses in the end plates which have the same half thickness as the TFC return legs, the incremental conductor carries a current of I and has a resistance of R_Q^{DISK}, yielding a resistive loss of $I^2R_Q^{DISK}$ which, when integrated over the entire end plate conductor yields:

$$P_Q^{PLATE} = \frac{I_o^2 \rho_{CU}}{2\pi W_{TFC}} (\ln R_{DISK} - \ln R_{CP}) \qquad [4.1.9]$$

where R_{CP} is the radius of the center post and R_{DISK} is the radius of the disk:

$$R_{DISK} = \frac{N * W_{TFC}}{2\pi} \qquad [4.1.10]$$

Since there are two plates, the total resistive losses

are given by:

$$P_{\Omega}^{PLATES} = \frac{I_o^2 \rho_{Cu}}{\pi W_{TFC}} (\ln R - \ln R_c) \qquad [4.1.11]$$

In the analysis of the center conductor post, the maximum allowable center post radius was determined by the geometry of the plasma. Specifically:

$$R = R_{CP} + W_{ws}' + 1.1a \qquad [4.1.12]$$

where W_{ws}' is the thickness of the inner first wall and shield. For a given value of the major and minor radii from the plasma parameters, R_{CP} can be calculated easily.

Peng [6] presents an expression for R_{CP} that is based on the center conductor post current density, J_c, and required B_T:

$$R_{CP} = r_c + [r_c^2 + 2(a + 0.1a + W_{ws})r_c]^{0.5} \qquad [4.1.13]$$

where,

$$r_c \equiv \frac{B_T}{\mu_o J_c} \qquad [4.1.14]$$

Note that here Peng's expression for R_{CP} was modified to conform to the geometry of our design which proposes an inboard shield, W_{ws}'.

The physical radius of the center conductor post,

R_{CP}, is related to the current-carrying radius by:

$$R_{CP} = \frac{R_{CP}^{\circ}}{F_P} \qquad [4.1.15]$$

where F_P is the packing fraction, and R_{CP}° is the required center post radius in the absence of coolant channels. The value of R_{CP}° is used to evaluate the center conductor post current, J_c as follows:

$$J_c = \frac{I_o}{\pi (R^{o}_{CP})^2} \qquad [4.1.16]$$

In this analysis, the maximum physically allowable value of R_{CP} is chosen and compared with a computation of R_{CP} based on Peng's equations. For all cases, the chosen value for R_{CP} was greater than that given by Peng, which is taken as a required minimum.

The resistive losses in the center conductor are easily determined by computing the resistance of the post:

$$R_{\Omega}^{CP} = \frac{\rho_{Cu} Z}{\pi (R_{CP}^{\circ})^2} \qquad [4.1.17]$$

and,

$$Z \equiv 2(K + 0.1)a + 2W_{MBB} + 2W_{TFC} \qquad [4.1.18]$$

Then:

$$P_{\Omega}^{CP} = \frac{I_{\Omega}^2 \rho_{Cu} Z}{\pi (R^{o}_{CP})^2} = I_{\Omega} J_c \rho_{Cu} Z \qquad [4.1.19]$$

4.2. Poloidal Field (PF) Components

The role of the poloidal field coils (PFC) is to provide the necessary vertical field to maintain the plasma equilibrium. Therefore, the force on the plasma from the field created by the PFC must balance the force created by the plasma current. The poloidal field, B_p, will scale directly with the plasma current, I_p. An analysis of the position and the field required based on MHD equilibrium [7] indicates that coils placed at a distance three times the minor radius from the plasma and a distance equal to the minor radius from the midplane will provide the required force balance. The current required in each coil is:

$$I_{PFC} = 0.3\ I_p \qquad [4.2.1]$$

Again, in order to determine the viability of normal coils, the resistive losses for the coils are calculated from the relation:

$$P_{\Omega}^{PFC} = I_{TFC}^2 R_{\Omega}^{PFC} = \frac{I_{PFC}^2 \rho_{Cu} l_{PFC}}{A_{PFC}} \qquad [4.2.2]$$

where P_{Ω}^{PFC} is the ohmic (resistive) losses, I_{PFC} is the current through the coil, R_{Ω}^{PFC} is the resistance of the coil, ρ_{Cu} is the resistivity of the coil material, l_{PFC} is the length of the coil ($l_{PFC} = 6\pi a$), and A_{PFC} is the coil cross sectional area.

4.3. Current Drive

A major part of the overall reactor power balance is the power required to drive the plasma current. In this study we will use an oscillating field current drive (OFCD OR F-Θ pumping) for current maintenance at steady state, and another non-inductive system, i.e. neutral beam injection, will be used for ramp-up. The concept of oscillating field current drive is currently being applied to the reverse-field pinch (RFP) and spheromak configurations [10]. Use of OFCD in tokamaks has been proposed and efficiencies similar to those in the RFP are expected for the spherical torus [19]. A high efficiency current drive system is important because of the high plasma currents characteristic of the spherical torus. An estimate will be made of the power drawn for the reactor regime of interest in this study.

Oscillating field current drive works by imposing an appropriately phased oscillating field upon the static fields of both the toroidal and poloidal systems. Most of the apparent power in this current drive system is reactive power and the amount of real power consumed is a complex function of the materials between the magnets and plasma, the power supply details, and the plasma currents. A rigorous estimation of this real power would require a fairly complete conceptual design for each configuration considered and is beyond the scope of this study.

The reactive power in the system is the power that is generated by oscillating the poloidal and toroidal fields. This reactive power can be estimated by [18]:

$$P_{REACTIVE} = V_{ETRL} \left(\frac{\omega\delta}{\mu_o}\right) [B_{to}^4 + B_{po}^4]^{0.5} \qquad [4.3.1]$$

where V_{ETRL} is the volume over which this energy is distributed and may be approximated by that volume enclosed by the TFC return legs, B_{to} and B_{po} are the toroidal and poloidal fields on axis, μ_o is the permeability of free space, ω is the frequency of oscillation, and δ is the ratio of static to oscillating fluxes.

The volume over which this energy is distributed, V_{ETRL}, may seem to underestimate the energy required to oscillate the poloidal field, however, this model significantly overstates the power required to oscillate the toroidal field which has been assumed to be the paramagnetic field on axis but actually has a 1/r dependence in the blanket and shield. It is hoped that these two estimations tend to offset each other.

There are limits on the frequency of oscillation, ω, first, so that the plasma appears as a perfect conductor, i.e. $\omega \gg \tau_R^{-1}$, where τ_R is the characteristic decay time of the toroidal plasma current; and, second, to allow for penetration of the oscillating magnetic field into the plasma interior, $\omega \leq \tau_T^{-1}$, where τ_T is the tearing time. To minimize the static to oscillating flux ratio, δ, and therefore the adverse effects on particle confinement, it is desirable to set ω at it's upper limit, $\omega \approx \tau_T^{-1}$. The usual expression for the tearing time, τ_T, is

$$\tau_T = \tau_R^{0.6} * \tau_A^{0.4} \qquad [4.3.2]$$

where τ_A is the alfven time,

$$\tau_A = (\mu_o \beta)^{0.5} / B_t \qquad [4.3.3]$$

and ρ is the mass density of the plasma. Now we can express the ratio of static to oscillating fluxes as:

$$\delta^2 = \omega^{-1}\gamma_R^{-1} = \frac{\gamma_I}{\gamma_R} \qquad [4.3.4].$$

An idea of the relative magnitudes of power for each configuration can be obtained by assuming that the real power is some constant fraction of the reactive power for each device. This should provide a reasonable basis for comparison because we are comparing devices with generally the same configuration. There is no justification for choosing a specific fraction without detailed studies or empirical data, however, a fraction of real to reactive power, f_{CD}, of 0.15 to 0.25 seems reasonable and yields total powers somewhat smaller than those typical for RF current drive systems currently being studied.

The current drive power can now be estimated by:

$$P_{CD} \approx f_{CD}\, V_{ETRL}\, \left(\frac{\omega\delta}{\mu_o}\right)[B_{to}^4+B_{po}^4]^{0.5} \qquad [4.3.5].$$

This yields current drive efficiencies of about 0.25 [A/W] for typical A=3 devices with frequencies of 2 Hz and $\delta \approx 1.3\%$. At low aspect ratios the current drive

efficiency improves to about 1 [A/W] due to the lower stored energy in the toroidal field, w and δ are also reduced at lower aspect ratios.

4.4. Superconducting Options

If the losses in the normal resistive coils are too great, superconducting coils will have to be considered. Based on the neutronics analysis conducted, superconducting poloidal field coils should be able to be employed without additional shielding.

To use superconducting magnets for the toroidal field coils, additional shielding will be required on the inboard side of the plasma and the outboard shield must be modified. Neutronics analysis indicates that approximately 50 [cm] of 90 vol% tungsten, 10 vol% heavy water will provide the necessary attenuation for the designs of interest in this study.

4.5. Analysis of Results

Parameters for the normal coils, as previously discussed, and results from the analysis of the normal coil losses are given by component in Table 4-1. Losses for the poloidal field coils range from about

500 [MW] to over 1200 [MW] for the design space under consideration. The toroidal field coil losses for the same design space vary from 3000 [MW] to over 14000 [MW] with most of the loss being in the center post. This results in total losses ranging from 3700 [MW] to 15000 [MW], which yields fissile fuel cost of more than an order of magnitude greater than present costs.

Based on these results, superconducting coils will be used for both the toroidal and poloidal field coils. The cost analysis has been modified to account for superconducting coils; however, the shield design must be modified as previously indicated.

The current drive powers shown in the table seem very reasonable, ranging from less than 15 [MW] to just under 40 [MW] for the cases under consideration. This gives efficiencies of up to 5 [A/W], which, if obtainable, will greatly reduce the cost of operating the reactor.

Table 4-1: Reactor Power Balance Results

Magnet System

#	R disk [m]	W tfc [m]	W pfc [m]	P tfc [MW]	P pfc [MW]	P cd [MW]	P total [MW]	Z coil [m]	P cp [MW]
101	3.6	1.0	1.0	13100	838	37.2	13940	17.6	10480
102	3.4	1.0	1.0	10860	681	36.4	11540	16.7	8690
103	3.1	1.0	1.0	8878	545	35.6	9424	15.9	7117
104	3.9	1.0	1.0	13480	877	32.7	14360	18.4	10770
105	3.6	1.0	1.0	11300	722	32.1	12020	17.6	9032
106	3.4	1.0	1.0	9360	587	31.4	9947	16.7	7493
107	3.5	1.0	1.0	11750	988	31.6	12740	18.3	9394
108	3.2	1.0	1.0	9730	803	30.9	10530	17.4	7787
109	3.0	1.0	1.0	7951	643	30.2	8594	16.5	6373
110	2.9	1.0	1.0	6395	506	29.5	6901	15.6	5139
111	2.9	1.0	1.0	8272	899	29.8	9171	17.2	6631
112	2.9	1.0	1.0	6645	707	29.1	7352	16.2	5342
113	2.9	1.0	1.0	5245	545	28.4	5790	15.3	4230
114	3.9	1.0	1.0	11490	747	27.9	12240	18.4	9174
115	3.7	1.0	1.0	11960	1022	27.5	12980	19.2	9548
116	3.5	1.0	1.0	10010	842	26.9	10860	18.3	8004
117	3.2	1.0	1.0	8290	684	26.3	8975	17.4	6635
118	3.0	1.0	1.0	8635	957	26.0	9592	18.1	6910
119	2.9	1.0	1.0	7048	766	25.4	7814	17.2	5650
120	2.9	1.0	1.0	5662	603	24.8	6264	16.2	4551
121	2.9	1.0	1.0	5896	866	24.4	6761	16.9	4742
122	2.9	1.0	1.0	4650	667	23.8	5317	15.9	3750
123	3.7	1.0	1.0	10050	859	23.1	10910	19.2	8023
124	3.5	1.0	1.0	10480	1201	22.8	11680	20.0	8368
125	3.3	1.0	1.0	8771	989	22.3	9760	19.1	7010
126	3.0	1.0	1.0	7256	804	21.8	8060	18.1	5806
127	2.9	1.0	1.0	5922	644	21.3	6566	17.2	4747
128	2.9	1.0	1.0	6172	925	21.0	7097	17.9	4951
129	2.9	1.0	1.0	4954	727	20.5	5681	16.9	3984
130	2.9	1.0	1.0	4076	831	19.8	4907	16.6	3288
131	2.9	1.0	1.0	3146	624	19.2	3770	15.6	2544

4.6. Conclusions

The reactor power balance for normal resistive copper coils has been examined. A current drive system based on oscillating poloidal and toroidal fields has been presented. Based on excessive resistive losses for the normal coils, a superconducting magnet system has been adopted.

Many issues remain to be resolved in the use of superconducting coils. These include refrigeration, placement, and fabrication, and are beyond the scope of this study. Issues with the oscillating field current drive system, such as efficiency and stability, are currently being addressed and do not bear further mention.

5. IMPURITY CONTROL

The impurity control system in the fusion reactor must be designed to accomplish the following tasks: reduce the impurity concentration in the plasma; decrease the particle flux on the first wall to reduce first wall sputtering, and; remove the alpha particle and hydrogen exhaust from the plasma during operation. The following goals are also desired: reduce heat load on the limiter or divertor plates to a manageable level; develop a vacuum system that is simple in design and minimizes radiation streaming; minimize the possibility of limiter damage due to plasma perturbation and disruptions; and design limiter or divertor plates with an operational lifetime of at least one year.

A limiter option and a divertor option will be qualitatively considered in this chapter. Both systems are currently being examined for the spherical torus in conjunction with other studies. Therefore, a detailed analysis will not be conducted here.

5.1. Limiter

A toroidal belt limiter centered on the midplane of the outboard wall/blanket/shield was chosen for this

option. The limiter is constructed in removable modules and extends around the entire torus. The midplane position was chosen because it has been shown [20] to be the least likely place for a thermal dump from plasma disruption and it helps maintain the symmetry of the plasma system. A plenum is located in the blanket behind the limiter to increase the buildup of helium and impurities. This "plenum" region is a chamber (.4[m] by 1.2[m]) extending around the entire circumference of the outboard blanket. Twenty-four pumping vents are located at the top and bottom of the plenum chamber, staggered throughout the blanket to accomplish plenum pumping. The limiter and entrance to the plenum chamber are cooled with water. A detailed cross sectional view is shown in Figure 5-1. Construction materials and coolant schemes will be discussed in further detail in a later section.

The heat flux to the limiter is kept low by radiating 75% to 80% of the charged particle power. This is accomplished by injecting between .01% and .05% iodine into the plasma edge region. While a larger radiative fraction is possible, it is not desirable because of the excessive thermal stresses on the first wall and the decrease in the fusion power.

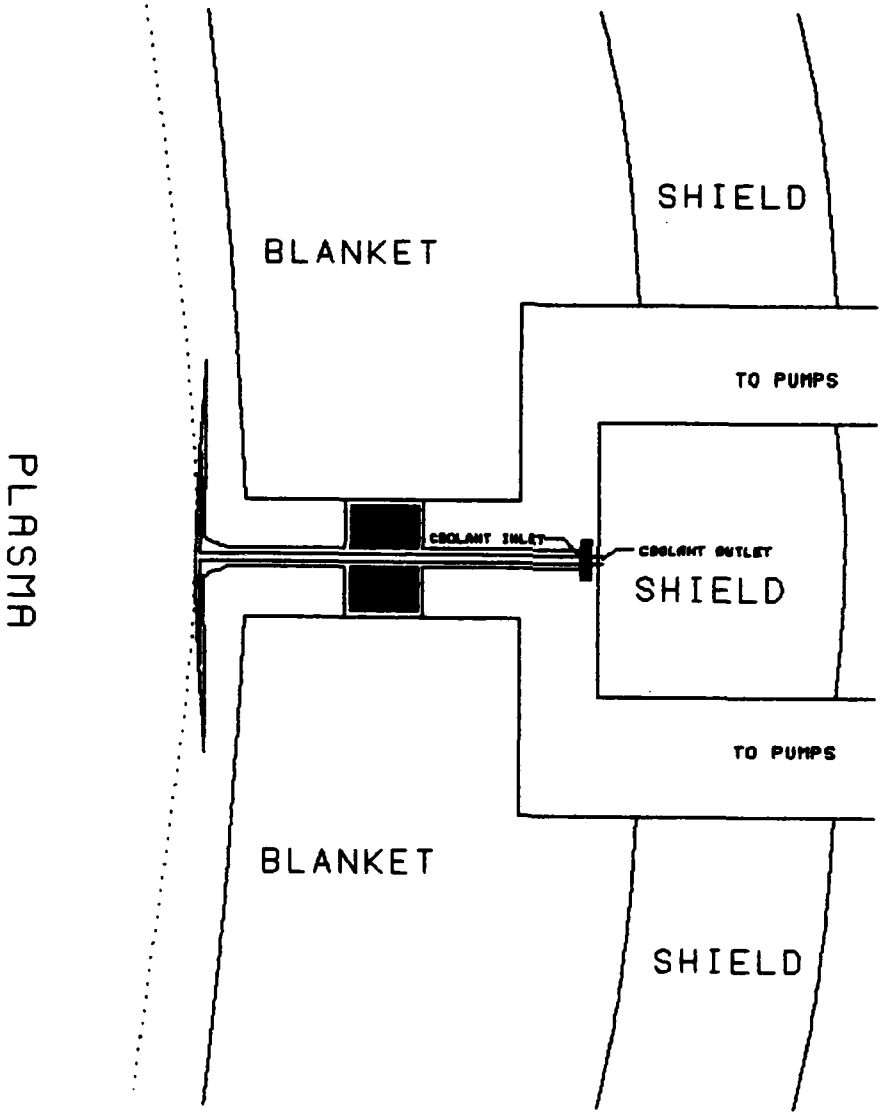

Figure 5-1: Detail of limiter system illustrating coolant flow, "plenum" region, and vacuum ducts.

The distance between the limiter wings and the first wall is designed such that 40% to 50% of the alpha particles reaching the limiter are reflected back into the plasma. The deuterium, tritium, and proton reflection is even greater than that for the alpha particles because charge-exchange of these particles competes with inversion (deionization). These two processes provide for a high helium pumping probability and enhanced deuterium and tritium recycling into the plasma.

5.1.1. Material Selection

Given the environment of a fusion reactor, especially the hostile environment seen by the limiter, construction materials for the limiter must have certain attributes. First, the limiter must have a high value of thermal conductivity to minimize the temperature change across the material and in turn to minimize the resultant thermal stress. Also, it must possess a high yield strength in order to withstand the inevitable thermal stresses, even at large levels of radiation damage. Good corrosion resistance properties are required to minimize internal material loss and to maintain a good coolant/wall boundary (i.e. reduce

degradation in heat transfer coefficients). Finally, the limiter must have a low cross section for activation to reduce maintenance difficulties and improve neutron economy in the blanket.
Since the limiter in a D-D system experiences large particle flux, it is necessary to have a low charge (Z) material on the limiter surface to reduce plasma radiative losses from sputtered impurities. For this case, beryllium was chosen due to its low Z and compatibility with potential structural materials.

Structural materials considered for the limiter and their properties are listed below in Table 5-1. HT-9 and PCA are common alloys of stainless steel.

Table 5-1: Candidate Structural Materials for the Limiter

MATERIAL	k [W/m²]	α [x10^{-6}K^{-1}]	E [MPa]	M.P. [°C]
Copper	393	17	110	1080
PCA	19.5	17.7	167	1400
HT-9	29	11.3	175	1420
VCrTi Alloy	24.2	9.6	120	1880

5.1.2. Design Issues

It is impossible to state with any certainty whether a limiter will provide the necessary exhaust and impurity removal without some experimental data and an extensive theoretical analysis. Additional analysis will be necessary to determine if any of the materials listed in Table 5-1 will be able to withstand the high particle fluxes for a reasonable period of time. Both of these analyses are beyond the scope of this project.

5.2. Divertor

A divertor impurity control system for the spherical torus is being explored as part of the Advanced Tokamak Reactor: Spherical Torus (ATR/ST) [19] study being conducted by Los Alamos National Laboratory. Data presented herein is based on two Tokamak Power Systems Studies Project Meetings, held May 15-16, 1985 (at Georgia Institute of Technology) and August 12-13, 1985 (at Massachusetts Institute of Technology).

Figures 5-2 and 5-3 show the location and design of the divertor system. The double-null poloidal-field divertor has the advantages of: vertical stability; reduced heat loads; a natural fit to the spherical

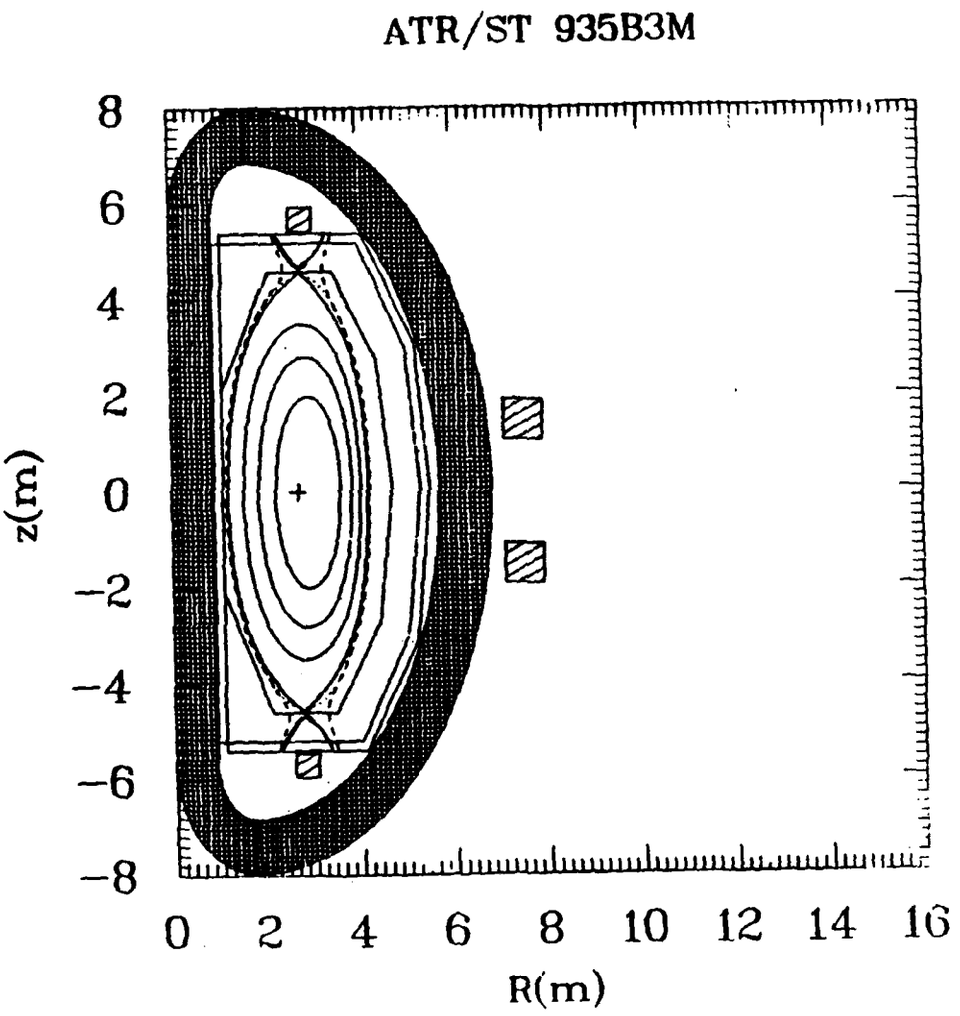

Figure 5-2: Overview of reactor illustrating divertor system.

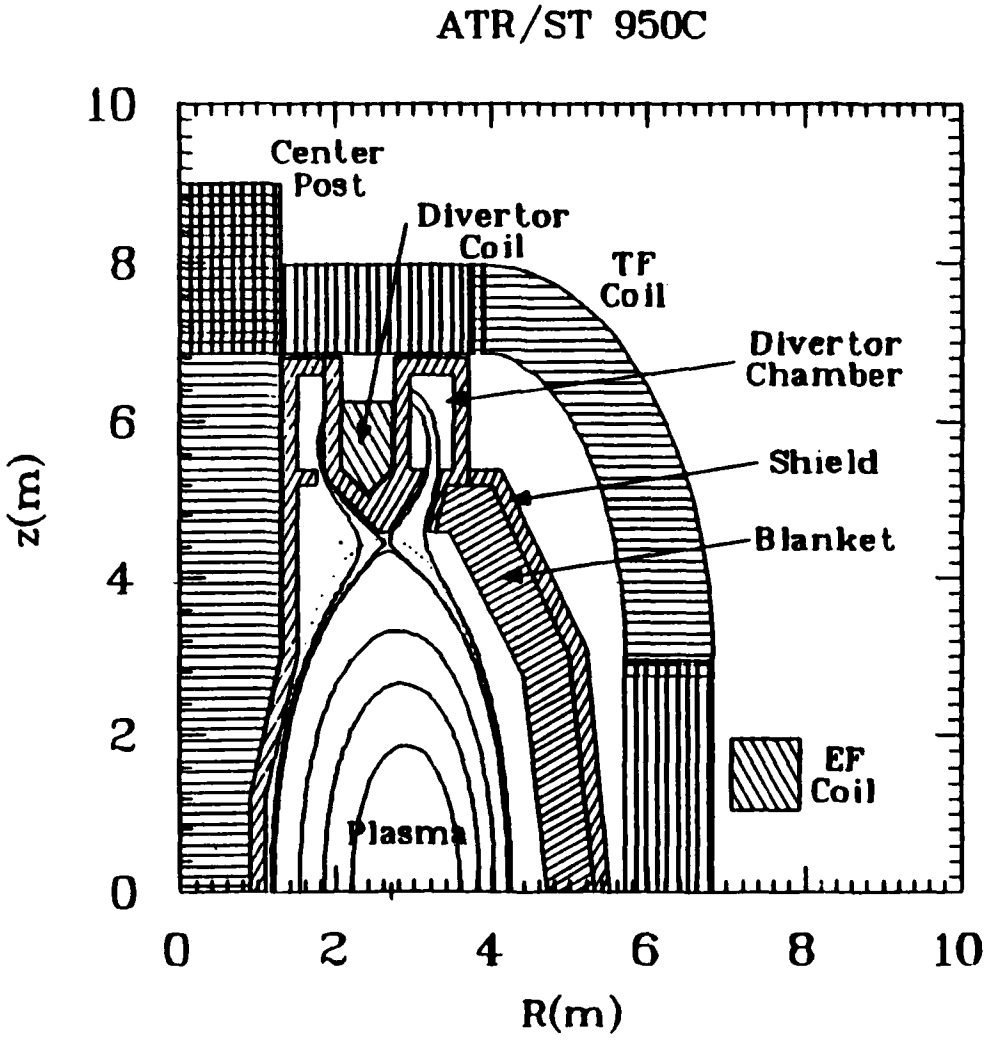

Figure 5-3: Cross section of poloidal divertor.

torus's elongated configuration; divertor coils inside the toroidal field coils, resulting in reduced divertor coil currents, better flux surface integrity, and more area for divertor channel; and reduced blanket impact. Table 5-2 lists the basic parameters for the divertor system. These are for a D-T system and will differ for the D-D system.

Table 5-2: Divertor Design Parameters

Scrapeoff thickness [m]	0.04
Radiation fraction, f_{RAD}	0.3
Particle confinement time, τ_p [s]	2.5 τ_E
Recycle coefficient	0.9
Divertor chamber area [m^2]	185
Transport power, P_{tr} [MW]	391
Plasma density [m^{-3}]	1.28
Divertor connection length [m]	21.7
Plasma surface area [m^2]	324.4
Diffusivity [m^2/s]	1
Edge-plasma density [$10^{18} m^{-3}$]	5-8
Edge-plasma temperature [keV]	1.0-0.4
Wall-plasma temperature [eV]	40-33
Average divertor heat flux [MW/m^2]	1.37
Divertor efficiency	0.997-0.999
Blanket loss	4%
First wall loss	9%

5.2.1. Design Issues

There are several issues which need to be addressed for the divertor option. The first is how the magnetics of the divertor will change the plasma shape and particle confinement. Second is what currents will be required and what will the associated losses be. Finally, will it be possible to develop a system to increase radiation in the divertor chamber. This is necessary to increase divertor plate lifetime and reduce stresses; however, the impurity concentration in the plasma must be kept low.

5.3. Conclusions

A divertor and a limiter impurity control system have been analyzed and the design issues associated with each have been presented. Sufficient information does not presently exist to choose one system over the other; further investigation and experimental data will be required before either option can be selected.

While the choice of an impurity control system will have effects on the overall system, the differences in effects created by choosing one over the other, assuming the same efficiency, should be minimal. Costs for the impurity control system are assumed to be

the same for either option, and are considered as such in the cost model. A 3% blanket volume reduction is considered in the neutronics analysis for the impurity control system.

6. FIRST WALL, BLANKET, SHIELD

Most recent hybrid breeder designs, including this design, favor the fission suppressed mode in which the neutrons are moderated and the fertile fuel is processed to remove the fissile isotopes before there is a sufficient build-up to present a large fission hazard. This mode of operation has the advantages of improved safety due to lower fission product afterheat and hazard, and a much higher net fissile output per installed thermal capacity [1]. Neutron multiplication is accomplished with non-fissioning multipliers such as beryllium or lead. However, this mode places a constraint on the design of the system because it requires a mobile blanket allowing the fissile material to be removed before the fission reaction rate becomes too high.

A simple first wall and blanket design, based on the Aqueous Self-Cooled Blanket [8] is proposed where the breeder material, in the form of a salt, is dissolved in heavy water, which acts as the coolant. This design minimizes the amount of structure, thereby reducing parasitic absorptions, and maximizes the breeder material present. This is possible because the neutron wall loading is less than 0.5 [MW/m^2] and

electricity production is not desired. Zircaloy has been chosen as the structural material because of its low neutron absorption and large database from use in fission reactors. This chapter details the designs and neutronics analyses of the first wall, blanket, and shield.

6.1. Design

The first wall is composed of thin zircaloy tubes with approximately 2 [mm] of beryllium coating on the plasma side to reduce erosion of the first wall. Cooling is accomplished by low pressure, low velocity (approximately 2 [ft³/min] at 1 atmosphere) breeder flowing through the tubes and into the moderator region. The breeding material is composed of heavy water, ^2H_2O (D_2O), with a small amount of uranium or thorium salt dissolved in it. Candidate salts and their solubilities in water are given in Table 6-1. Figure 6-1 illustrates a top view of the first wall and blanket.

Two blankets are used to provide fissile breeding. The first blanket (moderator) provides for neutron multiplication and moderation and is composed of 85 vol% beryllium, 5 vol% zircaloy, and 10 vol% breeder.

Table 6-1: Solubilities of Selected Uranium and Thorium Salts

SALT	SOLUBILITY [g/100cc]
UCl_4	260
UBr_4	> 250
$U(NO_3)_4$	∞
$ThCl_4$	> 250
$Th(NO_3)_4$	> 250

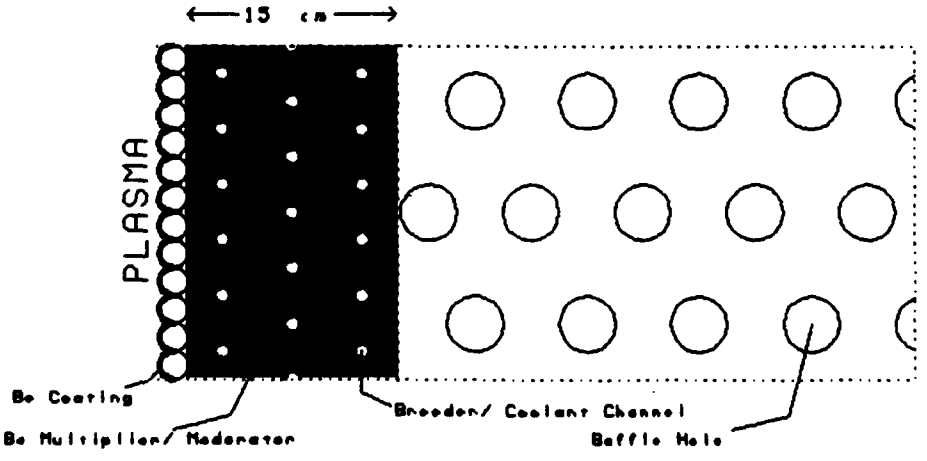

Figure 6-1: Top view of first wall and blanket.

The second blanket is a low velocity, low pressure "pool" of breeder with a 5 vol% zircaloy structure. Zircaloy baffle plates are employed horizontally in the blanket to prevent streaming and to maintain the flow of the breeder.

Three types of shielding are used in this reactor. Material composition for each shield is given in Table 6-2, with the locations being given in Figure 6-2. Shield material 3 is used to replace the inboard blanket and shield if the superconducting TF coil option is employed.

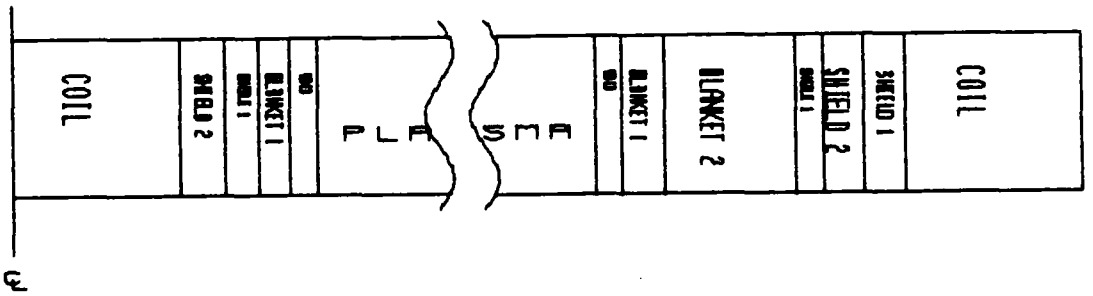

Figure 6-2: Blanket and shield positions.

Table 6-2: Candidate Shielding Materials

DESIGNATION	COMPOSITION	
Shield 1	Pb	90 vol%
	Fe^{1423}	5 vol%
	D_2O *	5 vol%
Shield 2	B_4C	85 vol%
	Fe^{1422}	10 vol%
	D_2O *	5 vol%
Shield 3	W	90 vol%
	D_2O *	10 vol%

* Breeder material may be substituted for D_2O if advantageous.

6.2. Neutronics

Neutronics analysis was accomplished using the one-dimensional transport code, ONEDANT [9]. Cross section data was compiled and grouped using TRANSX and the MATXS5 library [20]. The reactions of interest are given in Table 6-3. Cross sections were compiled and used for all materials present in the first wall, blanket, and shield as described in the previous section.

The reactor blanket and shield were initially modeled as a simple cylinder with the neutron source at the center, a small void, and then the blanket with a

Table 6-3: Breeding and Competing Reactions

Parasitic Reactions

$n + A^x \rightarrow A^{x+1} + \tau$

$n + A^x \rightarrow A^{x-1} + 2n$

$n + A^x \rightarrow B^{x-4} + \alpha$

$n + A^x \rightarrow B^{x-2} + {}^2H$

$n + A^x \rightarrow B^{x-1} + {}^1H$

$n + A^x \rightarrow B^{x-3} + {}^3H$

Uranium-Plutonium Cycle

$n + U^{238} \rightarrow U^{239} \rightarrow Np^{239} \rightarrow Pu^{239}$

$n + U^{238} \rightarrow U^{238} + \tau + n$

$n + U^{238} \rightarrow U^{237} + 2n$

$n + U^{238} \rightarrow FP + Xn + \tau$

Thorium-Uranium Cycle

$n + Th^{232} \rightarrow Th^{233} \rightarrow Pa^{233} \rightarrow U^{233}$

$n + Th^{232} \rightarrow Th^{232} + \tau + n$

$n + Th^{232} \rightarrow FP + Xn + \tau$

reflector outer boundary. After the optimum design space was found, a more detailed analysis was conducted in cylindrical geometry using the model shown in Figure 6-3. Table 6-4 illustrates the variation of fissile breeding, U^{238} (n,g) Pu^{239}, and fissioning, U^{238} (n,f) FP, with varying fertile material concentrations and varying moderator thicknesses. The variation of breeding and fissioning with moderator thickness is depicted graphically in Figure 6-4, while the variations with changes in U^{238} concentration are depicted in Figure 6-5. The reference design case was chosen as a 15 [cm] moderator and a 7 atom% U^{238}/D_2O breeding mixture, in both moderator and pool regions.

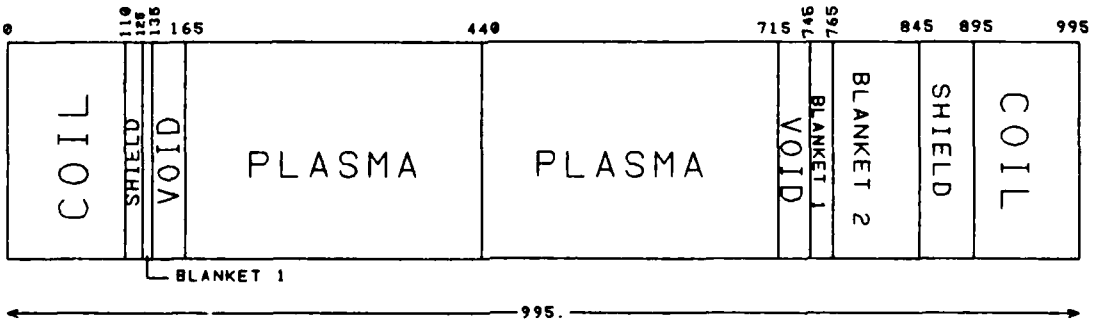

Figure 6-3: Model of reactor for neutronics analysis.

Table 6-4: Neutronics Analysis - Design Space Optimization

Region 1: 7% U238, Region 2: 15% U238

MODERATOR THICKNESS [cm]	(n,g) U-238 [#/fus n]	(n,f) U-238 [#/fus n]	n-heat (e-12) [W/fus n]
5.000	1.282	0.0535	2.724
10.000	1.354	0.0361	2.145
15.000	1.361	0.0237	1.843
20.000	1.326	0.0166	1.131
25.000	1.278	0.0124	1.616

15 [cm] Moderator: 7% U238

MAIN BLANKET CONC. U-238 [atm %]	(n,g) U-238 [#/fus n]	(n,f) U-238 [#/fus n]	n-heat (e-12) [W/fus n]
20.000	1.368	0.0287	1.977
15.000	1.361	0.0237	1.843
10.000	1.347	0.0182	1.701
7.000	1.331	0.0146	1.615
5.000	1.309	0.0121	1.564

Note: Breeding ratios assume 87% blanket coverage

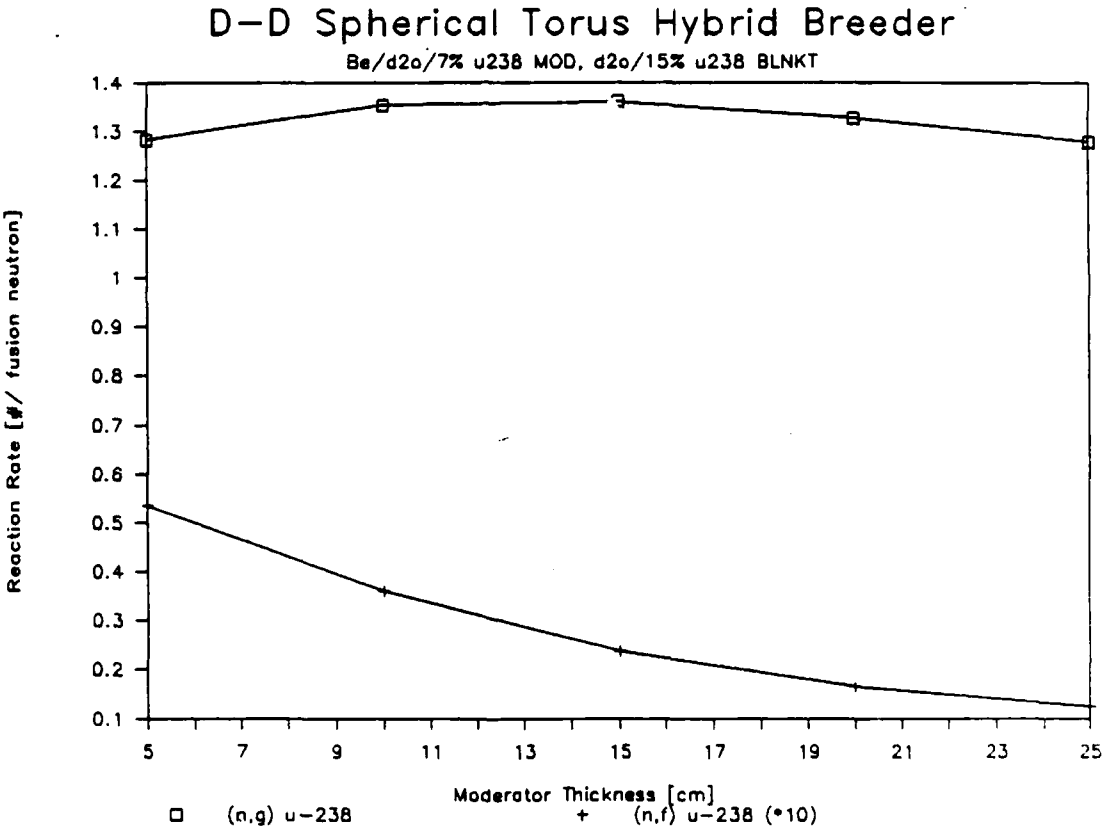

Figure 6-4: Fissile breeding and fissioning versus moderator thickness.

AD-A173 879 A FUSION BREEDER REACTOR BASED ON A CATALYZED D-D SPHERICAL TORUS(U) ARMY MILITARY PERSONNEL CENTER ALEXANDRIA VA K L WRISLEY 08 AUG 86 2/2

UNCLASSIFIED F/G 18/1 NL

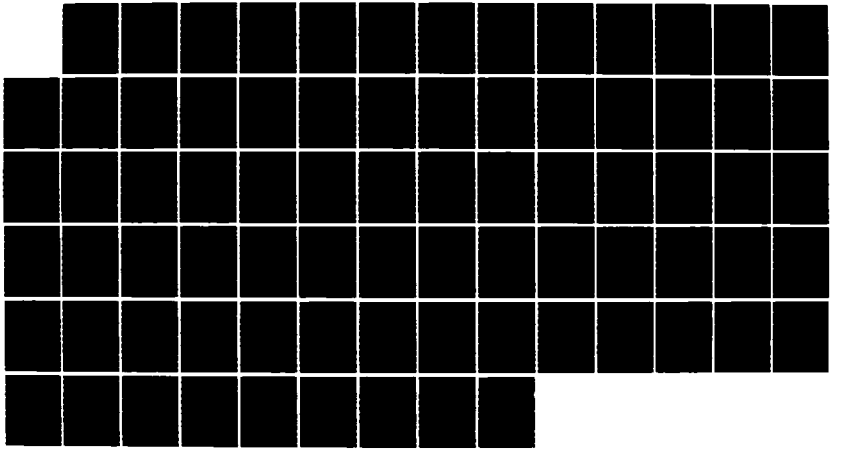

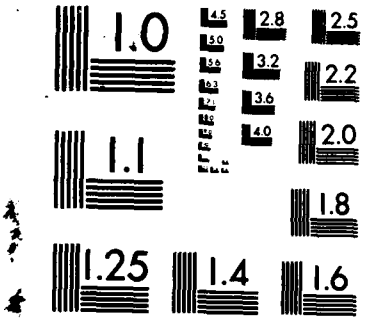

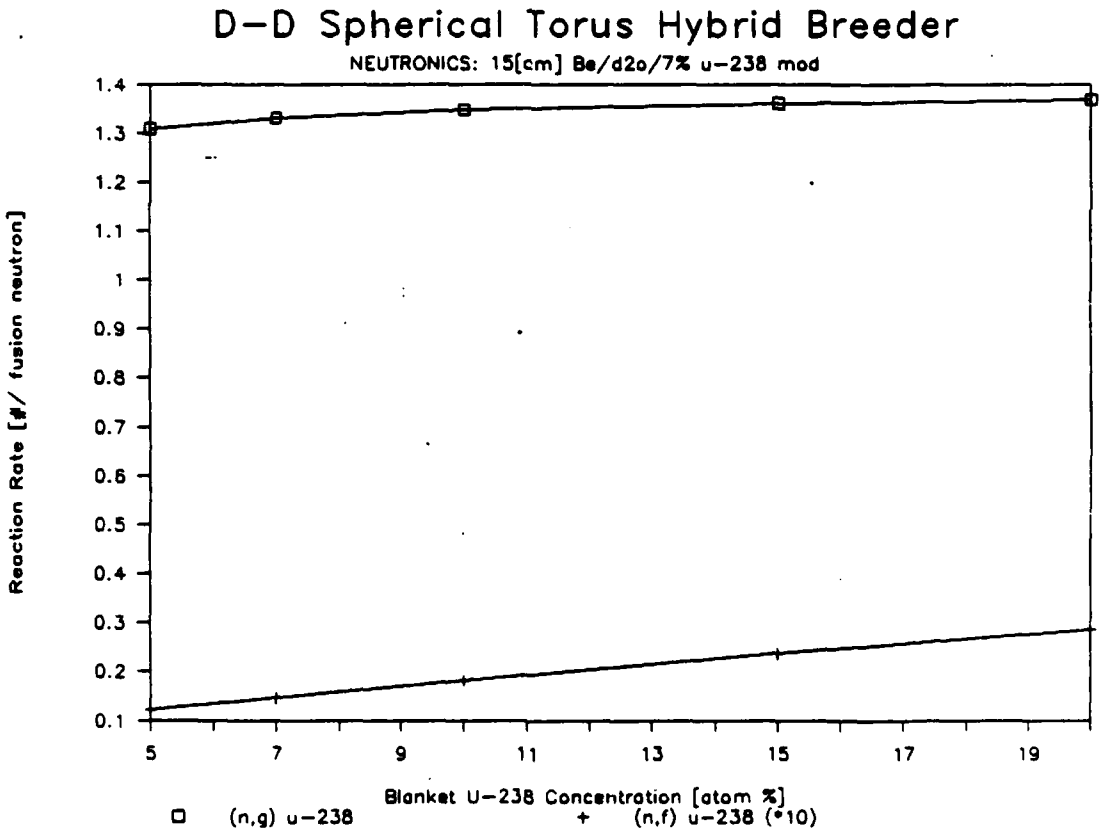

Figure 6-5: Fissile breeding and fissioning versus uranium concentration in second blanket.

6.3. Conclusions

A blanket design has been developed that provides good fissile breeding and a low fissioning rate. Steady state one-dimensional neutronics analysis was performed indicating a breeding ratio of 1.33 and a fissioning rate of 0.015 for 7% (atom) uranium 238 in heavy water. The fissioning rate listed is only for the U^{238} and additional fissioning will occur in the plutonium remaining in the breeder after processing. Additionally, the neutronics analysis indicates a biologically safe radiation level on the outside edge of the toroidal field coil during operation.

Stress analysis of the first wall and blanket remains to be done, as well as a dynamic neutronics analysis of the blanket considering fissile and fission product accumulation.

7. COST ANALYSIS

In order to evaluate the potential of the D-D Spherical Torus Hybrid Breeder, the selling cost of fissile material must be determined. The purpose of this chapter is to present the model used for making that determination. This will be divided into two major areas: the power flow model, which gives a cost of fuel based on the reactor cost; and the reactor costing model, which yields the total (direct and indirect) reactor cost. These are then combined to determine the cost of fissile fuel and the viability of this design.

7.1. Power Flow

In analyzing the economics of the hybrid system, it is beneficial to describe the performance in terms of the power flow model as shown in Figure 7-1. The notation used is given in Table 7-1.

The total thermal power in the hybrid can be expressed as:

$$P_T = P_{IN} + (1 - f_n)P_F + f_n M P_F \qquad [7.1.1]$$

and the fusion energy released in the production of a

Table 7-1: Definition of Economics and Power Flow Terms

P_T	Hybrid total thermal power
P_{IN}	Power supplied to drive the fusion reactor
η_P	Efficiency of current drive and auxiliary power systems,
P_P	Power going into the plasma
Q	Power amplification factor, $Q = P_F/\eta_P P_{IN}$
f_n	Fraction of fusion power removed by neutrons
M	Blanket energy multiplication
F	Fissile fuel production rate [fissile atoms/fusion neutron]
C	Conversion ratio
α	Capture to fission ratio
P_{fiss}	Power produced by fission reactors
E_{fiss}	Energy released per fission
E_{fus}	Energy released per fusion reaction
P_F	Fusion power
N	Number of fission reactors that can be supported by hybrid reactor of same thermal power
R_{el}	Ratio of total electric capacity to fusion power
η_e	Electrical conversion efficiency of fission reactors
η_H	Electrical conversion efficiency of fusion reactor
COF	Cost of fissile fuel, $\$/g_{fissile}$

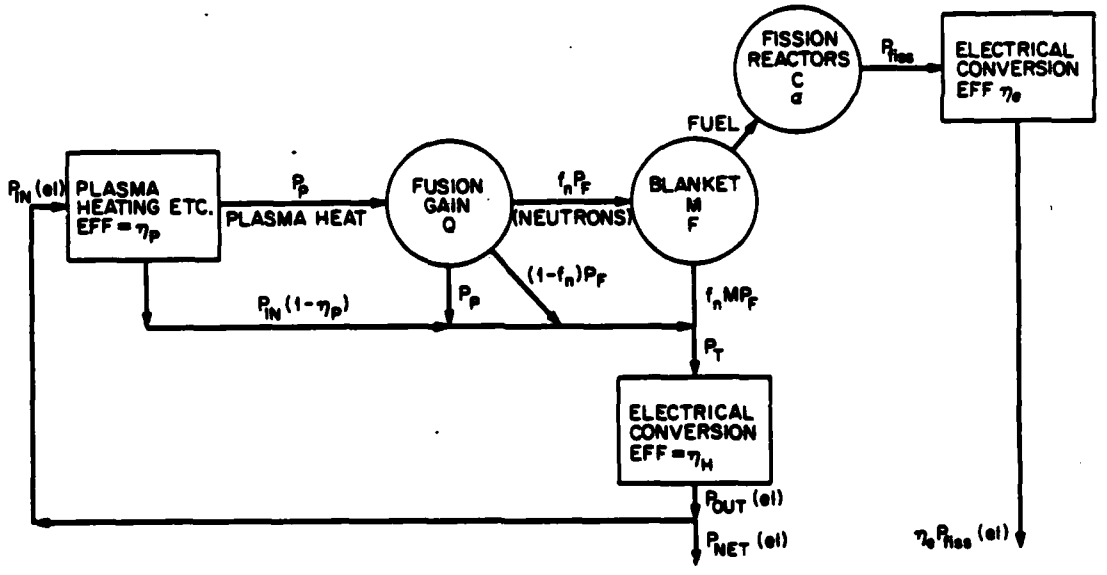

Figure 7-1: Diagram of the power flow for a hybrid (fission-fusion) device producing the makeup required for a number of fission reactors. The notation is explained in Table 7-1 and in the text.

fissile atom is E_{fus}/F.

Fissile atoms produced in the blanket are burned in fission reactors with the energy released per fissile atom produced being:

$$E_{fiss}/(1-C)(1+\alpha).$$

If it is assumed that all of the fissile material produced in the hybrid is consumed in the fission reactors, the ratio of fission to fusion power is:

$$\frac{P_{fiss}}{P_{fus}} = \frac{E_{fiss}}{E_{fus}} \times \frac{F}{(1-C)(1+\alpha)} \qquad [7.1.2]$$

From equations 7.1.1 and 7.1.2, N, the number of fission reactors that can be supported by a hybrid of the same thermal power is obtained:

$$N = \frac{P_{fiss}}{P_T} = \frac{E_{fiss}}{E_{fus}} \times \frac{F}{[(1/\eta_p Q)+1+f_n(M-1)]} \times \frac{1}{(1-C)(1+\alpha)} \qquad [7.1.3]$$

Finally, the ratio, R_{el}, of the total electrical capacity of the system to the fusion thermal power is given by :

$$R_{el} = (P_T\eta_H - P_{IN} + \eta_e P_{fiss})/P_T \qquad [7.1.4]$$

where η_e is the electrical efficiency of the fission reactors. To best realize the potential advantages of

the hybrid breeder, the support ratio, N, the ratio of total electric capacity to fusion power, R_{el}, and the hybrid conversion efficiency, η_H, need to be maximized.

7.2. Reactor Costing

Costing of the reactor was performed using accounts and data from the current Reverse-Field Pinch (RFP)/TITAN [10] reactor study modified to reflect no electrical generation and appropriate special materials. The costing by account is given in Table 7-2.

Because no electricity is being generated, there is no need for turbines and turbine related equipment. This leads to the elimination of accounts 21.3, 23, and 24. However, more power must be dissipated and, therefore, more (or larger) cooling towers are required. The special materials account is taken to be zero because water is used as the coolant and the cost of uranium salt is included in the fuel costs in determining "cost of fuel".

Table 7-2: Spherical Torus Hybrid Breeder Cost Analysis

ACCT #	ACCOUNT TITLE	(M$ 1980)
20.	Land and Land Rights	3.3
21.	Structures and Site Facilities	
21.1	Site Improvements and Facilities	11.15
21.2	Reactor Building	3e-4 Vrb +39.5
21.4	Cooling Structures	3.565 (P_{th}/1000)^0.3
21.5	Power Supply & Energy Storage	9.16
21.6	Miscellaneous Buildings	76.50
21.7	Ventilation Stack	1.81
21.98	Spare Parts (2 %)	
21.99	Contingency (15 %)	
22.	Reactor Plant Equipment	
22.1	Reactor Equipment	
22.1.1	Blanket and First Wall	0.047 Vbl
22.1.2	Shield	0.105 Vshld
22.1.3	Superconducting Magnets	0.584 Vc
21.1.5	Primary Structure and Support	0.1125 Vstr
21.1.6	Reactor Vacuum System	0.0051 Vvac
21.1.7	Power Supply	0.028 Pth + 1.00
21.1.8	Impurity Control System	14.3
21.1.9	Direct Energy Conversion	0.0
22.1.10	ECRH Breakdown System	2.82
22.2	Main Heat Transfer System	0.069 Pth
22.3	Auxiliary Cooling Systems	6.7e-4 Pth + 32.6
22.4	Radioactive Waste Treatment	1.2e-3 Pth
22.5	Fuel Handling and Storage	9.65e-3 Pth
22.6	Other Reactor Plant Equipment	0.011 Pth
22.7	Instrumentation and Control	23.41
22.98	Spare Parts (2 %)	
22.99	Contingency Allowance (15 %)	
24.	Electric Plant Equipment	45.40

Table 7-2: Spherical Torus Hybrid Breeder Cost Analysis (con't)

ACCT #	ACCOUNT TITLE	(M$ 1980)
25.	Miscellaneous Plant Equipment	
25.1	Transportation & Lifting Equip	15.68
25.2	Air & Water Service Systems	12.35
25.3	Communications Equipment	6.22
25.4	Furnishings & Fixtures	1.20
25.98	Spare Parts (3 %)	
25.99	Contingency Allowance (15 %)	
26.	Special Materials	0.0
90.	Total Direct Cost	
91.	Construction Facilities, Equip, Services	10%
92.	Engineering & Construction Management	8%
93.	Other Costs	5%
94.	Interest during Construction	10%/yr
95.	Escalation during Construction	5%/yr
99.	Total Cost	

7.3. Cost of Fuel

Based on the power flow described in the first section and the reactor cost obtained in the previous section, the cost of fissile fuel (COF) can be determined. The cost of fissile fuel is based on four accounts as given in Table 7-3: Return on Capital (ROC); Operations and Maintenance (O&M); Fuel; and Plant Capacity. The Operations and Maintenance account is further divided into three accounts: Operations, which accounts for day-to-day costs of operating and maintaining the plant; First Wall, Blanket, and Shield Replacement, which accounts for annual replacement of a portion of the first wall, blanket, and shield module; and Power, which accounts for the costs of electricity purchased from the line (because the reactor does not generate any electricity). The capacity is determined by taking the fissile fuel production rate multiplied by the plant availability, which is taken as 80%.

Table 7-3: Cost of Fuel Account Analysis

ACCOUNT TITLE	(M$ 1980)
Return on Capital (RoC) [M$/yr]	15% Acct. 99
Operations & Maintenance (O&M)	
Operations [M$/yr]	2% Acct. 99
First Wall Blanket Replacement	Acct 22.1.1/FWB$_{lifetime}$
Power [M$/yr]	Linecost x P$_{required}$
Fuel [M$/yr]	22.11e-6 F$_{fiss}$ * Availability
Capacity [kg/yr]	F$_{fiss}$ * Availability
Cost of Fissile Material (COF) [M$/kg]	RoC+O&M+Fuel/Capacity

7.4. Typical Results and Examples

The reactor costs and the costs leading to cost of fuel are given by account in Table 7-4. All values listed are in 1980 dollars; to convert to 1984 dollars, in order to compare with the fuel costs given by the Department of Energy [21], the 1980 dollars are multiplied by 1.21. Costs for Uranium 235 in 1984 ranged from 38 [$/gm] to almost 80 [$/gm]. Fuel costs (in 1984 dollars) from this reactor range from about 37 [$/gm] to almost 80 [$/gm]; however, extraction and processing costs have not been considered in the calculations for cost of fuel.

In analyzing the cost of fuel, it is seen that the costs come from two accounts: the return on capital; and the power component of operations and maintenance. Any changes in these two accounts will result in proportional changes in the cost of fissile fuel.

Table 7-4: Typical Results of Cost Analysis for the D-D Spherical Torus Hybrid Breeder

#	ACCT 20 [M$]	ACCT 21 [M$]	ACCT 22 [M$]	ACCT 24 [M$]	ACCT 25 [M$]	ACCT 90 [M$]	ACCT 91 [M$]	ACCT 92 [M$]	ACCT 93 [M$]
101	3.3	164.4	878.5	45.4	41.8	1134.6	113.5	90.8	56.7
102	3.3	163.9	767.6	45.4	41.8	1023.1	102.3	81.8	51.2
103	3.3	163.5	667.0	45.4	41.8	921.9	92.2	73.7	46.1
104	3.3	165.0	900.2	45.4	41.8	1157.0	115.7	92.6	57.9
105	3.3	164.4	793.8	45.4	41.8	1049.9	105.0	84.0	52.5
106	3.3	163.9	696.4	45.4	41.8	951.9	95.2	76.1	47.6
107	3.3	164.7	877.3	45.4	41.8	1133.7	113.4	90.7	56.7
108	3.3	164.1	765.3	45.4	41.8	1021.0	102.1	81.7	51.1
109	3.3	163.7	663.8	45.4	41.8	918.9	91.9	73.5	45.9
110	3.3	163.3	570.9	45.4	41.8	825.4	82.5	66.0	41.3
111	3.3	163.9	749.6	45.4	41.8	1004.9	100.5	80.4	50.2
112	3.3	163.4	638.5	45.4	41.8	893.3	89.3	71.5	44.7
113	3.3	163.0	539.9	45.4	41.8	794.2	79.4	63.5	39.7
114	3.3	165.0	813.0	45.4	41.8	1069.8	107.0	85.6	53.5
115	3.3	165.3	891.4	45.4	41.8	1148.6	114.9	91.9	57.4
116	3.3	164.7	785.1	45.4	41.8	1041.5	104.1	83.3	52.1

#	ACCT 94 [M$]	ACCT 95 [M$]	ACCT 99 [M$]	CAP RET [M$]	O&M [M$]	FUEL [M$]	Capacity [kg/yr]	COF [$/gm]
101	350.3	216.3	1962.1	294.3	125.2	0.18	7.96E+06	52.71
102	315.9	195.1	1769.3	265.4	120.2	0.15	6.47E+06	59.59
103	284.6	175.8	1594.3	239.1	115.6	0.12	5.18E+06	68.45
104	357.2	220.6	2000.9	300.1	125.1	0.17	7.21E+06	58.99
105	324.1	200.2	1815.6	272.4	121.5	0.14	5.94E+06	66.31
106	293.9	181.5	1646.1	246.9	118.3	0.11	4.83E+06	75.63
107	350.0	216.1	1960.6	294.1	117.3	0.19	8.42E+06	48.90
108	315.2	194.7	1765.8	264.9	112.4	0.16	6.84E+06	55.16
109	283.7	175.2	1589.2	238.4	107.9	0.13	5.48E+06	63.22
110	254.8	157.4	1427.5	214.1	105.4	0.10	4.31E+06	74.17
111	310.2	191.6	1737.9	260.7	110.4	0.19	8.24E+06	45.08
112	275.8	170.3	1544.8	231.7	105.5	0.15	6.48E+06	52.08
113	245.2	151.4	1373.4	206.0	101.0	0.12	4.99E+06	61.56
114	330.3	203.9	1850.0	277.5	128.9	0.12	5.25E+06	77.38
115	354.6	219.0	1986.3	298.0	120.9	0.17	7.45E+06	56.29
116	321.5	198.6	1801.1	270.2	117.7	0.14	6.14E+06	63.25

7.5. Conclusions

A cost model and analysis for the D-D Spherical Torus Hybrid breeder using superconducting coils has been presented. This model, based on RFPCR costing, indicates that fissile fuel can be produced at a cost close to or slightly higher than present-day costs. The cost of extraction and processing has not specifically been included in the model and will serve to increase the cost of fissile fuel.

8. RESULTS AND COMPARISON WITH PREVIOUS WORK

In this chapter, the results of this study will be examined and a comparison made with the previous designs presented in Chapter 1. The chapter is divided into two sections: presentation of results and comparison with previous work.

8.1. Presentation of Results

The computer code, listed in Appendix B, was used to do a parametric study of the potential design space for the D-D Spherical Torus Hybrid Breeder. The criteria and common parameters used for this design space study are given in Table 8-1. These values were chosen to meet the design objective of using a compact spherical torus reactor with a D-D fuel cycle, and to match the physics used from other studies, such as WILDCAT. The results of this design space study are given in Appendix A.

Table 8-1: Criteria and Common Parameters for Design Space Study

Particle Profile Factor, α_n	0.7
Temperature Profile Factor, α_T	0.7
D-shapeness, d	0.2
Alpha Removal Coefficient, R_α	0.5
He^3 Removal Coefficient, R_3	0.1
Proton Removal Coefficient, R_p	0.3
Number of TFC Return Legs, N_{TFC}	18
Packing Fraction, F_p	0.9
Current Drive Fraction, f_{CD}	0.2
Minimum Acceptable Power [MW]	700
Maximum Acceptable Current [MA]	71
Maximum Acceptable Fissile Fuel Cost [$/gm]	150
Plasma Temperature [keV]	
Maximum	35
Minimum	25
Magnetic Field on Axis, B_t [T]	
Maximum	7.5
Minimum	1.5
Major Radius, R [m]	
Maximum	8.5
Minimum	2.0
Aspect Ratio	
Maximum	2.3
Minimum	1.5

8.2. Comparison with Previous Designs

For comparison of the D-D Spherical Torus Hybrid Breeder with previous concepts, an optimum result from Appendix A will be used. The basic parameters for this design are given in Table 8-2. A comparison of this design with the Lawrence Livermore National Laboratory designs is given in Table 8-3.

Table 8-2: Basic Parameters for the Reference D-D Spherical Torus Hybrid Breeder

Major Radius, R [m]	6.0
Minor Radius, a [m]	2.9
Aspect Ratio, A	2.1
Toroidal Field on Axis, B_t [T]	6.5
Elongation, κ	1.9
Plasma Current, I_p [MA]	62
Fusion Power, P_{fus} [MW]	932
Thermal Power, $P_{thermal}$ [MW_t]	1146
Fissile Production, F [kg/yr] (@ 80%)	6478
Total Reactor Cost, Acct 99 [M$(1980)]	1544.8
Cost of Pu^{239} , COF [$/gm]	52.08
Neutron Wall Loading, P_{WL} [MW/m^2]	0.45
Neutron Production [$n/m^2/s$]	3.43×10^{17}

Table 8-3: Comparison of the D-D Spherical Torus Hybrid with Previous Designs

	Helium-Cooled Molten Salt Fusion Breeder [4]	Liquid-Metal-Cooled Fission-Suppressed Fusion Breeder [6]	D-D Spherical Torus Hybrid Breeder
P_{fusion} [MW]	3000	2600	932
$P_{electric}$ [MWe]	1380	1990	N/A
$P_{wall\ load}$ [MW/m^2]	2	1.7	0.45
Tritium Breeding Ratio, T [#/neutron]	1.0	1.06	N/A
Fissile Breeding Ratio, F [#/neutron]	0.6	0.84	1.34
Blanket Multiplication, M [E_{blnkt}/E_n]	1.6	2.4	1.23
Fissile Production [kg/yr] (@ 80% Capacity)	6380	6660	6478
Blanket Coolant	He	Li (liquid)	Heavy Water (breeder)
Structure	SS-316	SS-316	Zircaloy
Neutron Multiplier	Be Pebbles	Be Spheres	Be
Breeder	Molten Salt: LiF 70 mol%, BeF_2 12 mol%, ThF_4 18 mol%	Th (metal)	Aqueous: $UO_2(NO_3)_2$ 7 mol%, D_2O 93 mol%
Total Cost [M$] (Direct & Indirect)	4,867	6,300	1,545
Cost of Fuel [$/gm]	65.34	69.84	52.08

The obvious differences between this design and previous designs include: (1) the higher fissile breeding ratio, almost twice that of the other designs; (2) lower fusion power, a third of previous concepts; and (3) the much lower cost for this reactor design. This cost reduction is due to no electricity generation requirements, eliminating the need for turbine systems and generators, and also the reduced size of the plant.

Using the power flow model presented here, the cost of fuel for the two LLNL reactors was calculated and is also presented in Table 8-3. It should be noted that the costs for materials and fabrication of the breeder, except the uranium or thorium, and removal of the fissile material have not been included, but will be considerably higher for the LLNL designs.

9. CONCLUSIONS

A reactor design, designated the D-D Spherical Torus Hybrid Breeder, has been proposed that offers greater breeding at a lower cost than previous designs. This design uses a deuterium-deuterium fuel cycle to reduce neutron wall loading and to eliminate the need for tritium breeding. The reactor confinement scheme is based on the Spherical Torus compact reactor to increase neutron density and to reduce capital cost. Finally, the reactor uses a novel aqueous self-cooled blanket design which offers great advantage to the hybrid breeding blanket. In concluding this study, the advantages, disadvantages, and technological issues for each of the major systems will be summarized.

9.1. Catalyzed D-D Fuel Cycle

The fuel cycle employed in the D-D Spherical Torus Hybrid Breeder feeds deuterium into the plasma and recycles almost all of the tritium and about 90% of the helium-3 produced back into the plasma. This catalyzed mode of operation provides a higher fusion power and greater neutron production than does an uncatalyzed or semi-catalyzed D-D fuel cycle. The D-D fuel cycle

yields lower wall loading and also lower fusion power than a D-T cycle at the same particle density. This is a disadvantage for producing power, but an advantage for a system where all that is desired is a thermal neutron flux. The low neutron wall loading, less than 0.5 [MW/m²], allows the use of low absorption structural materials, namely zircaloy, rather than high strength materials such as stainless steel.

The D-D fuel cycle is not without its disadvantages. The plasma requires an order of magnitude better confinement, $\langle n\tau_E \rangle$, than the D-T cycle. It must also be operated at a higher plasma temperature, approximately 30 [keV], thus increasing surface erosion (sputtering) and the effects of impurities in the plasma. This necessitates increased particle removal and more efficient impurity control.

These disadvantages lead to the major issues concerning the use of the D-D fuel cycle. The first issue concerns the ability to confine a dense enough plasma, long enough and at the proper temperature for ignition to occur. This will probably involve initiating the reactor with a D-T fuel cycle, increasing the temperature by auxiliary means, and then decreasing and finally terminating the external tritium

fueling. This complex start-up cycle is going to require a high operating service availability (70%) to make the reactor economical.

The next issue is that of impurity control. This system must be able to accommodate a large particle flux and heat load, and keep impurity concentrations in the plasma to a very low level to minimize radiation losses. Another issue is whether the deuterium, tritium, and helium-3 in the exhaust are able to be efficiently separated from the hydrogen and helium-4 and recycled to the plasma.

The final issue is to be able to maintain the plasma temperature by auxiliary means. This must be accomplished without serious degradation of particle and energy confinement.

9.2. Spherical Torus Reactor Design

By using a compact high aspect ratio design, the capital cost of the reactor is reduced and, therefore, the cost of the fissile material is reduced. The technological issues associated with the reactor, however, are numerous. First, because the plasma current scales inversely with the aspect ratio, the compact reactor must have a means to maintain high

plasma current. Also, due to the small size, the current must be driven non-inductively, because there is no room for a solenoid in the center of the reactor. This means that a high efficiency current drive system, potentially the OFCD, must be developed. An issue with the OFCD is what effect the field oscillations will have on particle confinement.

The high power density and compact size of the spherical torus make design and placement of an impurity control system difficult. Because of the small surface area presented to the plasma, a limiter or divertor and the associated exhaust system can easily remove a large fraction of first wall area and blanket volume. This would be very detrimental to the production of fissile material.

9.3. Aqueous Self-Cooled Blanket

The aqueous self-cooled blanket (ASCB) used for a fissile breeder in a deuterium-deuterium fueled reactor seems to offer a large number of advantages and few, if any, disadvantages. The ASCB provides for simplified breeder material fabrication and reprocessing; a lower fissioning rate which yields greater fissile

production; and increased safety.

Technological issues associated with this ASCB design are two-fold. First is whether a 5 vol% zircaloy structure is sufficient to provide the necessary strength and support to the blanket. Second, can the fission-products and fissile material be almost totally removed during the online processing of the breeder/coolant.

In conclusion, the D-D Spherical Torus Hybrid Breeder offers the potential for a large, low-cost fissile material source. The associated technological issues may, however, hamper the realization of such a reactor as the need for alternate fissile material sources arises.

REFERENCES

1. M.J. Saltmarsh, et al., "An Optimization of the Fission-Fusion Hybrid Concept", Oak Ridge National Laboratory, ORNL/PPA-79/3 (1979).

2. R.W. Moir, et al., "Design of a Helium Cooled Molten Salt Breeder", Fusion Tech., 8, 465 (1985).

3. D.H. Berwald, et al., "Updated Reference Design of a Liquid-Metal-Cooled Tandem-Mirror Fusion Breeder", Fusion Tech. (1986) (in press).

4. K. Evans, et al., "WILDCAT: A Catalyzed D-D Tokamak Reactor", Argonne National Laboratory, ANL/FPP/TM-150 (1981).

5. "STARFIRE: A Commercial Tokamak Fusion Power Plant Study", ANL/FPP-80-1, Argonne National Laboratory, 1980.

6. Y-K. M. Peng, "Spherical Torus Compact Fusion at Low Field", Oak Ridge National Laboratory, ORNL/FEDC-84/7 (1984).

7. Y-K. M. Peng and D.J. Strickler, "Features of Spherical Torus Plasmas", ORNL/FEDC-85/6, Oak Ridge National Laboratory, 1985.

8. D. Steiner, et al., "A Self-Cooled Heavy Water Breeding Blanket", Proceedings of the 11th Symposium on Fusion Engineering, November 1985.

9. R.D. O'Dell, F.W. Brinkley, and D.R. Marr, "A Code Package for One-Dimensional, Diffusion-Accelerated Neutral-Particle Transport", Los Alamos National Laboratory, LA-9184-M, February 1982.

10. R.L. Hagenson, R.A. Krakowski, "Compact Reversed-Field Pinch Reactors (CRFPR): Sensitivity Study and Design-Point Determination", Los Alamos National Laboratory, LA-9389-MS, July 1982.

11. T.J. Dolan, Fusion Research, Pergamon Press, 1982.

12. N.A. Uckan, "Physics Basis for Trade-Off Studies", Oak Ridge National Laboratory, Jan. 1985 (unpublished).

13. C.S Chang and F.L. Hinton, "Effect of Finite Aspect Ratio on the Neo-Classical Ion Thermal Conductivity in the Banana Regime", Phys. Fluids, 25, (1493), 1982.

14. T. Ohkawa, "Energy Confinement Times of Tokamak Plasmas with Auxiliary Heating", Plasma Phys. and Contr. Fusion, 26, 1984.

15. C.E. Singer, "Semi-Empirical Transport in Tokamaks", Journal of Fusion Energy, 3, 1983.

16. W. Pfeiffer and R.E. Waltz, "Empirical Scaling Laws for Energy Confinement in Ohmically Heated Tokamaks", Nuclear Fusion, 19, 1976.

17. S.M. Kaye and R. J. Goldston, "Global Energy Confinement Sealing for Neutral-Beam-Heated Tokamak", PPPL-2157, 1984.

18. P.M. Bellan, "Physical Model of Current Drive by AC Helicity Injection", Journal of Applied Physics, 27(8), August 1984.

19. R.L. Miller, et al., "Advanced Tokamak Reactors Based on the Spherical Torus (ATR/ST)", Los Alamos National Laboratory, LA-10740-MS, June 1986.

20. R.E. MacFarlane, "TRANSX-CTR: A Code for Interfacing MATXS Cross-Section Libraries to Nuclear Transport Codes for Fusion Systems Analysis".

21. "Historical Plant Cost and Annual Production Expenses for Selected Electric Plants 1984", Department of Energy, DOE/EIA-0455(84), 1984.

A. Results of Design Space Analysis

This appendix lists the results of the design space analysis for the D-D Spherical Torus Hybrid Breeder. This appendix is provided so that a consolidated set of results exists for reference. The data numbering system used is consistant throughout the appendix, as well as throughout the thesis. A glossary of terms is included in the first section with the tables of results appearing in the following section.

A.1. Glossary of Terms

The terms used in the tables of results, in the approximate order in which they appear, are given in Table A-1 through Table A-4.

Table A-1: Glossary of Terms - Plasma Parameters

R	Major Radius [m]
a	Minor Radius [m]
A	Aspect Ratio, R/a
kappa	Plasma Elongation
Bt	Toroidal Field on Axis [T]
beta	Plasma Beta
Ip	Plasma Current [MA]
P fusion	Plasma Fusion Power [MW]
n tot	Total Particle Density [#/m^3]
V	Plasma Volume [m^3]
F	Fissile Production Rate [kg/yr]
P equiv	Power Produced by Burning All of the Fissile Material Produced
n d	Density of Deuterium
n t	Density of Tritium
n He3	Density of Helium-3
n He4	Density of Helium-4 (Alpha Particles)
n p	Density of Protons
n e	Density of Electrons
fm	Paramagnetism Factor
flux n	Neutron Production Rate [#/m^2s]
fp	Profile Factor Associated with Subsequent Reaction Power
P xx	Power [MW] associated with xx reaction
dt	D-T Reaction
ddt	Tritium Producing Chain of D-D Reaction
dd3	He^3 Producing Chain of D-D Reaction
d3	D-He^3 Reaction
tt	T-T Reaction
P wl xx	Neutron Wall Loading [MW/m^2] Associated with xx Reaction
$\langle v \rangle$ xx	Reaction Rate Parameter associated with xx Reaction
S	First Wall Surface Area [m^2]
Bt max	Maximum Toroidal Field Generated

Table A-2: Glossary of Terms - Plasma Power Balance

P aux	Required Auxialiary Power [MW] Associated with Listed Scaling Law (Negative Numbers Imply Ignition)
Q plasma	Plasma Energy Gain, P_{fusion}/P_{aux}, Associated with Listed Scaling Law (Negative Numbers Imply Ignition)
P brem	Power [MW] Lost from the Plasma Due to Bremmstralhung Radiation
P part	Fusion Energy [MW] Retained by the Charged Particles
Tau e	Energy Confinement Time [s] associated with listed scaling laws
P tr	Power [MW] Lost Due to Particle Transport

Table A-3: Glossary of Terms - Reactor Power Balance (Resistive Coils)

R disk	Radius of Disk Connecting TFC Return Legs and Centerpost
W tfc	Width of a Side of the TFC Return Legs
W pfc	Width of a Side of the PFC Coils
P tfc	Resistive Losses [MW] in the Toroidal Field Coil (All Components)
P pfc	Resistive Losses [MW] in the Poloidal Field Coils (Both Coils)
P cd	Power Required to Drive the Plasma Current
P total	Total Power Required for Magnets and Current Drive Systems
Z coil	Height of Center Conductor Post
P cp	Resistive Losses in the Centerpost

Table A-4: Glossary of Terms - Cost Analysis

ACCT xx	Costing Account Number from Table 7-2
CAP RET	Return on Capital [M$/yr]
O&M	Operations and Maintenance [M$/yr]
Capacity	Capacity Factor [kg fissile material/yr]
COF	Cost of Fissile Fuel [$/gm]

A.2. Tables of Results

Results are grouped into tables by area: plasma parameters; plasma power balance; reactor power balance; and cost analysis. Within each table, results are grouped by temperature.

Table A-5: Results - Plasma Parameters

#	R [m]	a [m]	A	kappa	Bt [T]	beta	Ip [MA]	P fusion [MW]	n tot [m-3]	V [m3]	F [kg/yr] (@ 80%)	P equiv [MW]
35 [keV]												
1	7.5	3.3	2.3	1.8	7.0	0.091	63.1	1032	1.31E+20	2803	7159	67180
2	7.0	3.0	2.3	1.8	7.0	0.091	58.9	839	1.31E+20	2279	5821	54620
3	6.5	2.8	2.3	1.8	7.0	0.091	54.7	672	1.31E+20	1825	4660	43730
4	8.0	3.5	2.3	1.8	6.5	0.091	62.5	929	1.13E+20	3401	6484	60850
5	7.5	3.3	2.3	1.8	6.5	0.091	58.6	765	1.13E+20	2803	5342	50140
6	7.5	3.4	2.2	1.8	6.5	0.096	67.1	1090	1.28E+20	3093	7568	71020
7	7.0	3.2	2.2	1.8	6.5	0.096	62.6	886	1.28E+20	2515	6153	57740
8	6.5	3.0	2.2	1.8	6.5	0.096	58.1	710	1.28E+20	2013	4926	46230
9	6.5	3.1	2.1	1.9	6.5	0.100	67.1	1074	1.50E+20	2231	7403	69470
10	6.0	2.9	2.1	1.9	6.5	0.100	62.0	845	1.50E+20	1754	5822	54640
11	5.5	2.6	2.1	1.9	6.5	0.100	56.8	651	1.50E+20	1351	4485	42090
12	8.0	3.6	2.2	1.8	6.0	0.096	66.0	958	1.09E+20	3754	6695	62830
13	7.5	3.4	2.2	1.8	6.0	0.096	61.9	789	1.09E+20	3093	5516	51770
14	7.0	3.2	2.2	1.8	6.0	0.096	57.8	642	1.09E+20	2515	4485	42090
15	7.0	3.3	2.1	1.9	6.0	0.100	66.7	971	1.27E+20	2786	6744	63290
16	6.5	3.1	2.1	1.9	6.0	0.100	62.0	777	1.27E+20	2231	5399	50670
17	6.0	2.9	2.1	1.9	6.0	0.100	57.2	612	1.27E+20	1754	4246	39850
18	6.0	3.0	2.0	1.9	6.0	0.107	66.9	925	1.48E+20	1952	6378	59860
19	5.5	2.8	2.0	1.9	6.0	0.107	61.3	713	1.48E+20	1504	4913	46110
20	8.0	3.8	2.1	1.9	5.5	0.100	69.9	1020	1.07E+20	4158	7138	66990
21	7.5	3.6	2.1	1.9	5.5	0.100	65.6	841	1.07E+20	3426	5882	55200
22	7.0	3.3	2.1	1.9	5.5	0.100	61.2	684	1.07E+20	2786	4782	44880
23	6.5	3.3	2.0	1.9	5.5	0.107	66.4	828	1.25E+20	2482	5754	54000
24	6.0	3.0	2.0	1.9	5.5	0.107	61.3	651	1.25E+20	1952	4526	42470
25	5.5	2.9	1.9	1.9	5.5	0.115	66.7	779	1.47E+20	1681	5374	50430
26	8.0	3.8	2.1	1.9	5.0	0.100	63.6	695	8.86E+19	4158	4895	45940
27	7.5	3.8	2.0	1.9	5.0	0.107	69.7	866	1.03E+20	3812	6066	56920
28	7.0	3.5	2.0	1.9	5.0	0.107	65.0	704	1.03E+20	3100	4931	46280
29	6.0	3.2	1.9	1.9	5.0	0.115	66.2	688	1.21E+20	2182	4790	44960
30	8.0	4.0	2.0	1.9	4.5	0.107	66.9	687	8.36E+19	4627	4850	45510
31	7.0	3.7	1.9	1.9	4.5	0.115	69.5	715	9.83E+19	3465	5016	47070
32	8.0	4.2	1.9	1.9	4.0	0.115	70.6	664	7.77E+19	5173	4694	44060
30 [keV]												
101	7.5	3.3	2.3	1.8	7.0	0.091	63.1	1139	1.53E+20	2803	7963	74730
102	7.0	3.0	2.3	1.8	7.0	0.091	58.9	926	1.53E+20	2279	6474	60760
103	6.5	2.8	2.3	1.8	7.0	0.091	54.7	742	1.53E+20	1825	5184	48650
104	8.0	3.5	2.3	1.8	6.5	0.091	62.5	1026	1.32E+20	3401	7211	67670
105	7.5	3.3	2.3	1.8	6.5	0.091	58.6	846	1.32E+20	2803	5942	55760
106	7.0	3.0	2.3	1.8	6.5	0.091	54.7	687	1.32E+20	2279	4831	45340

Table A-5 (cont.)

#	R [m]	a [m]	A	kappa	Bt [T]	beta	Ip [MA]	P fusion [MW]	n tot [m-3]	V [m3]	F [kg/yr] (@ 80%)	P equiv [MW]
107	7.5	3.4	2.2	1.8	6.5	0.096	67.1	1203	1.50E+20	3093	8416	78990
108	7.0	3.2	2.2	1.8	6.5	0.096	62.6	978	1.50E+20	2515	6844	64230
109	6.5	3.0	2.2	1.8	6.5	0.096	58.1	783	1.50E+20	2013	5479	51420
110	6.0	2.7	2.2	1.8	6.5	0.096	53.6	616	1.50E+20	1584	4310	40450
111	6.5	3.1	2.1	1.9	6.5	0.100	67.1	1185	1.74E+20	2231	8232	77290
112	6.0	2.9	2.1	1.9	6.5	0.100	62.0	932	1.74E+20	1754	6478	60790
113	5.5	2.6	2.1	1.9	6.5	0.100	56.8	718	1.74E+20	1351	4990	46820
114	8.0	3.5	2.3	1.8	6.0	0.091	57.7	744	1.12E+20	3401	5254	49300
115	8.0	3.6	2.2	1.8	6.0	0.096	66.0	1058	1.28E+20	3754	7446	69870
116	7.5	3.4	2.2	1.8	6.0	0.096	61.9	872	1.28E+20	3093	6134	57570
117	7.0	3.2	2.2	1.8	6.0	0.096	57.8	709	1.28E+20	2515	4988	46810
118	7.0	3.3	2.1	1.9	6.0	0.100	66.7	1072	1.49E+20	2786	7501	70390
119	6.5	3.1	2.1	1.9	6.0	0.100	62.0	858	1.49E+20	2231	6006	56360
120	6.0	2.9	2.1	1.9	6.0	0.100	57.2	675	1.49E+20	1754	4723	44330
121	6.0	3.0	2.0	1.9	6.0	0.107	66.9	1021	1.73E+20	1952	7096	66590
122	5.5	2.8	2.0	1.9	6.0	0.107	61.3	786	1.73E+20	1504	5466	51290
123	8.0	3.6	2.2	1.8	5.5	0.096	60.5	746	1.07E+20	3754	5276	49510
124	8.0	3.8	2.1	1.9	5.5	0.100	69.9	1128	1.25E+20	4158	7938	74500
125	7.5	3.6	2.1	1.9	5.5	0.100	65.6	929	1.25E+20	3426	6541	61380
126	7.0	3.3	2.1	1.9	5.5	0.100	61.2	755	1.25E+20	2786	5318	49910
127	6.5	3.1	2.1	1.9	5.5	0.100	56.8	605	1.25E+20	2231	4258	39960
128	6.5	3.3	2.0	1.9	5.5	0.107	66.4	914	1.46E+20	2482	6400	60060
129	6.0	3.0	2.0	1.9	5.5	0.107	61.3	719	1.46E+20	1952	5034	47240
130	5.5	2.9	1.9	1.9	5.5	0.115	66.7	859	1.71E+20	1681	5978	56100
131	5.0	2.6	1.9	1.9	5.5	0.115	60.7	646	1.71E+20	1263	4491	42150
132	8.0	3.8	2.1	1.9	5.0	0.100	63.6	769	1.03E+20	4158	5442	51080
133	7.5	3.6	2.1	1.9	5.0	0.100	59.6	633	1.03E+20	3426	4485	42090
134	7.5	3.8	2.0	1.9	5.0	0.107	69.7	957	1.20E+20	3812	6745	63300
135	7.0	3.5	2.0	1.9	5.0	0.107	65.0	778	1.20E+20	3100	5484	51460
136	6.5	3.3	2.0	1.9	5.0	0.107	60.4	623	1.20E+20	2482	4390	41200
137	6.0	3.2	1.9	1.9	5.0	0.115	66.2	760	1.41E+20	2182	5328	50000
138	8.0	4.0	2.0	1.9	4.5	0.107	66.9	760	9.75E+19	4627	5393	50610
139	7.5	3.8	2.0	1.9	4.5	0.107	62.7	627	9.75E+19	3812	4443	41700
140	7.0	3.7	1.9	1.9	4.5	0.115	69.5	790	1.15E+20	3465	5578	52340
141	6.5	3.4	1.9	1.9	4.5	0.115	64.5	633	1.15E+20	2775	4466	41910
142	8.0	4.2	1.9	1.9	4.0	0.115	70.6	735	9.07E+19	5173	5220	48980
143	7.5	3.9	1.9	1.9	4.0	0.115	66.2	605	9.07E+19	4262	4301	40360
25 [keV]												
201	7.5	3.3	2.3	1.8	7.0	0.091	63.1	1261	1.83E+20	2803	8888	83420
202	7.0	3.0	2.3	1.8	7.0	0.091	58.9	1025	1.83E+20	2279	7227	67830

Table A-5 (cont.)

#	R [m]	a [m]	A	kappa	Bt [T]	beta	Ip [MA]	P fusion [MW]	n tot [m-3]	V [m3]	F [kg/yr] (@ 80%)	P equiv [MW]
203	6.5	2.8	2.3	1.8	7.0	0.091	54.7	821	1.83E+20	1825	5786	54300
204	6.0	2.6	2.3	1.8	7.0	0.091	50.5	646	1.83E+20	1435	4551	42710
205	8.0	3.5	2.3	1.8	6.5	0.091	62.5	1137	1.58E+20	3401	8048	75530
206	7.5	3.3	2.3	1.8	6.5	0.091	58.6	937	1.58E+20	2803	6631	62230
207	7.0	3.0	2.3	1.8	6.5	0.091	54.7	762	1.58E+20	2279	5392	50600
208	6.5	2.8	2.3	1.8	6.5	0.091	50.8	610	1.58E+20	1825	4317	40510
209	7.5	3.4	2.2	1.8	6.5	0.096	67.1	1332	1.80E+20	3093	9400	88180
210	7.0	3.2	2.2	1.8	6.5	0.096	62.6	1083	1.80E+20	2515	7640	71690
211	6.5	3.0	2.2	1.8	6.5	0.096	58.1	867	1.80E+20	2013	6117	57400
212	6.0	2.7	2.2	1.8	6.5	0.096	53.6	682	1.80E+20	1584	4811	45150
213	6.5	3.1	2.1	1.9	6.5	0.100	67.1	1310	2.09E+20	2231	9192	86300
214	6.0	2.9	2.1	1.9	6.5	0.100	62.0	1030	2.09E+20	1754	7233	67870
215	5.5	2.6	2.1	1.9	6.5	0.100	56.8	794	2.09E+20	1351	5571	52280
216	8.0	3.5	2.3	1.8	6.0	0.091	57.7	825	1.35E+20	3401	5862	55010
217	7.5	3.3	2.3	1.8	6.0	0.091	54.1	680	1.35E+20	2803	4830	45330
218	8.0	3.6	2.2	1.8	6.0	0.096	66.0	1173	1.53E+20	3754	8312	77980
219	7.5	3.4	2.2	1.8	6.0	0.096	61.9	966	1.53E+20	3093	6846	64250
220	7.0	3.2	2.2	1.8	6.0	0.096	57.8	786	1.53E+20	2515	5566	52240
221	6.5	3.0	2.2	1.8	6.0	0.096	53.6	629	1.53E+20	2013	4457	41830
222	7.0	3.3	2.1	1.9	6.0	0.100	66.7	1187	1.79E+20	2786	8376	78580
223	6.5	3.1	2.1	1.9	6.0	0.100	62.0	950	1.79E+20	2231	6704	62910
224	6.0	2.9	2.1	1.9	6.0	0.100	57.2	747	1.79E+20	1754	5273	49480
225	6.0	3.0	2.0	1.9	6.0	0.107	66.9	1129	2.08E+20	1952	7923	74350
226	5.5	2.8	2.0	1.9	6.0	0.107	61.3	869	2.08E+20	1504	6103	57270
227	5.0	2.5	2.0	1.9	6.0	0.107	55.8	653	2.08E+20	1130	4585	43030
228	8.0	3.6	2.2	1.8	5.5	0.096	60.5	827	1.29E+20	3754	5886	55240
229	7.5	3.4	2.2	1.8	5.5	0.096	56.7	682	1.29E+20	3093	4850	45520
230	8.0	3.8	2.1	1.9	5.5	0.100	69.9	1250	1.50E+20	4158	8856	83140
231	7.5	3.6	2.1	1.9	5.5	0.100	65.6	1030	1.50E+20	3426	7300	68500
232	7.0	3.3	2.1	1.9	5.5	0.100	61.2	837	1.50E+20	2786	5935	55700
233	6.5	3.1	2.1	1.9	5.5	0.100	56.8	670	1.50E+20	2231	4752	44590
234	6.5	3.3	2.0	1.9	5.5	0.107	66.4	1012	1.75E+20	2482	7144	67050
235	6.0	3.0	2.0	1.9	5.5	0.107	61.3	796	1.75E+20	1952	5619	52730
236	5.5	2.8	2.0	1.9	5.5	0.107	56.2	613	1.75E+20	1504	4328	40620
237	5.5	2.9	1.9	1.9	5.5	0.115	66.7	951	2.05E+20	1681	6675	62640
238	5.0	2.6	1.9	1.9	5.5	0.115	60.7	714	2.05E+20	1263	5015	47060
239	8.0	3.8	2.1	1.9	5.0	0.100	63.6	853	1.24E+20	4158	6073	56990
240	7.5	3.6	2.1	1.9	5.0	0.100	59.6	703	1.24E+20	3426	5004	46960
241	7.5	3.8	2.0	1.9	5.0	0.107	69.7	1061	1.44E+20	3812	7527	70640
242	7.0	3.5	2.0	1.9	5.0	0.107	65.0	863	1.44E+20	3100	6120	57430
243	6.5	3.3	2.0	1.9	5.0	0.107	60.4	691	1.44E+20	2482	4900	45980

Table A-5 (cont.)

#	n d [m-3]	n t [m-3]	n He3 [m-3]	n He4 [m-3]	n p [m-3]	n e [m-3]	fm	flux n [#/m2/s]	fp
35 [keV]									
1	1.29E+20	6.91E+17	8.53E+17	1.87E+17	3.11E+17	1.32E+20	1.00	2.78E+17	1.3
2	1.29E+20	6.91E+17	8.53E+17	1.87E+17	3.11E+17	1.32E+20	1.00	2.59E+17	1.3
3	1.29E+20	6.91E+17	8.53E+17	1.87E+17	3.11E+17	1.32E+20	1.00	2.41E+17	1.3
4	1.11E+20	5.97E+17	6.42E+17	1.38E+17	2.30E+17	1.14E+20	1.00	2.21E+17	1.3
5	1.11E+20	5.97E+17	6.42E+17	1.38E+17	2.30E+17	1.14E+20	1.00	2.07E+17	1.3
6	1.26E+20	6.77E+17	8.18E+17	1.79E+17	2.98E+17	1.29E+20	1.04	2.75E+17	1.3
7	1.26E+20	6.77E+17	8.18E+17	1.79E+17	2.98E+17	1.29E+20	1.04	2.56E+17	1.3
8	1.26E+20	6.77E+17	8.18E+17	1.79E+17	2.98E+17	1.29E+20	1.04	2.38E+17	1.3
9	1.47E+20	7.88E+17	1.10E+18	2.45E+17	4.08E+17	1.51E+20	1.10	3.34E+17	1.3
10	1.47E+20	7.88E+17	1.10E+18	2.45E+17	4.08E+17	1.51E+20	1.10	3.08E+17	1.3
11	1.47E+20	7.88E+17	1.10E+18	2.45E+17	4.08E+17	1.51E+20	1.10	2.83E+17	1.3
12	1.08E+20	5.78E+17	6.02E+17	1.29E+17	2.15E+17	1.10E+20	1.04	2.14E+17	1.3
13	1.08E+20	5.78E+17	6.02E+17	1.29E+17	2.15E+17	1.10E+20	1.04	2.00E+17	1.3
14	1.08E+20	5.78E+17	6.02E+17	1.29E+17	2.15E+17	1.10E+20	1.04	1.87E+17	1.3
15	1.26E+20	6.73E+17	8.09E+17	1.77E+17	2.95E+17	1.28E+20	1.10	2.62E+17	1.3
16	1.26E+20	6.73E+17	8.09E+17	1.77E+17	2.95E+17	1.28E+20	1.10	2.44E+17	1.3
17	1.26E+20	6.73E+17	8.09E+17	1.77E+17	2.95E+17	1.28E+20	1.10	2.25E+17	1.3
18	1.46E+20	7.82E+17	1.08E+18	2.41E+17	4.02E+17	1.50E+20	1.15	3.15E+17	1.3
19	1.46E+20	7.82E+17	1.08E+18	2.41E+17	4.02E+17	1.50E+20	1.15	2.88E+17	1.3
20	1.06E+20	5.67E+17	5.80E+17	1.24E+17	2.07E+17	1.08E+20	1.10	2.13E+17	1.3
21	1.06E+20	5.67E+17	5.80E+17	1.24E+17	2.07E+17	1.08E+20	1.10	1.99E+17	1.3
22	1.06E+20	5.67E+17	5.80E+17	1.24E+17	2.07E+17	1.08E+20	1.10	1.86E+17	1.3
23	1.23E+20	6.59E+17	7.76E+17	1.69E+17	2.82E+17	1.26E+20	1.15	2.42E+17	1.3
24	1.23E+20	6.59E+17	7.76E+17	1.69E+17	2.82E+17	1.26E+20	1.15	2.23E+17	1.3
25	1.44E+20	7.74E+17	1.06E+18	2.36E+17	3.93E+17	1.48E+20	1.20	2.93E+17	1.3
26	8.75E+19	4.69E+17	4.02E+17	8.43E+16	1.41E+17	8.91E+19	1.10	1.46E+17	1.3
27	1.02E+20	5.46E+17	5.39E+17	1.15E+17	1.91E+17	1.04E+20	1.15	1.92E+17	1.3
28	1.02E+20	5.46E+17	5.39E+17	1.15E+17	1.91E+17	1.04E+20	1.15	1.79E+17	1.3
29	1.20E+20	6.41E+17	7.36E+17	1.60E+17	2.66E+17	1.22E+20	1.20	2.20E+17	1.3
30	8.26E+19	4.43E+17	3.59E+17	7.49E+16	1.25E+17	8.40E+19	1.15	1.35E+17	1.3
31	9.70E+19	5.21E+17	4.91E+17	1.04E+17	1.74E+17	9.89E+19	1.20	1.69E+17	1.3
32	7.68E+19	4.12E+17	3.11E+17	6.47E+16	1.08E+17	7.81E+19	1.20	1.21E+17	1.3
30 [keV]									
101	1.51E+20	7.02E+17	9.59E+17	2.06E+17	3.43E+17	1.54E+20	1.00	3.09E+17	1.4
102	1.51E+20	7.02E+17	9.59E+17	2.06E+17	3.43E+17	1.54E+20	1.00	2.89E+17	1.4
103	1.51E+20	7.02E+17	9.59E+17	2.06E+17	3.43E+17	1.54E+20	1.00	2.68E+17	1.4
104	1.30E+20	6.07E+17	7.21E+17	1.52E+17	2.54E+17	1.33E+20	1.00	2.46E+17	1.4
105	1.30E+20	6.07E+17	7.21E+17	1.52E+17	2.54E+17	1.33E+20	1.00	2.31E+17	1.4
106	1.30E+20	6.07E+17	7.21E+17	1.52E+17	2.54E+17	1.33E+20	1.00	2.15E+17	1.4

Table A-5 (cont.)

#	n d [m-3]	n t [m-3]	n He3 [m-3]	n He4 [m-3]	n p [m-3]	n e [m-3]	fm	flux n [#/m2/s]	fp
107	1.47E+20	6.87E+17	9.19E+17	1.97E+17	3.28E+17	1.51E+20	1.04	3.06E+17	1.4
108	1.47E+20	6.87E+17	9.19E+17	1.97E+17	3.28E+17	1.51E+20	1.04	2.85E+17	1.4
109	1.47E+20	6.87E+17	9.19E+17	1.97E+17	3.28E+17	1.51E+20	1.04	2.65E+17	1.4
110	1.47E+20	6.87E+17	9.19E+17	1.97E+17	3.28E+17	1.51E+20	1.04	2.44E+17	1.4
111	1.72E+20	8.00E+17	1.24E+18	2.69E+17	4.49E+17	1.76E+20	1.10	3.72E+17	1.4
112	1.72E+20	8.00E+17	1.24E+18	2.69E+17	4.49E+17	1.76E+20	1.10	3.43E+17	1.4
113	1.72E+20	8.00E+17	1.24E+18	2.69E+17	4.49E+17	1.76E+20	1.10	3.14E+17	1.4
114	1.11E+20	5.18E+17	5.29E+17	1.10E+17	1.84E+17	1.13E+20	1.00	1.79E+17	1.4
115	1.26E+20	5.87E+17	6.76E+17	1.42E+17	2.37E+17	1.28E+20	1.04	2.37E+17	1.4
116	1.26E+20	5.87E+17	6.76E+17	1.42E+17	2.37E+17	1.28E+20	1.04	2.23E+17	1.4
117	1.26E+20	5.87E+17	6.76E+17	1.42E+17	2.37E+17	1.28E+20	1.04	2.08E+17	1.4
118	1.47E+20	6.84E+17	9.10E+17	1.95E+17	3.25E+17	1.50E+20	1.10	2.92E+17	1.4
119	1.47E+20	6.84E+17	9.10E+17	1.95E+17	3.25E+17	1.50E+20	1.10	2.71E+17	1.4
120	1.47E+20	6.84E+17	9.10E+17	1.95E+17	3.25E+17	1.50E+20	1.10	2.50E+17	1.4
121	1.70E+20	7.94E+17	1.22E+18	2.65E+17	4.42E+17	1.75E+20	1.15	3.50E+17	1.4
122	1.70E+20	7.94E+17	1.22E+18	2.65E+17	4.42E+17	1.75E+20	1.15	3.21E+17	1.4
123	1.06E+20	4.94E+17	4.83E+17	1.00E+17	1.67E+17	1.08E+20	1.04	1.68E+17	1.4
124	1.23E+20	5.76E+17	6.51E+17	1.37E+17	2.28E+17	1.26E+20	1.10	2.36E+17	1.4
125	1.23E+20	5.76E+17	6.51E+17	1.37E+17	2.28E+17	1.26E+20	1.10	2.22E+17	1.4
126	1.23E+20	5.76E+17	6.51E+17	1.37E+17	2.28E+17	1.26E+20	1.10	2.07E+17	1.4
127	1.23E+20	5.76E+17	6.51E+17	1.37E+17	2.28E+17	1.26E+20	1.10	1.92E+17	1.4
128	1.44E+20	6.69E+17	8.73E+17	1.86E+17	3.11E+17	1.47E+20	1.15	2.69E+17	1.4
129	1.44E+20	6.69E+17	8.73E+17	1.86E+17	3.11E+17	1.47E+20	1.15	2.48E+17	1.4
130	1.69E+20	7.86E+17	1.19E+18	2.59E+17	4.32E+17	1.73E+20	1.20	3.26E+17	1.4
131	1.69E+20	7.86E+17	1.19E+18	2.59E+17	4.32E+17	1.73E+20	1.20	2.97E+17	1.4
132	1.02E+20	4.77E+17	4.50E+17	9.31E+16	1.55E+17	1.04E+20	1.10	1.62E+17	1.4
133	1.02E+20	4.77E+17	4.50E+17	9.31E+16	1.55E+17	1.04E+20	1.10	1.52E+17	1.4
134	1.19E+20	5.54E+17	6.04E+17	1.27E+17	2.11E+17	1.21E+20	1.15	2.13E+17	1.4
135	1.19E+20	5.54E+17	6.04E+17	1.27E+17	2.11E+17	1.21E+20	1.15	1.99E+17	1.4
136	1.19E+20	5.54E+17	6.04E+17	1.27E+17	2.11E+17	1.21E+20	1.15	1.85E+17	1.4
137	1.40E+20	6.51E+17	8.27E+17	1.76E+17	2.94E+17	1.43E+20	1.20	2.44E+17	1.4
138	9.64E+19	4.50E+17	4.02E+17	8.27E+16	1.38E+17	9.80E+19	1.15	1.50E+17	1.4
139	9.64E+19	4.50E+17	4.02E+17	8.27E+16	1.38E+17	9.80E+19	1.15	1.40E+17	1.4
140	1.13E+20	5.29E+17	5.51E+17	1.15E+17	1.92E+17	1.15E+20	1.20	1.88E+17	1.4
141	1.13E+20	5.29E+17	5.51E+17	1.15E+17	1.92E+17	1.15E+20	1.20	1.75E+17	1.4
142	8.97E+19	4.19E+17	3.49E+17	7.15E+16	1.19E+17	9.11E+19	1.20	1.35E+17	1.4
143	8.97E+19	4.19E+17	3.49E+17	7.15E+16	1.19E+17	9.11E+19	1.20	1.26E+17	1.4
25 [keV]									
201	1.81E+20	7.24E+17	1.08E+18	2.27E+17	3.78E+17	1.85E+20	1.00	3.45E+17	1.5
202	1.81E+20	7.24E+17	1.08E+18	2.27E+17	3.78E+17	1.85E+20	1.00	3.22E+17	1.5

Table A-5 (cont.)

#	n d [m-3]	n t [m-3]	n He3 [m-3]	n He4 [m-3]	n p [m-3]	n e [m-3]	fm	flux n [#/m2/s]	fp
203	1.81E+20	7.24E+17	1.08E+18	2.27E+17	3.78E+17	1.85E+20	1.00	2.99E+17	1.5
204	1.81E+20	7.24E+17	1.08E+18	2.27E+17	3.78E+17	1.85E+20	1.00	2.76E+17	1.5
205	1.56E+20	6.26E+17	8.13E+17	1.68E+17	2.81E+17	1.59E+20	1.00	2.75E+17	1.5
206	1.56E+20	6.26E+17	8.13E+17	1.68E+17	2.81E+17	1.59E+20	1.00	2.57E+17	1.5
207	1.56E+20	6.26E+17	8.13E+17	1.68E+17	2.81E+17	1.59E+20	1.00	2.40E+17	1.5
208	1.56E+20	6.26E+17	8.13E+17	1.68E+17	2.81E+17	1.59E+20	1.00	2.23E+17	1.5
209	1.77E+20	7.09E+17	1.04E+18	2.17E+17	3.62E+17	1.81E+20	1.04	3.41E+17	1.5
210	1.77E+20	7.09E+17	1.04E+18	2.17E+17	3.62E+17	1.81E+20	1.04	3.18E+17	1.5
211	1.77E+20	7.09E+17	1.04E+18	2.17E+17	3.62E+17	1.81E+20	1.04	2.96E+17	1.5
212	1.77E+20	7.09E+17	1.04E+18	2.17E+17	3.62E+17	1.81E+20	1.04	2.73E+17	1.5
213	2.06E+20	8.26E+17	1.40E+18	2.97E+17	4.95E+17	2.11E+20	1.10	4.15E+17	1.5
214	2.06E+20	8.26E+17	1.40E+18	2.97E+17	4.95E+17	2.11E+20	1.10	3.83E+17	1.5
215	2.06E+20	8.26E+17	1.40E+18	2.97E+17	4.95E+17	2.11E+20	1.10	3.51E+17	1.5
216	1.33E+20	5.34E+17	5.96E+17	1.22E+17	2.03E+17	1.36E+20	1.00	2.00E+17	1.5
217	1.33E+20	5.34E+17	5.96E+17	1.22E+17	2.03E+17	1.36E+20	1.00	1.88E+17	1.5
218	1.51E+20	6.05E+17	7.62E+17	1.57E+17	2.62E+17	1.54E+20	1.04	2.65E+17	1.5
219	1.51E+20	6.05E+17	7.62E+17	1.57E+17	2.62E+17	1.54E+20	1.04	2.48E+17	1.5
220	1.51E+20	6.05E+17	7.62E+17	1.57E+17	2.62E+17	1.54E+20	1.04	2.32E+17	1.5
221	1.51E+20	6.05E+17	7.62E+17	1.57E+17	2.62E+17	1.54E+20	1.04	2.15E+17	1.5
222	1.76E+20	7.05E+17	1.03E+18	2.15E+17	3.58E+17	1.80E+20	1.10	3.26E+17	1.5
223	1.76E+20	7.05E+17	1.03E+18	2.15E+17	3.58E+17	1.80E+20	1.10	3.02E+17	1.5
224	1.76E+20	7.05E+17	1.03E+18	2.15E+17	3.58E+17	1.80E+20	1.10	2.79E+17	1.5
225	2.05E+20	8.19E+17	1.38E+18	2.92E+17	4.87E+17	2.09E+20	1.15	3.91E+17	1.5
226	2.05E+20	8.19E+17	1.38E+18	2.92E+17	4.87E+17	2.09E+20	1.15	3.58E+17	1.5
227	2.05E+20	8.19E+17	1.38E+18	2.92E+17	4.87E+17	2.09E+20	1.15	3.26E+17	1.5
228	1.27E+20	5.09E+17	5.43E+17	1.11E+17	1.85E+17	1.29E+20	1.04	1.88E+17	1.5
229	1.27E+20	5.09E+17	5.43E+17	1.11E+17	1.85E+17	1.29E+20	1.04	1.76E+17	1.5
230	1.48E+20	5.94E+17	7.34E+17	1.51E+17	2.52E+17	1.51E+20	1.10	2.64E+17	1.5
231	1.48E+20	5.94E+17	7.34E+17	1.51E+17	2.52E+17	1.51E+20	1.10	2.47E+17	1.5
232	1.48E+20	5.94E+17	7.34E+17	1.51E+17	2.52E+17	1.51E+20	1.10	2.31E+17	1.5
233	1.48E+20	5.94E+17	7.34E+17	1.51E+17	2.52E+17	1.51E+20	1.10	2.14E+17	1.5
234	1.72E+20	6.90E+17	9.85E+17	2.06E+17	3.43E+17	1.76E+20	1.15	3.00E+17	1.5
235	1.72E+20	6.90E+17	9.85E+17	2.06E+17	3.43E+17	1.76E+20	1.15	2.77E+17	1.5
236	1.72E+20	6.90E+17	9.85E+17	2.06E+17	3.43E+17	1.76E+20	1.15	2.54E+17	1.5
237	2.03E+20	8.11E+17	1.35E+18	2.86E+17	4.76E+17	2.07E+20	1.20	3.64E+17	1.5
238	2.03E+20	8.11E+17	1.35E+18	2.86E+17	4.76E+17	2.07E+20	1.20	3.31E+17	1.5
239	1.23E+20	4.91E+17	5.06E+17	1.03E+17	1.72E+17	1.25E+20	1.10	1.81E+17	1.5
240	1.23E+20	4.91E+17	5.06E+17	1.03E+17	1.72E+17	1.25E+20	1.10	1.70E+17	1.5
241	1.43E+20	5.71E+17	6.81E+17	1.40E+17	2.34E+17	1.45E+20	1.15	2.38E+17	1.5
242	1.43E+20	5.71E+17	6.81E+17	1.40E+17	2.34E+17	1.45E+20	1.15	2.22E+17	1.5
243	1.43E+20	5.71E+17	6.81E+17	1.40E+17	2.34E+17	1.45E+20	1.15	2.06E+17	1.5

Table A-5 (cont.)

#	P dt [MW]	fp	P ddt [MW]	fp	P dd3 [MW]	fp	P d3 [MW]	fp	P tt [MW]	P wl tot [MW/m2]	P wl dt [MW/m2]
35 [keV]											
1	688.2	1.8	157.7	1.8	134.4	2.5	51.7	1.69	0.011	0.362	0.306
2	559.6	1.8	128.2	1.8	109.3	2.5	42.0	1.69	0.009	0.338	0.286
3	448.0	1.8	102.6	1.8	87.5	2.5	33.7	1.69	0.007	0.314	0.265
4	623.4	1.8	142.8	1.8	121.7	2.5	40.8	1.69	0.010	0.288	0.244
5	513.6	1.8	117.7	1.8	100.3	2.5	33.7	1.69	0.009	0.270	0.228
6	727.5	1.8	166.7	1.8	142.1	2.5	53.6	1.69	0.012	0.358	0.303
7	591.5	1.8	135.5	1.8	115.5	2.5	43.6	1.69	0.010	0.334	0.282
8	473.6	1.8	108.5	1.8	92.5	2.5	34.9	1.69	0.008	0.310	0.262
9	711.7	1.8	163.1	1.8	139.0	2.5	60.4	1.69	0.012	0.435	0.368
10	559.8	1.8	128.2	1.8	109.3	2.5	47.5	1.69	0.009	0.402	0.340
11	431.2	1.8	98.8	1.8	84.2	2.5	36.6	1.69	0.007	0.368	0.311
12	643.6	1.8	147.5	1.8	125.7	2.5	40.9	1.69	0.011	0.278	0.235
13	530.3	1.8	121.5	1.8	103.6	2.5	33.7	1.69	0.009	0.261	0.221
14	431.2	1.8	98.8	1.8	84.2	2.5	27.4	1.69	0.007	0.243	0.206
15	648.3	1.8	148.5	1.8	126.6	2.5	47.5	1.69	0.011	0.342	0.289
16	519.1	1.8	118.9	1.8	101.4	2.5	38.0	1.69	0.009	0.317	0.268
17	408.3	1.8	93.5	1.8	79.7	2.5	29.9	1.69	0.007	0.293	0.248
18	613.2	1.8	140.5	1.8	119.8	2.5	51.7	1.69	0.010	0.410	0.347
19	472.3	1.8	108.2	1.8	92.3	2.5	39.8	1.69	0.008	0.376	0.318
20	686.2	1.8	157.2	1.8	134.0	2.5	42.8	1.69	0.011	0.277	0.234
21	565.4	1.8	129.5	1.8	110.4	2.5	35.3	1.69	0.009	0.260	0.220
22	459.7	1.8	105.3	1.8	89.8	2.5	28.7	1.69	0.008	0.242	0.205
23	553.2	1.8	126.7	1.8	108.0	2.5	39.7	1.69	0.009	0.315	0.266
24	435.1	1.8	99.7	1.8	85.0	2.5	31.3	1.69	0.007	0.291	0.246
25	516.6	1.8	118.4	1.8	100.9	2.5	43.1	1.69	0.009	0.382	0.323
26	470.6	1.8	107.8	1.8	91.9	2.5	24.5	1.69	0.008	0.190	0.161
27	583.1	1.8	133.6	1.8	113.9	2.5	35.1	1.69	0.010	0.249	0.211
28	474.1	1.8	108.6	1.8	92.6	2.5	28.5	1.69	0.008	0.233	0.197
29	460.6	1.8	105.5	1.8	90.0	2.5	32.3	1.69	0.008	0.286	0.242
30	466.2	1.8	106.8	1.8	91.1	2.5	23.0	1.69	0.008	0.175	0.148
31	482.2	1.8	110.5	1.8	94.2	2.5	27.8	1.69	0.008	0.220	0.186
32	451.3	1.8	103.4	1.8	88.2	2.5	20.8	1.69	0.008	0.158	0.133
30 [keV]											
101	766.5	1.8	175.6	1.8	149.3	2.8	47.9	1.72	0.010	0.403	0.341
102	623.2	1.8	142.8	1.8	121.4	2.8	38.9	1.72	0.008	0.376	0.318
103	499.00	1.8	114.30	1.8	97.21	2.8	31.17	1.72	0.006	0.349	0.296
104	694.10	1.8	159.00	1.8	135.20	2.8	37.75	1.72	0.009	0.321	0.271
105	571.90	1.8	131.00	1.8	111.40	2.8	31.11	1.72	0.007	0.301	0.254
106	465.00	1.8	106.50	1.8	90.59	2.8	25.29	1.72	0.006	0.281	0.237

Table A-5 (cont.)

#	P dt [MW]	fp	P ddt [MW]	fp	P dd3 [MW]	fp	P d3 [MW]	fp	P tt [MW]	P wl tot [MW/m2]	P wl dt [MW/m2]
107	810.30	1.8	185.60	1.8	157.90	2.8	49.61	1.72	0.010	0.398	0.337
108	658.80	1.8	150.90	1.8	128.30	2.8	40.33	1.72	0.008	0.372	0.315
109	527.4	1.8	120.8	1.8	102.8	2.8	32.3	1.72	0.007	0.345	0.292
110	414.80	1.8	95.05	1.8	80.82	2.8	25.40	1.72	0.005	0.319	0.270
111	792.70	1.8	181.60	1.8	154.40	2.8	56.02	1.72	0.010	0.484	0.410
112	623.50	1.8	142.90	1.8	121.50	2.8	44.06	1.72	0.008	0.447	0.378
113	480.30	1.8	110.00	1.8	93.56	2.8	33.94	1.72	0.006	0.410	0.347
114	505.70	1.8	115.90	1.8	98.52	2.8	23.65	1.72	0.006	0.234	0.198
115	716.70	1.8	164.20	1.8	139.60	2.8	37.77	1.72	0.009	0.310	0.262
116	590.50	1.8	135.30	1.8	115.00	2.8	31.12	1.72	0.008	0.290	0.246
117	480.10	1.8	110.00	1.8	93.54	2.8	25.30	1.72	0.006	0.271	0.229
118	722.00	1.8	165.40	1.8	140.70	2.8	43.98	1.72	0.009	0.380	0.322
119	578.10	1.8	132.40	1.8	112.60	2.8	35.22	1.72	0.007	0.353	0.299
120	454.70	1.8	104.20	1.8	88.58	2.8	27.70	1.72	0.006	0.326	0.276
121	683.00	1.8	156.50	1.8	133.10	2.8	47.92	1.71	0.009	0.456	0.386
122	526.10	1.8	120.50	1.8	102.50	2.8	36.91	1.71	0.007	0.418	0.354
123	507.80	1.8	116.30	1.8	98.94	2.8	22.70	1.72	0.007	0.219	0.186
124	764.10	1.8	175.10	1.8	148.90	2.8	39.54	1.72	0.010	0.308	0.261
125	629.60	1.8	144.30	1.8	122.70	2.8	32.58	1.72	0.008	0.289	0.244
126	511.90	1.8	117.30	1.8	99.73	2.8	26.49	1.72	0.007	0.270	0.228
127	409.90	1.8	93.90	1.8	79.85	2.8	21.21	1.72	0.005	0.250	0.212
128	616.10	1.8	141.20	1.8	120.00	2.8	36.78	1.71	0.008	0.351	0.297
129	484.60	1.8	111.00	1.8	94.40	2.8	28.93	1.71	0.006	0.324	0.274
130	575.50	1.8	131.80	1.8	112.10	2.8	39.97	1.71	0.007	0.426	0.360
131	432.40	1.8	99.06	1.8	84.23	2.8	30.03	1.71	0.006	0.387	0.327
132	523.90	1.8	120.00	1.8	102.10	2.8	22.63	1.72	0.007	0.211	0.179
133	431.70	1.8	98.90	1.8	84.10	2.8	18.65	1.72	0.006	0.198	0.168
134	649.30	1.8	148.80	1.8	126.50	2.8	32.41	1.71	0.008	0.278	0.235
135	527.90	1.8	120.90	1.8	102.80	2.8	26.35	1.71	0.007	0.259	0.219
136	422.60	1.8	96.83	1.8	82.34	2.8	21.10	1.71	0.005	0.241	0.204
137	512.90	1.8	117.50	1.8	99.92	2.8	29.84	1.71	0.007	0.319	0.270
138	519.10	1.8	118.90	1.8	101.10	2.8	21.21	1.71	0.007	0.195	0.165
139	427.70	1.8	97.99	1.8	83.32	2.8	17.48	1.71	0.005	0.183	0.155
140	536.90	1.8	123.00	1.8	104.60	2.8	25.62	1.71	0.007	0.245	0.207
141	429.80	1.8	98.48	1.8	83.74	2.8	20.51	1.71	0.006	0.228	0.193
142	502.40	1.8	115.10	1.8	97.89	2.8	19.16	1.71	0.006	0.176	0.149
143	414.00	1.8	94.85	1.8	80.66	2.8	15.78	1.71	0.005	0.165	0.139
25 [keV]											
201	857.50	1.9	196.50	1.9	166.40	3.1	40.82	1.76	0.008	0.451	0.381
202	697.10	1.9	159.70	1.9	135.30	3.1	33.19	1.76	0.007	0.421	0.356

Table A-5 (cont.)

#	P dt [MW]	fp	P ddt [MW]	fp	P dd3 [MW]	fp	P d3 [MW]	fp	P tt [MW]	P wl tot [MW/m2]	P wl dt [MW/m2]
203	558.20	1.9	127.90	1.9	108.30	3.1	26.57	1.76	0.005	0.391	0.331
204	439.00	1.9	100.60	1.9	85.18	3.1	20.90	1.76	0.004	0.360	0.305
205	776.30	1.9	177.90	1.9	150.60	3.1	32.11	1.76	0.007	0.359	0.304
206	639.70	1.9	146.60	1.9	124.10	3.1	26.46	1.76	0.006	0.336	0.285
207	520.10	1.9	119.20	1.9	100.90	3.1	21.51	1.76	0.005	0.314	0.266
208	416.4	1.9	95.4	1.9	80.8	3.1	17.2	1.76	0.004	0.291	0.247
209	906.4	1.9	207.7	1.9	175.9	3.1	42.3	1.76	0.009	0.445	0.377
210	736.9	1.9	168.8	1.9	143.0	3.1	34.4	1.76	0.007	0.416	0.352
211	590.0	1.9	135.2	1.9	114.5	3.1	27.5	1.76	0.006	0.386	0.327
212	464.1	1.9	106.3	1.9	90.0	3.1	21.6	1.76	0.004	0.356	0.302
213	887.0	1.9	203.2	1.9	172.1	3.1	47.9	1.76	0.009	0.542	0.459
214	697.6	1.9	159.8	1.9	135.4	3.1	37.6	1.76	0.007	0.500	0.423
215	537.4	1.9	123.1	1.9	104.3	3.1	29.0	1.76	0.005	0.458	0.388
216	565.4	1.9	129.5	1.9	109.7	3.1	20.1	1.76	0.005	0.261	0.221
217	465.9	1.9	106.7	1.9	90.4	3.1	16.5	1.76	0.004	0.245	0.207
218	801.5	1.9	183.6	1.9	155.5	3.1	32.1	1.76	0.008	0.346	0.293
219	660.4	1.9	151.3	1.9	128.1	3.1	26.5	1.76	0.006	0.324	0.275
220	536.9	1.9	123.0	1.9	104.2	3.1	21.5	1.76	0.005	0.303	0.256
221	429.9	1.9	98.5	1.9	83.4	3.1	17.2	1.76	0.004	0.281	0.238
222	807.7	1.9	185.0	1.9	156.7	3.1	37.5	1.76	0.008	0.425	0.360
223	646.7	1.9	148.2	1.9	125.5	3.1	30.0	1.76	0.006	0.395	0.334
224	508.6	1.9	116.5	1.9	98.7	3.1	23.6	1.76	0.005	0.365	0.309
225	764.3	1.9	175.1	1.9	148.3	3.1	40.9	1.76	0.007	0.510	0.432
226	588.7	1.9	134.9	1.9	114.2	3.1	31.5	1.76	0.006	0.468	0.396
227	442.3	1.9	101.3	1.9	85.8	3.1	23.7	1.76	0.004	0.425	0.360
228	567.8	1.9	130.1	1.9	110.2	3.1	19.3	1.76	0.005	0.245	0.208
229	467.9	1.9	107.2	1.9	90.8	3.1	15.9	1.76	0.005	0.230	0.195
230	854.5	1.9	195.8	1.9	165.8	3.1	33.6	1.76	0.008	0.344	0.292
231	704.1	1.9	161.3	1.9	136.6	3.1	27.7	1.76	0.007	0.323	0.273
232	572.5	1.9	131.2	1.9	111.1	3.1	22.5	1.76	0.006	0.301	0.255
233	458.4	1.9	105.0	1.9	88.9	3.1	18.0	1.76	0.004	0.280	0.237
234	689.1	1.9	157.9	1.9	133.7	3.1	31.3	1.76	0.007	0.392	0.332
235	542.0	1.9	124.2	1.9	105.2	3.1	24.6	1.76	0.005	0.362	0.306
236	417.5	1.9	95.7	1.9	81.0	3.1	19.0	1.76	0.004	0.332	0.281
237	643.9	1.9	147.5	1.9	124.9	3.1	34.1	1.76	0.006	0.476	0.403
238	483.8	1.9	110.8	1.9	93.9	3.1	25.7	1.76	0.005	0.433	0.366
239	585.8	1.9	134.2	1.9	113.7	3.1	19.2	1.76	0.006	0.236	0.200
240	482.6	1.9	110.6	1.9	93.7	3.1	15.8	1.76	0.005	0.221	0.187
241	726.1	1.9	166.3	1.9	140.9	3.1	27.5	1.76	0.007	0.310	0.263
242	590.3	1.9	135.2	1.9	114.5	3.1	22.4	1.76	0.006	0.290	0.245
243	472.6	1.9	108.3	1.9	91.7	3.1	17.9	1.76	0.005	0.269	0.228

Table A-5 (cont.)

#	P wl d3 [MW/m2]	⟨ v⟩ dt [m3/s]	⟨ v⟩ ddt [m3/s]	⟨ v⟩ dd3 [m3/s]	⟨ v⟩ d3 [m3/s]	⟨ v⟩ tt [m3/s]	S [m2]	Bt max [T]
35 [keV]								
1	0.056	7.48E-22	6.00E-24	6.27E-24	2.28E-23	5.60E-24	1802	13.4
2	0.052	7.48E-22	6.00E-24	6.27E-24	2.28E-23	5.60E-24	1570	13.4
3	0.048	7.48E-22	6.00E-24	6.27E-24	2.28E-23	5.60E-24	1354	13.4
4	0.044	7.48E-22	6.00E-24	6.27E-24	2.28E-23	5.60E-24	2050	12.5
5	0.042	7.48E-22	6.00E-24	6.27E-24	2.28E-23	5.60E-24	1802	12.5
6	0.055	7.48E-22	6.00E-24	6.27E-24	2.29E-23	5.60E-24	1927	13.0
7	0.052	7.48E-22	6.00E-24	6.27E-24	2.29E-23	5.60E-24	1679	13.0
8	0.048	7.48E-22	6.00E-24	6.27E-24	2.29E-23	5.60E-24	1448	13.0
9	0.067	7.49E-22	6.01E-24	6.27E-24	2.29E-23	5.60E-24	1551	13.7
10	0.062	7.49E-22	6.01E-24	6.27E-24	2.29E-23	5.60E-24	1321	13.7
11	0.057	7.49E-22	6.01E-24	6.27E-24	2.29E-23	5.60E-24	1110	13.7
12	0.043	7.48E-22	6.00E-24	6.27E-24	2.29E-23	5.60E-24	2193	12.0
13	0.040	7.48E-22	6.00E-24	6.27E-24	2.29E-23	5.60E-24	1927	12.0
14	0.038	7.48E-22	6.00E-24	6.27E-24	2.29E-23	5.60E-24	1679	12.0
15	0.053	7.49E-22	6.01E-24	6.27E-24	2.29E-23	5.60E-24	1799	12.6
16	0.049	7.49E-22	6.01E-24	6.27E-24	2.29E-23	5.60E-24	1551	12.6
17	0.045	7.49E-22	6.01E-24	6.27E-24	2.29E-23	5.60E-24	1321	12.6
18	0.063	7.49E-22	6.01E-24	6.28E-24	2.29E-23	5.60E-24	1418	13.3
19	0.058	7.49E-22	6.01E-24	6.28E-24	2.29E-23	5.60E-24	1192	13.3
20	0.043	7.49E-22	6.01E-24	6.27E-24	2.29E-23	5.60E-24	2349	11.6
21	0.040	7.49E-22	6.01E-24	6.27E-24	2.29E-23	5.60E-24	2065	11.6
22	0.037	7.49E-22	6.01E-24	6.27E-24	2.29E-23	5.60E-24	1799	11.6
23	0.049	7.49E-22	6.01E-24	6.28E-24	2.29E-23	5.60E-24	1664	12.2
24	0.045	7.49E-22	6.01E-24	6.28E-24	2.29E-23	5.60E-24	1418	12.2
25	0.059	7.49E-22	6.01E-24	6.28E-24	2.29E-23	5.60E-24	1281	13.1
26	0.029	7.49E-22	6.01E-24	6.27E-24	2.29E-23	5.60E-24	2349	10.5
27	0.039	7.49E-22	6.01E-24	6.28E-24	2.29E-23	5.60E-24	2216	11.1
28	0.036	7.49E-22	6.01E-24	6.28E-24	2.29E-23	5.60E-24	1930	11.1
29	0.044	7.49E-22	6.01E-24	6.28E-24	2.29E-23	5.60E-24	1525	11.9
30	0.027	7.49E-22	6.01E-24	6.28E-24	2.29E-23	5.60E-24	2521	10.0
31	0.034	7.49E-22	6.01E-24	6.28E-24	2.29E-23	5.60E-24	2075	10.7
32	0.024	7.49E-22	6.01E-24	6.28E-24	2.29E-23	5.60E-24	2711	9.5
30 [keV]								
101	0.062	6.73E-22	4.78E-24	4.97E-24	1.46E-23	4.56E-24	1802	13.4
102	0.058	6.73E-22	4.78E-24	4.97E-24	1.46E-23	4.56E-24	1570	13.4
103	0.054	6.73E-22	4.78E-24	4.97E-24	1.46E-23	4.56E-24	1354	13.4
104	0.049	6.73E-22	4.78E-24	4.97E-24	1.46E-23	4.56E-24	2050	12.5
105	0.046	6.73E-22	4.78E-24	4.97E-24	1.46E-23	4.56E-24	1802	12.5
106	0.043	6.73E-22	4.78E-24	4.97E-24	1.46E-23	4.56E-24	1570	12.5

Table A-5 (cont.)

#	P wl d3 [MW/m2]	⟨ v⟩ dt [m3/s]	⟨ v⟩ ddt [m3/s]	⟨ v⟩ dd3 [m3/s]	⟨ v⟩ d3 [m3/s]	⟨ v⟩ tt [m3/s]	S [m2]	Bt max [T]
107	0.061	6.73E-22	4.78E-24	4.97E-24	1.46E-23	4.56E-24	1927	13.0
108	0.057	6.73E-22	4.78E-24	4.97E-24	1.46E-23	4.56E-24	1679	13.0
109	0.053	6.73E-22	4.78E-24	4.97E-24	1.46E-23	4.56E-24	1448	13.0
110	0.049	6.73E-22	4.78E-24	4.97E-24	1.46E-23	4.56E-24	1234	13.0
111	0.075	6.73E-22	4.78E-24	4.97E-24	1.46E-23	4.56E-24	1551	13.7
112	0.069	6.73E-22	4.78E-24	4.97E-24	1.46E-23	4.56E-24	1321	13.7
113	0.063	6.73E-22	4.78E-24	4.97E-24	1.46E-23	4.56E-24	1110	13.7
114	0.036	6.73E-22	4.78E-24	4.97E-24	1.46E-23	4.56E-24	2050	11.5
115	0.048	6.73E-22	4.78E-24	4.97E-24	1.46E-23	4.56E-24	2193	12.0
116	0.045	6.73E-22	4.78E-24	4.97E-24	1.46E-23	4.56E-24	1927	12.0
117	0.042	6.73E-22	4.78E-24	4.97E-24	1.46E-23	4.56E-24	1679	12.0
118	0.059	6.73E-22	4.78E-24	4.97E-24	1.46E-23	4.56E-24	1799	12.6
119	0.054	6.73E-22	4.78E-24	4.97E-24	1.46E-23	4.56E-24	1551	12.6
120	0.050	6.73E-22	4.78E-24	4.97E-24	1.46E-23	4.56E-24	1321	12.6
121	0.070	6.73E-22	4.78E-24	4.97E-24	1.46E-23	4.57E-24	1418	13.3
122	0.064	6.73E-22	4.78E-24	4.97E-24	1.46E-23	4.57E-24	1192	13.3
123	0.034	6.73E-22	4.78E-24	4.97E-24	1.46E-23	4.56E-24	2193	11.0
124	0.047	6.73E-22	4.78E-24	4.97E-24	1.46E-23	4.56E-24	2349	11.6
125	0.045	6.73E-22	4.78E-24	4.97E-24	1.46E-23	4.56E-24	2065	11.6
126	0.042	6.73E-22	4.78E-24	4.97E-24	1.46E-23	4.56E-24	1799	11.6
127	0.039	6.73E-22	4.78E-24	4.97E-24	1.46E-23	4.56E-24	1551	11.6
128	0.054	6.73E-22	4.78E-24	4.97E-24	1.46E-23	4.57E-24	1664	12.2
129	0.050	6.73E-22	4.78E-24	4.97E-24	1.46E-23	4.57E-24	1418	12.2
130	0.066	6.73E-22	4.78E-24	4.97E-24	1.46E-23	4.57E-24	1281	13.1
131	0.060	6.73E-22	4.78E-24	4.97E-24	1.46E-23	4.57E-24	1059	13.1
132	0.033	6.73E-22	4.78E-24	4.97E-24	1.46E-23	4.56E-24	2349	10.5
133	0.031	6.73E-22	4.78E-24	4.97E-24	1.46E-23	4.56E-24	2065	10.5
134	0.043	6.73E-22	4.78E-24	4.97E-24	1.46E-23	4.57E-24	2216	11.1
135	0.040	6.73E-22	4.78E-24	4.97E-24	1.46E-23	4.57E-24	1930	11.1
136	0.037	6.73E-22	4.78E-24	4.97E-24	1.46E-23	4.57E-24	1664	11.1
137	0.049	6.73E-22	4.78E-24	4.97E-24	1.46E-23	4.57E-24	1525	11.9
138	0.030	6.73E-22	4.78E-24	4.97E-24	1.46E-23	4.57E-24	2521	10.0
139	0.028	6.73E-22	4.78E-24	4.97E-24	1.46E-23	4.57E-24	2216	10.0
140	0.038	6.73E-22	4.78E-24	4.97E-24	1.46E-23	4.57E-24	2075	10.7
141	0.035	6.73E-22	4.78E-24	4.97E-24	1.46E-23	4.57E-24	1789	10.7
142	0.027	6.73E-22	4.78E-24	4.97E-24	1.46E-23	4.57E-24	2711	9.5
143	0.025	6.73E-22	4.78E-24	4.97E-24	1.46E-23	4.57E-24	2382	9.5
25 [keV]								
201	0.069	5.68E-22	3.58E-24	3.70E-24	8.24E-24	3.53E-24	1802	13.4
202	0.065	5.68E-22	3.58E-24	3.70E-24	8.24E-24	3.53E-24	1570	13.4

Table A-5 (cont.)

#	P wl d3 [MW/m2]	⟨ v⟩ dt [m3/s]	⟨ v⟩ ddt [m3/s]	⟨ v⟩ dd3 [m3/s]	⟨ v⟩ d3 [m3/s]	⟨ v⟩ tt [m3/s]	S [m2]	Bt max [T]
203	0.060	5.68E-22	3.58E-24	3.70E-24	8.24E-24	3.53E-24	1354	13.4
204	0.055	5.68E-22	3.58E-24	3.70E-24	8.24E-24	3.53E-24	1153	13.4
205	0.055	5.68E-22	3.58E-24	3.70E-24	8.24E-24	3.53E-24	2050	12.5
206	0.052	5.68E-22	3.58E-24	3.70E-24	8.24E-24	3.53E-24	1802	12.5
207	0.048	5.68E-22	3.58E-24	3.70E-24	8.24E-24	3.53E-24	1570	12.5
208	0.045	5.68E-22	3.58E-24	3.70E-24	8.24E-24	3.53E-24	1354	12.5
209	0.068	5.68E-22	3.58E-24	3.70E-24	8.24E-24	3.53E-24	1927	13.0
210	0.064	5.68E-22	3.58E-24	3.70E-24	8.24E-24	3.53E-24	1679	13.0
211	0.059	5.68E-22	3.58E-24	3.70E-24	8.24E-24	3.53E-24	1448	13.0
212	0.055	5.68E-22	3.58E-24	3.70E-24	8.24E-24	3.53E-24	1234	13.0
213	0.083	5.68E-22	3.58E-24	3.70E-24	8.25E-24	3.53E-24	1551	13.7
214	0.077	5.68E-22	3.58E-24	3.70E-24	8.25E-24	3.53E-24	1321	13.7
215	0.070	5.68E-22	3.58E-24	3.70E-24	8.25E-24	3.53E-24	1110	13.7
216	0.040	5.68E-22	3.58E-24	3.70E-24	8.24E-24	3.53E-24	2050	11.5
217	0.038	5.68E-22	3.58E-24	3.70E-24	8.24E-24	3.53E-24	1802	11.5
218	0.053	5.68E-22	3.58E-24	3.70E-24	8.24E-24	3.53E-24	2193	12.0
219	0.050	5.68E-22	3.58E-24	3.70E-24	8.24E-24	3.53E-24	1927	12.0
220	0.046	5.68E-22	3.58E-24	3.70E-24	8.24E-24	3.53E-24	1679	12.0
221	0.043	5.68E-22	3.58E-24	3.70E-24	8.24E-24	3.53E-24	1448	12.0
222	0.065	5.68E-22	3.58E-24	3.70E-24	8.25E-24	3.53E-24	1799	12.6
223	0.061	5.68E-22	3.58E-24	3.70E-24	8.25E-24	3.53E-24	1551	12.6
224	0.056	5.68E-22	3.58E-24	3.70E-24	8.25E-24	3.53E-24	1321	12.6
225	0.078	5.68E-22	3.59E-24	3.70E-24	8.25E-24	3.53E-24	1418	13.3
226	0.072	5.68E-22	3.59E-24	3.70E-24	8.25E-24	3.53E-24	1192	13.3
227	0.065	5.68E-22	3.59E-24	3.70E-24	8.25E-24	3.53E-24	985	13.3
228	0.038	5.68E-22	3.58E-24	3.70E-24	8.24E-24	3.53E-24	2193	11.0
229	0.035	5.68E-22	3.58E-24	3.70E-24	8.24E-24	3.53E-24	1927	11.0
230	0.053	5.68E-22	3.58E-24	3.70E-24	8.25E-24	3.53E-24	2349	11.6
231	0.050	5.68E-22	3.58E-24	3.70E-24	8.25E-24	3.53E-24	2065	11.6
232	0.046	5.68E-22	3.58E-24	3.70E-24	8.25E-24	3.53E-24	1799	11.6
233	0.043	5.68E-22	3.58E-24	3.70E-24	8.25E-24	3.53E-24	1551	11.6
234	0.060	5.68E-22	3.59E-24	3.70E-24	8.25E-24	3.53E-24	1664	12.2
235	0.056	5.68E-22	3.59E-24	3.70E-24	8.25E-24	3.53E-24	1418	12.2
236	0.051	5.68E-22	3.59E-24	3.70E-24	8.25E-24	3.53E-24	1192	12.2
237	0.073	5.68E-22	3.59E-24	3.71E-24	8.26E-24	3.53E-24	1281	13.1
238	0.066	5.68E-22	3.59E-24	3.71E-24	8.26E-24	3.53E-24	1059	13.1
239	0.036	5.68E-22	3.58E-24	3.70E-24	8.25E-24	3.53E-24	2349	10.5
240	0.034	5.68E-22	3.58E-24	3.70E-24	8.25E-24	3.53E-24	2065	10.5
241	0.048	5.68E-22	3.59E-24	3.70E-24	8.25E-24	3.53E-24	2216	11.1
242	0.044	5.68E-22	3.59E-24	3.70E-24	8.25E-24	3.53E-24	1930	11.1
243	0.041	5.68E-22	3.59E-24	3.70E-24	8.25E-24	3.53E-24	1664	11.1

Table A-6: Results - Plasma Power Balance

#	NEO-ALCATOR P aux [MW]	NEO-ALCATOR Q plasma [P o/P i]	Pfeiffer-Waltz P aux [MW]	Pfeiffer-Waltz Q plasma [P o/P i]	GMS (Mirnov) P aux [MW]	GMS (Mirnov) Q plasma [P o/P i]	ASDEX P aux [MW]	ASDEX Q plasma [P o/P i]	Goldston-Kaye P aux [MW]	Goldston-Kaye Q plasma [P o/P i]
35 [keV]										
1	-83.6	-15.2	832.5	1.5	31.5	40.3	-55.0	-23.1	167.2	7.6
2	-42.5	-24.3	845.8	1.2	41.0	25.2	-24.5	-42.2	172.5	6.0
3	-7.0	-118.8	852.4	1.0	47.2	17.5	0.5	1662.4	173.4	4.8
4	-58.2	-19.6	869.6	1.3	70.5	16.2	-31.3	-36.6	205.8	5.6
5	-24.1	-39.1	877.5	1.1	73.4	12.8	-6.9	-135.9	205.2	4.6
6	-88.3	-15.2	881.7	1.5	23.3	57.5	-64.0	-21.0	151.3	8.9
7	-45.0	-24.2	895.6	1.2	34.7	31.5	-31.4	-34.7	159.3	6.8
8	-7.6	-115.4	902.3	1.0	42.3	20.6	-4.7	-184.9	162.4	5.4
9	-81.4	-16.2	902.5	1.5	-17.3	-76.5	-69.4	-19.0	96.2	13.7
10	-31.8	-32.7	917.5	1.1	1.6	633.4	-31.7	-32.7	111.1	9.3
11	10.1	78.9	922.9	0.9	15.2	52.5	-1.8	-438.0	119.4	6.7
12	-56.6	-20.9	924.6	1.3	67.4	17.5	-34.8	-33.9	194.3	6.1
13	-21.5	-45.2	931.9	1.0	71.0	13.7	-9.7	-100.6	195.3	5.0
14	9.1	86.6	933.6	0.9	72.1	11.0	11.1	71.4	192.7	4.1
15	-55.0	-21.7	944.7	1.3	23.8	50.2	-44.0	-27.2	136.9	8.7
16	-14.0	-68.5	953.2	1.0	34.1	28.0	-14.0	-68.2	144.1	6.6
17	21.1	35.7	954.0	0.8	40.8	18.5	10.0	75.6	146.5	5.1
18	-40.4	-28.2	970.5	1.2	-11.6	-97.8	-45.3	-25.1	87.8	12.9
19	5.5	159.4	977.5	0.9	5.4	163.3	-11.7	-74.6	100.9	8.7
20	-61.3	-20.5	979.9	1.3	61.3	20.5	-43.0	-29.3	174.5	7.2
21	-24.0	-43.2	987.8	1.1	66.3	15.6	-15.8	-65.4	178.3	5.8
22	8.6	98.5	989.6	0.9	68.7	12.3	6.6	128.3	178.3	4.7
23	-15.6	-65.2	1012.7	1.0	26.7	38.1	-21.7	-46.9	125.9	8.1
24	21.6	37.1	1013.7	0.8	35.2	22.8	4.3	187.6	131.3	6.1
25	0.9	1100.3	1038.2	0.9	-6.3	-153.1	-23.3	-41.1	78.5	12.2
26	8.8	97.8	1028.7	0.8	107.0	8.0	12.2	70.1	217.2	4.0
27	-19.9	-53.5	1053.9	1.0	63.2	16.9	-19.0	-56.2	162.3	6.6
28	13.4	64.6	1054.7	0.8	66.3	13.1	4.2	207.4	164.2	5.3
29	23.6	35.9	1080.4	0.8	29.0	29.2	-1.8	-480.0	113.4	7.5
30	19.5	43.5	1099.6	0.8	108.3	7.8	14.3	59.4	205.1	4.1
31	21.3	41.4	1128.0	0.8	64.1	13.8	2.6	339.6	148.2	6.0
32	34.4	23.8	1179.1	0.7	109.9	7.5	17.9	45.9	191.2	4.3
30 [keV]										
101	-92.1	-15.2	707.3	2.0	41.4	33.9	-45.1	-31.1	142.4	9.9
102	-52.6	-21.7	722.6	1.6	49.4	23.1	-16.1	-70.9	149.5	7.6
103	-18.4	-49.6	731.6	1.3	54.2	16.8	7.5	121.1	152.2	6.0
104	-68.3	-18.5	741.3	1.7	79.0	16.0	-22.8	-55.4	178.3	7.1
105	-35.4	-29.5	751.4	1.4	80.6	12.9	0.3	3295.5	179.7	5.8
106	-6.6	-127.9	756.3	1.1	80.1	10.6	19.3	44.0	177.8	4.8

Table A-6 (cont.)

#	NEO-ALCATOR P aux [MW]	NEO-ALCATOR Q plasma [P o/P i]	Pfeiffer-Waltz P aux [MW]	Pfeiffer-Waltz Q plasma [P o/P i]	GMS (Mirnov) P aux [MW]	GMS (Mirnov) Q plasma [P o/P i]	ASDEX P aux [MW]	ASDEX Q plasma [P o/P i]	Goldston-Kaye P aux [MW]	Goldston-Kaye Q plasma [P o/P i]
107	-97.4	-15.2	749.0	2.0	33.6	44.0	-53.7	-27.6	127.4	11.6
108	-55.7	-21.6	765.1	1.6	43.4	27.8	-22.7	-53.0	136.9	8.8
109	-19.7	-48.9	774.4	1.3	49.6	19.4	2.6	373.9	141.8	6.8
110	11.0	68.8	777.1	1.0	52.8	14.4	22.6	33.5	142.5	5.3
111	-90.8	-16.0	767.8	1.9	-6.1	-237.2	-58.3	-25.0	78.0	18.7
112	-43.1	-26.6	785.3	1.5	10.8	106.3	-22.6	-50.7	94.1	12.2
113	-2.9	-299.8	793.7	1.1	22.7	38.9	5.6	157.0	103.8	8.5
114	-15.0	-61.1	780.7	1.2	112.3	8.2	18.3	50.0	209.9	4.4
115	-67.5	-19.3	788.6	1.7	76.0	17.2	-26.3	-49.7	167.6	7.8
116	-33.6	-32.0	798.3	1.4	78.3	13.7	-2.3	-463.7	170.4	6.3
117	-4.1	-213.0	802.6	1.1	78.3	11.2	17.3	50.5	169.8	5.2
118	-66.1	-20.0	806.3	1.6	33.2	39.7	-34.5	-38.3	115.7	11.4
119	-26.6	-39.8	817.4	1.3	42.0	25.2	-6.1	-173.0	124.5	8.5
120	7.1	117.0	821.4	1.0	47.3	17.6	16.5	50.3	128.5	6.5
121	-52.2	-24.1	830.0	1.5	-1.7	-721.7	-35.5	-35.4	72.2	17.4
122	-8.2	-118.2	840.3	1.2	13.4	72.2	-3.7	-261.6	86.4	11.2
123	-8.9	-103.8	831.2	1.1	112.8	8.2	19.1	48.2	203.0	4.5
124	-72.8	-19.1	835.7	1.7	70.3	19.8	-34.0	-40.9	148.9	9.3
125	-36.8	-31.1	846.0	1.4	74.1	15.5	-8.1	-141.3	154.4	7.4
126	-5.4	-171.8	850.7	1.1	75.3	12.4	13.2	70.8	156.3	6.0
127	21.7	34.4	849.9	0.9	74.2	10.0	30.1	24.8	154.7	4.8
128	-29.0	-38.8	868.4	1.3	35.0	32.1	-13.4	-84.0	107.4	10.5
129	6.8	130.9	872.6	1.0	42.1	21.1	11.2	79.3	114.3	7.7
130	-13.5	-78.5	891.9	1.2	2.4	439.5	-14.6	-72.3	65.4	16.2
131	26.4	30.1	893.7	0.9	15.6	51.1	12.8	62.0	77.6	10.2
132	-5.7	-165.8	884.2	1.1	113.1	8.4	18.3	51.8	191.2	5.0
133	18.2	42.9	882.9	0.9	107.7	7.3	33.0	23.7	186.9	4.2
134	-33.8	-34.9	903.1	1.3	71.1	16.6	-11.1	-106.0	139.7	8.5
135	-1.6	-586.0	907.0	1.1	72.9	13.2	10.9	88.4	143.3	6.7
136	26.2	29.4	905.2	0.9	72.5	10.6	28.5	27.0	143.4	5.4
137	7.8	120.3	930.1	1.0	36.2	25.9	5.4	173.1	97.7	9.6
138	3.7	254.2	946.1	1.0	114.2	8.2	20.2	46.5	180.2	5.2
139	27.2	28.4	942.9	0.8	108.5	7.1	34.5	22.4	176.7	4.4
140	4.9	197.6	970.6	1.0	70.8	13.8	9.3	105.1	128.6	7.6
141	33.0	23.6	967.3	0.8	70.7	11.0	27.2	28.7	130.3	6.0
142	17.0	53.4	1015.8	0.9	115.6	7.9	23.5	38.6	167.8	5.4
143	39.6	18.9	1010.1	0.7	109.5	6.8	37.0	20.2	164.9	4.5
25 [keV]										
201	-80.8	-19.2	599.6	2.6	71.2	21.8	-15.3	-101.4	135.3	11.5
202	-46.3	-27.3	613.5	2.1	74.1	17.0	8.6	146.8	140.8	9.0

Table A-6 (cont.)

#	NEO-ALCATOR P aux [MW]	NEO-ALCATOR Q plasma [P o/P i]	Pfeiffer-Waltz P aux [MW]	Pfeiffer-Waltz Q plasma [P o/P i]	GMS (Mirnov) P aux [MW]	GMS (Mirnov) Q plasma [P o/P i]	ASDEX P aux [MW]	ASDEX Q plasma [P o/P i]	Goldston-Kaye P aux [MW]	Goldston-Kaye Q plasma [P o/P i]
203	-16.6	-60.9	621.8	1.6	74.5	13.6	27.8	36.4	142.4	7.1
204	8.7	91.3	624.7	1.3	72.7	11.0	42.6	18.7	140.5	5.7
205	-60.8	-23.1	628.3	2.2	105.0	13.4	3.2	441.2	166.1	8.4
206	-32.0	-36.1	637.7	1.8	102.5	11.3	22.2	52.1	166.7	6.9
207	-6.9	-135.7	642.5	1.5	98.3	9.6	37.5	25.1	164.4	5.7
208	14.7	51.3	642.9	1.2	92.6	8.1	49.3	15.3	159.5	4.7
209	-85.7	-19.2	634.7	2.6	64.8	25.3	-22.5	-72.9	122.0	13.5
210	-49.4	-27.0	649.3	2.1	69.2	19.3	3.1	428.7	129.7	10.3
211	-18.0	-59.4	658.0	1.6	70.8	15.1	23.8	45.0	133.2	8.0
212	8.7	96.4	661.0	1.3	70.0	12.0	39.8	21.1	133.1	6.3
213	-79.1	-20.4	651.9	2.5	26.1	61.8	-26.0	-62.0	79.1	20.4
214	-37.7	-33.7	667.7	1.9	36.8	34.5	3.4	372.3	92.3	13.8
215	-2.8	-345.7	675.5	1.5	43.3	22.6	26.3	37.2	99.9	9.8
216	-14.8	-68.7	662.4	1.5	131.0	7.8	37.0	27.5	192.7	5.3
217	5.6	149.3	663.7	1.3	122.6	6.8	48.4	17.3	186.7	4.5
218	-60.4	-24.0	668.2	2.2	102.5	14.1	0.3	5149.5	156.5	9.2
219	-30.8	-38.7	677.3	1.8	100.6	11.9	20.0	59.6	158.4	7.5
220	-5.0	-193.4	681.7	1.4	96.9	10.0	35.9	27.0	157.3	6.2
221	17.2	45.1	681.6	1.1	91.6	8.5	48.2	16.1	153.4	5.1
222	-58.4	-25.0	684.2	2.1	61.4	23.8	-6.3	-230.7	111.3	13.1
223	-24.0	-48.7	694.4	1.7	65.1	18.0	17.0	69.0	118.2	9.9
224	5.3	175.3	698.5	1.3	66.0	14.0	35.2	26.2	121.0	7.6
225	-45.6	-30.5	705.5	2.0	26.5	52.4	-7.2	-193.1	73.2	19.0
226	-7.5	-143.5	714.9	1.5	35.8	29.9	18.7	57.2	84.8	12.6
227	24.1	33.4	716.2	1.1	41.0	19.6	38.0	21.1	90.7	8.9
228	-9.8	-104.4	705.2	1.5	131.4	7.8	37.7	27.1	186.5	5.5
229	10.6	79.2	705.4	1.2	122.9	6.9	49.0	17.2	181.0	4.7
230	-65.2	-23.6	708.0	2.2	98.5	15.7	-5.8	-264.5	140.1	11.0
231	-33.7	-37.6	717.7	1.8	97.7	13.0	15.5	81.8	144.4	8.8
232	-6.3	-163.7	722.4	1.4	94.9	10.9	32.8	31.5	145.5	7.1
233	17.3	47.7	722.4	1.1	90.4	9.1	46.3	17.9	143.5	5.8
234	-26.4	-47.3	737.6	1.7	59.4	21.0	11.0	113.7	103.2	12.1
235	4.8	205.8	741.9	1.3	61.8	15.9	30.9	31.8	108.6	9.0
236	30.9	24.4	739.8	1.0	61.5	12.3	45.8	16.5	109.9	6.9
237	-12.2	-96.2	758.7	1.5	26.7	43.8	9.7	120.8	66.5	17.6
238	22.4	39.3	760.9	1.2	34.5	25.5	31.8	27.7	76.3	11.5
239	-7.3	-145.0	750.1	1.4	132.2	8.0	37.3	28.2	175.9	6.0
240	13.7	63.3	749.7	1.2	123.8	7.0	49.1	17.7	171.7	5.1
241	-31.5	-41.6	766.0	1.7	95.2	13.8	13.0	100.7	131.3	10.0
242	-3.3	-323.2	770.1	1.4	93.0	11.4	30.9	34.4	133.9	7.9
243	21.0	40.6	769.3	1.1	89.0	9.6	45.0	18.9	133.5	6.4

Table A-6 (cont.)

#	P brem [MW]	P part [MW]	neo-ALCATOR Tau e [s]	neo-ALCATOR P tr [MW]	Pfeiffer-Walt Tau e [s]	Pfeiffer-Walt P tr [MW]	GMS (Mirnov) Tau e [s]	GMS (Mirnov) P tr [MW]	ASDEX Tau e [s]	ASDEX P tr [MW]	Goldston-Kaye Tau e [s]	Goldston-Kaye P tr [MW]
35 [keV]												
1	157.3	380.7	53.5	139.8	7.1	1055.9	29.4	254.9	44.4	168.4	19.2	390.6
2	127.9	309.5	43.7	139.2	5.9	1027.5	27.3	222.7	38.7	157.1	17.2	354.2
3	102.4	247.8	35.2	138.5	4.9	997.8	25.3	192.6	33.4	145.9	15.3	318.8
4	141.5	338.8	56.3	139.1	7.3	1066.9	29.2	267.8	47.2	166.0	19.4	403.1
5	116.6	279.1	46.6	138.5	6.2	1040.0	27.3	236.0	41.4	155.6	17.5	367.8
6	166.1	401.3	55.0	147.0	7.2	1116.9	31.2	258.6	47.2	171.2	20.9	386.6
7	135.0	326.3	44.9	146.3	6.0	1086.9	29.1	225.9	41.1	159.8	18.7	350.5
8	108.1	261.2	36.1	145.6	5.0	1055.5	26.9	195.4	35.4	148.4	16.7	315.6
9	163.8	400.5	43.8	155.3	6.0	1139.2	31.0	219.5	40.6	167.4	20.4	333.0
10	128.8	315.0	34.6	154.5	4.9	1103.7	28.5	187.9	34.6	154.5	18.0	297.3
11	99.2	242.7	26.8	153.6	3.9	1066.3	26.0	158.7	29.1	141.6	15.7	262.9
12	145.9	348.5	57.2	146.1	7.4	1127.2	30.9	270.0	49.8	167.8	21.0	397.0
13	120.2	287.1	47.3	145.5	6.3	1098.8	28.9	237.9	43.8	157.3	19.0	362.2
14	97.7	233.5	38.6	144.9	5.2	1069.3	26.9	207.8	38.1	146.8	17.0	328.4
15	148.0	357.4	46.9	154.5	6.3	1154.1	31.0	233.2	43.7	165.5	20.9	346.3
16	118.5	286.1	37.7	153.7	5.2	1120.8	28.7	201.8	37.7	153.6	18.6	311.8
17	93.2	225.1	29.8	152.9	4.2	1085.9	26.4	172.6	32.1	141.8	16.4	278.4
18	141.1	344.7	36.2	163.3	5.0	1174.2	30.8	192.1	37.3	158.4	20.3	291.5
19	108.7	265.5	28.0	162.4	4.0	1134.4	28.0	162.2	31.3	145.2	17.6	257.8
20	155.4	370.8	58.9	154.1	7.6	1195.3	32.8	276.7	52.7	172.4	23.3	389.8
21	128.1	305.5	48.7	153.5	6.4	1165.2	30.7	243.8	46.3	161.6	21.0	355.7
22	104.1	248.4	39.8	152.8	5.4	1133.9	28.6	213.0	40.3	150.9	18.9	322.6
23	126.1	304.1	38.9	162.4	5.3	1190.7	30.8	204.7	40.4	156.3	20.8	303.9
24	99.2	239.2	30.7	161.6	4.3	1153.7	28.3	175.2	34.4	144.3	18.3	271.3
25	118.8	290.0	29.2	172.1	4.2	1209.4	30.5	165.0	34.0	148.0	20.1	249.7
26	105.8	249.5	49.2	152.4	6.4	1172.3	29.9	250.7	48.1	155.9	20.8	360.9
27	131.9	313.8	49.4	162.0	6.5	1235.8	32.7	245.2	49.2	163.0	23.3	344.2
28	107.2	255.1	40.4	161.3	5.4	1202.6	30.4	214.2	42.8	152.1	20.9	312.2
29	104.9	252.4	31.5	171.1	4.4	1227.9	30.6	176.5	37.0	145.7	20.7	260.9
30	104.6	245.9	49.0	160.7	6.4	1240.8	31.6	249.5	50.6	155.5	22.7	346.3
31	108.8	258.2	40.7	170.7	5.4	1277.3	32.5	213.4	45.7	152.0	23.3	297.5
32	101.1	236.5	48.2	169.9	6.2	1314.6	33.4	245.4	53.4	153.3	25.1	326.6
30 [keV]												
101	198.0	414.1	60.3	124.0	8.1	923.4	29.1	257.5	43.7	171.0	20.9	358.6
102	161.0	336.7	49.4	123.2	6.8	898.4	27.0	225.2	38.1	159.6	18.7	325.3
103	128.9	269.6	39.8	122.3	5.6	872.3	25.0	194.9	32.9	148.2	16.6	292.9
104	178.1	369.4	63.6	123.0	8.4	932.6	29.0	270.3	46.5	168.5	21.2	369.7
105	146.8	304.4	52.8	122.3	7.1	909.0	27.1	238.3	40.8	157.9	19.1	337.4
106	119.3	247.5	43.2	121.5	5.9	884.4	25.2	208.3	35.6	147.4	17.1	306.0

Table A-6 (cont.)

#	P brem [MW]	P part [MW]	neo-ALCATOR Tau e [s]	neo-ALCATOR P tr [MW]	Pfeiffer-Walt Tau e [s]	Pfeiffer-Walt P tr [MW]	GMS (Mirnov) Tau e [s]	GMS (Mirnov) P tr [MW]	ASDEX Tau e [s]	ASDEX P tr [MW]	Goldston-Kaye Tau e [s]	Goldston-Kaye P tr [MW]
107	209.1	436.8	62.0	130.3	8.3	976.6	30.9	261.3	46.4	174.0	22.8	355.0
108	170.0	355.1	50.8	129.4	6.9	950.2	28.8	228.5	40.4	162.4	20.4	322.0
109	136.1	284.3	40.9	128.5	5.7	922.6	26.6	197.8	34.9	150.8	18.1	290.0
110	107.1	223.6	32.4	127.6	4.6	893.7	24.4	169.4	29.7	139.2	16.0	259.0
111	206.2	434.8	49.4	137.8	6.8	996.4	30.6	222.5	39.9	170.3	22.2	306.6
112	162.2	342.0	39.1	136.7	5.5	965.1	28.1	190.6	34.0	157.2	19.5	273.9
113	124.9	263.4	30.4	135.6	4.4	932.3	25.6	161.2	28.6	144.1	17.0	242.3
114	129.0	265.3	55.0	121.3	7.3	917.0	26.8	248.6	43.1	154.7	19.3	346.2
115	183.7	380.2	64.7	129.1	8.5	985.2	30.7	272.5	49.1	170.3	22.9	364.2
116	151.3	313.3	53.6	128.3	7.2	960.2	28.7	240.3	43.1	159.6	20.7	332.4
117	123.0	254.7	43.9	127.6	6.0	934.3	26.7	210.0	37.6	149.0	18.6	301.4
118	186.3	389.0	53.0	136.7	7.2	1009.0	30.7	235.9	43.0	168.2	22.7	318.4
119	149.2	311.4	42.7	135.7	5.9	979.7	28.4	204.3	37.1	156.2	20.2	286.8
120	117.3	245.0	33.8	134.8	4.8	949.0	26.1	175.0	31.6	144.2	17.8	256.2
121	177.6	374.3	40.9	144.5	5.8	1026.7	30.3	195.0	36.6	161.3	22.0	268.9
122	136.8	288.3	31.7	143.4	4.6	991.8	27.6	164.9	30.8	147.8	19.1	237.9
123	129.3	265.4	55.2	127.2	7.3	967.3	28.2	248.9	45.2	155.2	20.7	339.1
124	195.7	404.7	66.7	136.2	8.7	1044.7	32.5	279.3	51.9	175.0	25.4	357.8
125	161.2	333.4	55.3	135.4	7.4	1018.2	30.4	246.2	45.6	164.1	22.9	326.6
126	131.1	271.1	45.2	134.6	6.1	990.7	28.3	215.3	39.7	153.2	20.5	296.3
127	105.0	217.1	36.4	133.8	5.1	962.0	26.1	186.3	34.2	142.2	18.3	266.8
128	158.8	331.2	44.0	143.3	6.1	1040.7	30.4	207.4	39.7	159.0	22.6	279.7
129	124.9	260.5	34.9	142.3	4.9	1008.2	27.9	177.6	33.8	146.7	19.9	249.9
130	149.5	314.9	33.1	151.9	4.8	1057.3	30.0	167.8	33.4	150.8	21.8	230.8
131	112.3	236.6	25.1	150.7	3.7	1018.0	27.0	139.8	27.6	137.1	18.7	201.9
132	133.2	273.0	56.0	134.0	7.3	1023.9	29.7	252.9	47.5	158.0	22.7	330.9
133	109.8	224.9	46.4	133.4	6.2	998.1	27.7	222.9	41.7	148.2	20.5	302.0
134	166.0	342.6	56.1	142.8	7.4	1079.7	32.3	247.7	48.4	165.5	25.3	316.3
135	135.0	278.6	45.9	142.0	6.2	1050.6	30.1	216.5	42.2	154.5	22.7	286.9
136	108.1	223.0	36.9	141.1	5.1	1020.2	27.8	187.5	36.4	143.4	20.2	258.4
137	132.0	274.9	35.8	150.7	5.0	1072.9	30.1	179.1	36.4	148.3	22.4	240.5
138	131.8	269.2	55.8	141.2	7.3	1083.5	31.3	251.7	49.9	157.7	24.8	317.7
139	108.6	221.8	46.2	140.5	6.1	1056.2	29.3	221.8	43.9	147.8	22.4	289.9
140	137.0	282.1	46.3	150.0	6.2	1115.7	32.2	215.9	45.0	154.4	25.4	273.7
141	109.7	225.9	37.3	149.2	5.1	1083.5	29.7	186.9	38.8	143.3	22.6	246.5
142	127.3	259.2	55.0	149.0	7.1	1147.7	33.1	247.6	52.7	155.5	27.3	299.8
143	104.9	213.6	45.5	148.3	6.0	1118.8	30.9	218.2	46.3	145.8	24.7	273.6
25 [keV]												
201	259.9	450.4	68.2	109.7	9.5	790.1	28.6	261.6	42.7	175.1	23.0	325.7
202	211.3	366.2	56.1	108.5	7.9	768.4	26.6	229.0	37.2	163.5	20.6	295.6

Table A-6 (cont.)

#	P brem [MW]	P part [MW]	neo-ALCATOR Tau e [s]	neo-ALCATOR P tr [MW]	Pfeiffer-Walt Tau e [s]	Pfeiffer-Walt P tr [MW]	GMS (Mirnov) Tau e [s]	GMS (Mirnov) P tr [MW]	ASDEX Tau e [s]	ASDEX P tr [MW]	Goldston-Kaye Tau e [s]	Goldston-Kaye P tr [MW]
203	169.2	293.2	45.4	107.4	6.5	745.8	24.5	198.5	32.1	151.8	18.3	266.3
204	133.1	230.6	36.1	106.2	5.3	722.2	22.5	170.2	27.3	140.1	16.1	238.0
205	233.9	402.9	72.3	108.3	9.8	797.4	28.6	274.0	45.5	172.2	23.4	335.2
206	192.7	332.0	60.1	107.3	8.3	776.9	26.7	241.8	40.0	161.5	21.1	306.0
207	156.7	269.9	49.3	106.3	6.9	755.7	24.8	211.5	34.8	150.7	18.9	277.7
208	125.4	216.1	39.9	105.4	5.7	733.6	22.9	183.3	30.0	139.9	16.8	250.2
209	274.5	475.2	70.3	115.0	9.7	835.4	30.4	265.5	45.3	178.2	25.0	322.7
210	223.2	386.3	57.7	113.8	8.1	812.5	28.3	232.4	39.5	166.3	22.4	292.9
211	178.7	309.3	46.7	112.6	6.7	788.7	26.1	201.4	34.1	154.4	19.9	263.9
212	140.5	243.3	37.1	111.5	5.4	763.7	23.9	172.7	29.0	142.5	17.5	235.8
213	270.6	471.5	55.8	121.8	8.0	852.8	30.0	227.0	38.9	174.9	24.3	280.0
214	212.8	370.9	44.4	120.4	6.5	825.7	27.5	194.8	33.1	161.4	21.4	250.3
215	163.9	285.7	34.7	118.9	5.2	797.3	25.0	165.0	27.8	148.0	18.6	221.6
216	169.3	290.1	62.9	106.0	8.5	783.2	26.5	251.8	42.3	157.9	21.3	313.5
217	139.5	239.1	52.3	105.2	7.2	763.2	24.7	222.1	37.1	148.0	19.2	286.2
218	241.1	414.9	73.7	113.4	9.9	842.0	30.2	276.3	48.0	174.1	25.3	330.3
219	198.7	341.9	61.2	112.4	8.4	820.5	28.2	243.8	42.2	163.2	22.8	301.6
220	161.5	278.0	50.2	111.4	7.0	798.1	26.2	213.3	36.7	152.3	20.5	273.7
221	129.3	222.6	40.6	110.4	5.8	774.8	24.2	184.9	31.7	141.4	18.2	246.6
222	244.5	423.2	60.2	120.3	8.4	862.9	30.1	240.1	42.0	172.4	25.0	290.0
223	195.8	338.9	48.7	119.0	6.9	837.5	27.8	208.2	36.2	160.1	22.2	261.3
224	154.0	266.5	38.7	117.8	5.6	811.0	25.5	178.6	30.9	147.7	19.5	233.6
225	233.1	406.0	46.4	127.3	6.7	878.4	29.6	199.4	35.6	165.7	24.0	246.1
226	179.5	312.7	36.2	125.7	5.4	848.1	26.9	169.0	29.9	151.9	20.9	217.9
227	134.9	234.9	27.5	124.2	4.2	816.2	24.2	141.1	24.8	138.1	17.9	190.8
228	169.8	290.5	63.3	110.9	8.5	825.9	27.8	252.1	44.3	158.3	22.9	307.1
229	139.9	239.3	52.6	110.1	7.2	804.9	26.0	222.3	39.0	148.4	20.6	280.4
230	256.9	441.8	75.9	119.6	10.2	892.8	32.0	283.3	50.7	179.0	27.9	325.0
231	211.7	364.0	63.1	118.6	8.6	870.0	29.9	250.0	44.6	167.8	25.2	296.7
232	172.1	296.0	51.7	117.5	7.2	846.3	27.8	218.8	38.8	156.7	22.6	269.3
233	137.8	237.0	41.8	116.5	5.9	821.5	25.7	189.6	33.5	145.5	20.1	242.6
234	208.5	360.5	50.2	125.6	7.1	889.6	29.8	211.4	38.7	163.0	24.7	255.3
235	164.0	283.5	39.9	124.3	5.8	861.5	27.4	181.4	33.0	150.5	21.8	228.2
236	126.3	218.4	31.1	123.0	4.6	831.9	24.9	153.6	27.7	137.9	18.9	202.0
237	196.3	341.7	37.8	133.3	5.6	904.1	29.2	172.1	32.4	155.1	23.7	211.9
238	147.5	256.7	28.7	131.6	4.3	870.2	26.3	143.8	26.8	141.0	20.4	185.6
239	175.0	299.0	64.3	116.7	8.6	874.1	29.3	256.2	46.5	161.3	25.0	299.9
240	144.2	246.3	53.3	115.9	7.3	851.9	27.4	226.0	40.9	151.3	22.6	273.9
241	218.0	374.3	64.1	124.9	8.7	922.4	31.8	251.5	47.3	169.3	27.9	287.6
242	177.2	304.3	52.6	123.8	7.3	897.2	29.6	220.1	41.2	158.0	25.0	261.0
243	141.9	243.7	42.5	122.7	6.0	871.0	27.3	190.8	35.5	146.8	22.2	235.2

Table A-7: Results - Reactor Power Balance

#	R disk [m]	W tfc [m]	W pfc [m]	P tfc [MW]	P pfc [MW]	P cd [MW]	P total [MW]	Z coil [m]	P cp [MW]
35 [keV]									
1	3.6	1.0	1.0	13100	838	31.4	13940	17.6	10480
2	3.4	1.0	1.0	10860	681	30.7	11540	16.7	8690
3	3.1	1.0	1.0	8878	545	30.1	9424	15.9	7117
4	3.9	1.0	1.0	13480	877	27.6	14360	18.4	10770
5	3.6	1.0	1.0	11300	722	27.1	12020	17.6	9032
6	3.5	1.0	1.0	11750	988	26.6	12740	18.3	9394
7	3.2	1.0	1.0	9730	803	26.1	10530	17.4	7787
8	3.0	1.0	1.0	7951	643	25.5	8594	16.5	6373
9	2.9	1.0	1.0	8272	899	25.2	9171	17.2	6631
10	2.9	1.0	1.0	6645	707	24.6	7352	16.2	5342
11	2.9	1.0	1.0	5245	545	23.9	5790	15.3	4230
12	3.7	1.0	1.0	11960	1022	23.2	12980	19.2	9548
13	3.5	1.0	1.0	10010	842	22.7	10860	18.3	8004
14	3.2	1.0	1.0	8290	684	22.2	8975	17.4	6635
15	3.0	1.0	1.0	8635	957	21.9	9592	18.1	6910
16	2.9	1.0	1.0	7048	766	21.4	7814	17.2	5650
17	2.9	1.0	1.0	5662	603	20.9	6264	16.2	4551
18	2.9	1.0	1.0	5896	866	20.6	6761	16.9	4742
19	2.9	1.0	1.0	4650	667	20.1	5317	15.9	3750
20	3.5	1.0	1.0	10480	1201	19.2	11680	20.0	8368
21	3.3	1.0	1.0	8771	989	18.8	9760	19.1	7010
22	3.0	1.0	1.0	7256	804	18.4	8060	18.1	5806
23	2.9	1.0	1.0	6172	925	17.8	7097	17.9	4951
24	2.9	1.0	1.0	4954	727	17.3	5681	16.9	3984
25	2.9	1.0	1.0	4076	831	16.7	4907	16.6	3288
26	3.5	1.0	1.0	8663	992	15.9	9655	20.0	6916
27	3.1	1.0	1.0	7572	1174	15.4	8746	19.9	6051
28	2.9	1.0	1.0	6259	955	15.0	7214	18.9	5008
29	2.9	1.0	1.0	4274	892	14.1	5166	17.7	3439
30	3.3	1.0	1.0	7335	1154	12.7	8489	20.9	5855
31	2.9	1.0	1.0	5301	1147	12.0	6447	19.8	4245
32	3.1	1.0	1.0	6074	1353	9.9	7426	21.9	4848
30 [keV]									
101	3.6	1.0	1.0	13100	838	37.2	13940	17.6	10480
102	3.4	1.0	1.0	10860	681	36.4	11540	16.7	8690
103	3.1	1.0	1.0	8878	545	35.6	9424	15.9	7117
104	3.9	1.0	1.0	13480	877	32.7	14360	18.4	10770
105	3.6	1.0	1.0	11300	722	32.1	12020	17.6	9032
106	3.4	1.0	1.0	9360	587	31.4	9947	16.7	7493

Table A-7 (cont.)

#	R disk [m]	W tfc [m]	W pfc [m]	P tfc [MW]	P pfc [MW]	P cd [MW]	P total [MW]	Z coil [m]	P cp [MW]
107	3.5	1.0	1.0	11750	988	31.6	12740	18.3	9394
108	3.2	1.0	1.0	9730	803	30.9	10530	17.4	7787
109	3.0	1.0	1.0	7951	643	30.2	8594	16.5	6373
110	2.9	1.0	1.0	6395	506	29.5	6901	15.6	5139
111	2.9	1.0	1.0	8272	899	29.8	9171	17.2	6631
112	2.9	1.0	1.0	6645	707	29.1	7352	16.2	5342
113	2.9	1.0	1.0	5245	545	28.4	5790	15.3	4230
114	3.9	1.0	1.0	11490	747	27.9	12240	18.4	9174
115	3.7	1.0	1.0	11960	1022	27.5	12980	19.2	9548
116	3.5	1.0	1.0	10010	842	26.9	10860	18.3	8004
117	3.2	1.0	1.0	8290	684	26.3	8975	17.4	6635
118	3.0	1.0	1.0	8635	957	26.0	9592	18.1	6910
119	2.9	1.0	1.0	7048	766	25.4	7814	17.2	5650
120	2.9	1.0	1.0	5662	603	24.8	6264	16.2	4551
121	2.9	1.0	1.0	5896	866	24.4	6761	16.9	4742
122	2.9	1.0	1.0	4650	667	23.8	5317	15.9	3750
123	3.7	1.0	1.0	10050	859	23.1	10910	19.2	8023
124	3.5	1.0	1.0	10480	1201	22.8	11680	20.0	8368
125	3.3	1.0	1.0	8771	989	22.3	9760	19.1	7010
126	3.0	1.0	1.0	7256	804	21.8	8060	18.1	5806
127	2.9	1.0	1.0	5922	644	21.3	6566	17.2	4747
128	2.9	1.0	1.0	6172	925	21.0	7097	17.9	4951
129	2.9	1.0	1.0	4954	727	20.5	5681	16.9	3984
130	2.9	1.0	1.0	4076	831	19.8	4907	16.6	3288
131	2.9	1.0	1.0	3146	624	19.2	3770	15.6	2544
132	3.5	1.0	1.0	8663	992	18.8	9655	20.0	6916
133	3.3	1.0	1.0	7249	818	18.4	8066	19.1	5793
134	3.1	1.0	1.0	7572	1174	18.2	8746	19.9	6051
135	2.9	1.0	1.0	6259	955	17.8	7214	18.9	5008
136	2.9	1.0	1.0	5101	764	17.4	5865	17.9	4091
137	2.9	1.0	1.0	4274	892	16.8	5166	17.7	3439
138	3.3	1.0	1.0	7335	1154	15.1	8489	20.9	5855
139	3.1	1.0	1.0	6134	951	14.7	7085	19.9	4902
140	2.9	1.0	1.0	5301	1147	14.3	6447	19.8	4245
141	2.9	1.0	1.0	4317	918	13.9	5235	18.7	3465
142	3.1	1.0	1.0	6074	1353	11.8	7426	21.9	4848
143	2.9	1.0	1.0	5075	1115	11.5	6190	20.8	4055
25 [keV]									
201	3.6	1.0	1.0	13100	838	45.4	13940	17.6	10480
202	3.4	1.0	1.0	10860	681	44.5	11540	16.7	8690

Table A-7 (cont.)

#	R disk [m]	W tfc [m]	W pfc [m]	P tfc [MW]	P pfc [MW]	P cd [MW]	P total [MW]	Z coil [m]	P cp [MW]
203	3.1	1.0	1.0	8878	545	43.5	9424	15.9	7117
204	2.9	1.0	1.0	7153	429	42.5	7582	15.1	5745
205	3.9	1.0	1.0	13480	877	40.0	14360	18.4	10770
206	3.6	1.0	1.0	11300	722	39.2	12020	17.6	9032
207	3.4	1.0	1.0	9360	587	38.4	9947	16.7	7493
208	3.1	1.0	1.0	7655	470	37.5	8126	15.9	6137
209	3.5	1.0	1.0	11750	988	38.6	12740	18.3	9394
210	3.2	1.0	1.0	9730	803	37.8	10530	17.4	7787
211	3.0	1.0	1.0	7951	643	36.9	8594	16.5	6373
212	2.9	1.0	1.0	6395	506	36.1	6901	15.6	5139
213	2.9	1.0	1.0	8272	899	36.4	9171	17.2	6631
214	2.9	1.0	1.0	6645	707	35.6	7352	16.2	5342
215	2.9	1.0	1.0	5245	545	34.7	5790	15.3	4230
216	3.9	1.0	1.0	11490	747	34.1	12240	18.4	9174
217	3.6	1.0	1.0	9627	615	33.4	10240	17.6	7696
218	3.7	1.0	1.0	11960	1022	33.5	12980	19.2	9548
219	3.5	1.0	1.0	10010	842	32.9	10860	18.3	8004
220	3.2	1.0	1.0	8290	684	32.2	8975	17.4	6635
221	3.0	1.0	1.0	6775	548	31.5	7323	16.5	5430
222	3.0	1.0	1.0	8635	957	31.8	9592	18.1	6910
223	2.9	1.0	1.0	7048	766	31.0	7814	17.2	5650
224	2.9	1.0	1.0	5662	603	30.3	6264	16.2	4551
225	2.9	1.0	1.0	5896	866	29.9	6761	16.9	4742
226	2.9	1.0	1.0	4650	667	29.1	5317	15.9	3750
227	2.9	1.0	1.0	3593	501	28.3	4093	14.9	2906
228	3.7	1.0	1.0	10050	859	28.2	10910	19.2	8023
229	3.5	1.0	1.0	8415	707	27.6	9122	18.3	6726
230	3.5	1.0	1.0	10480	1201	27.8	11680	20.0	8368
231	3.3	1.0	1.0	8771	989	27.3	9760	19.1	7010
232	3.0	1.0	1.0	7256	804	26.7	8060	18.1	5806
233	2.9	1.0	1.0	5922	644	26.1	6566	17.2	4747
234	2.9	1.0	1.0	6172	925	25.7	7097	17.9	4951
235	2.9	1.0	1.0	4954	727	25.1	5681	16.9	3984
236	2.9	1.0	1.0	3907	560	24.5	4468	15.9	3151
237	2.9	1.0	1.0	4076	831	24.1	4907	16.6	3288
238	2.9	1.0	1.0	3146	624	23.5	3770	15.6	2544
239	3.5	1.0	1.0	8663	992	23.0	9655	20.0	6916
240	3.3	1.0	1.0	7249	818	22.5	8066	19.1	5793
241	3.1	1.0	1.0	7572	1174	22.2	8746	19.9	6051
242	2.9	1.0	1.0	6259	955	21.8	7214	18.9	5008
243	2.9	1.0	1.0	5101	764	21.3	5865	17.9	4091

Table A-8: Results - Cost Analysis

#	ACCT 20 [M$]	ACCT 21 [M$]	ACCT 22 [M$]	ACCT 24 [M$]	ACCT 25 [M$]	ACCT 90 [M$]	ACCT 91 [M$]	ACCT 92 [M$]	ACCT 93 [M$]	ACCT 94 [M$]
35 [keV]										
1	3.3	164.4	860.0	45.4	41.8	1116.1	111.6	89.3	55.8	344.6
2	3.3	163.9	752.6	45.4	41.8	1008.1	100.8	80.6	50.4	311.2
3	3.3	163.5	655.0	45.4	41.8	909.9	91.0	72.8	45.5	280.9
4	3.3	165.0	883.5	45.4	41.8	1140.3	114.0	91.2	57.0	352.0
5	3.3	164.4	780.0	45.4	41.8	1036.1	103.6	82.9	51.8	319.9
6	3.3	164.7	857.8	45.4	41.8	1114.2	111.4	89.1	55.7	344.0
7	3.3	164.1	749.5	45.4	41.8	1005.2	100.5	80.4	50.3	310.3
8	3.3	163.7	651.1	45.4	41.8	906.2	90.6	72.5	45.3	279.8
9	3.3	163.9	730.5	45.4	41.8	985.9	98.6	78.9	49.3	304.4
10	3.3	163.4	623.6	45.4	41.8	878.3	87.8	70.3	43.9	271.2
11	3.3	163.0	528.4	45.4	41.8	782.6	78.3	62.6	39.1	241.6
12	3.3	165.3	874.1	45.4	41.8	1131.3	113.1	90.5	56.6	349.3
13	3.3	164.7	770.8	45.4	41.8	1027.2	102.7	82.2	51.4	317.1
14	3.3	164.1	676.3	45.4	41.8	932.0	93.2	74.6	46.6	287.7
15	3.3	164.4	752.7	45.4	41.8	1008.7	100.9	80.7	50.4	311.4
16	3.3	163.8	651.8	45.4	41.8	907.1	90.7	72.6	45.4	280.0
17	3.3	163.4	559.5	45.4	41.8	814.3	81.4	65.1	40.7	251.4
18	3.3	163.6	627.6	45.4	41.8	882.5	88.3	70.6	44.1	272.5
19	3.3	163.2	530.4	45.4	41.8	784.8	78.5	62.8	39.2	242.3
20	3.3	165.6	870.5	45.4	41.8	1128.1	112.8	90.2	56.4	348.3
21	3.3	164.9	766.3	45.4	41.8	1023.0	102.3	81.8	51.2	315.8
22	3.3	164.3	671.2	45.4	41.8	927.1	92.7	74.2	46.4	286.2
23	3.3	164.1	648.7	45.4	41.8	904.2	90.4	72.3	45.2	279.2
24	3.3	163.6	555.9	45.4	41.8	810.8	81.1	64.9	40.5	250.3
25	3.3	163.3	533.2	45.4	41.8	787.8	78.8	63.0	39.4	243.2
26	3.3	165.6	773.2	45.4	41.8	1030.8	103.1	82.5	51.5	318.2
27	3.3	165.2	757.2	45.4	41.8	1014.3	101.4	81.1	50.7	313.1
28	3.3	164.6	662.1	45.4	41.8	918.4	91.8	73.5	45.9	283.5
29	3.3	163.8	551.8	45.4	41.8	807.0	80.7	64.6	40.4	249.2
30	3.3	165.9	756.1	45.4	41.8	1014.0	101.4	81.1	50.7	313.1
31	3.3	164.9	650.1	45.4	41.8	906.7	90.7	72.5	45.3	279.9
32	3.3	166.4	736.1	45.4	41.8	994.6	99.5	79.6	49.7	307.1
30 [keV]										
101	3.3	164.4	878.5	45.4	41.8	1134.6	113.5	90.8	56.7	350.3
102	3.3	163.9	767.6	45.4	41.8	1023.1	102.3	81.8	51.2	315.9
103	3.3	163.5	667.0	45.4	41.8	921.9	92.2	73.7	46.1	284.6
104	3.3	165.0	900.2	45.4	41.8	1157.0	115.7	92.6	57.9	357.2
105	3.3	164.4	793.8	45.4	41.8	1049.9	105.0	84.0	52.5	324.1
106	3.3	163.9	696.4	45.4	41.8	951.9	95.2	76.1	47.6	293.9

Table A-8 (cont.)

#	ACCT 20 [M$]	ACCT 21 [M$]	ACCT 22 [M$]	ACCT 24 [M$]	ACCT 25 [M$]	ACCT 90 [M$]	ACCT 91 [M$]	ACCT 92 [M$]	ACCT 93 [M$]	ACCT 94 [M$]
107	3.3	164.7	877.3	45.4	41.8	1133.7	113.4	90.7	56.7	350.0
108	3.3	164.1	765.3	45.4	41.8	1021.0	102.1	81.7	51.1	315.2
109	3.3	163.7	663.8	45.4	41.8	918.9	91.9	73.5	45.9	283.7
110	3.3	163.3	570.9	45.4	41.8	825.4	82.5	66.0	41.3	254.8
111	3.3	163.9	749.6	45.4	41.8	1004.9	100.5	80.4	50.2	310.2
112	3.3	163.4	638.5	45.4	41.8	893.3	89.3	71.5	44.7	275.8
113	3.3	163.0	539.9	45.4	41.8	794.2	79.4	63.5	39.7	245.2
114	3.3	165.0	813.0	45.4	41.8	1069.8	107.0	85.6	53.5	330.3
115	3.3	165.3	891.4	45.4	41.8	1148.6	114.9	91.9	57.4	354.6
116	3.3	164.7	785.1	45.4	41.8	1041.5	104.1	83.3	52.1	321.5
117	3.3	164.1	687.9	45.4	41.8	943.6	94.4	75.5	47.2	291.3
118	3.3	164.4	770.1	45.4	41.8	1026.1	102.6	82.1	51.3	316.8
119	3.3	163.8	665.7	45.4	41.8	921.0	92.1	73.7	46.0	284.3
120	3.3	163.4	570.5	45.4	41.8	825.2	82.5	66.0	41.3	254.8
121	3.3	163.6	644.0	45.4	41.8	898.9	89.9	71.9	44.9	277.5
122	3.3	163.2	543.0	45.4	41.8	797.4	79.7	63.8	39.9	246.2
123	3.3	165.3	797.8	45.4	41.8	1054.9	105.5	84.4	52.7	325.7
124	3.3	165.6	888.9	45.4	41.8	1146.5	114.6	91.7	57.3	354.0
125	3.3	164.9	781.5	45.4	41.8	1038.2	103.8	83.1	51.9	320.5
126	3.3	164.3	683.5	45.4	41.8	939.5	93.9	75.2	47.0	290.0
127	3.3	163.8	594.0	45.4	41.8	849.4	84.9	67.9	42.5	262.2
128	3.3	164.1	663.5	45.4	41.8	919.1	91.9	73.5	46.0	283.7
129	3.3	163.6	567.5	45.4	41.8	822.5	82.2	65.8	41.1	253.9
130	3.3	163.3	547.0	45.4	41.8	801.6	80.2	64.1	40.1	247.5
131	3.3	162.9	456.3	45.4	41.8	710.4	71.0	56.8	35.5	219.3
132	3.3	165.6	785.9	45.4	41.8	1043.4	104.3	83.5	52.2	322.1
133	3.3	164.9	693.9	45.4	41.8	950.6	95.1	76.1	47.5	293.5
134	3.3	165.2	772.9	45.4	41.8	1030.0	103.0	82.4	51.5	318.0
135	3.3	164.6	674.3	45.4	41.8	931.1	93.1	74.5	46.6	287.5
136	3.3	164.0	584.5	45.4	41.8	840.1	84.0	67.2	42.0	259.4
137	3.3	163.8	564.2	45.4	41.8	819.4	81.9	65.6	41.0	253.0
138	3.3	165.9	768.6	45.4	41.8	1026.6	102.7	82.1	51.3	316.9
139	3.3	165.2	678.0	45.4	41.8	935.1	93.5	74.8	46.8	288.7
140	3.3	164.9	663.0	45.4	41.8	919.7	92.0	73.6	46.0	283.9
141	3.3	164.3	573.6	45.4	41.8	829.5	83.0	66.4	41.5	256.1
142	3.3	166.4	748.3	45.4	41.8	1006.7	100.7	80.5	50.3	310.8
143	3.3	165.6	659.4	45.4	41.8	916.3	91.7	73.4	45.8	283.1
25 [keV]										
201	3.3	164.4	899.4	45.4	41.8	1155.5	115.6	92.4	57.8	356.7
202	3.3	163.9	784.6	45.4	41.8	1040.1	104.0	83.2	52.0	321.1

Table A-8 (cont.)

#	ACCT 20 [M$]	ACCT 21 [M$]	ACCT 22 [M$]	ACCT 24 [M$]	ACCT 25 [M$]	ACCT 90 [M$]	ACCT 91 [M$]	ACCT 92 [M$]	ACCT 93 [M$]	ACCT 94 [M$]
203	3.3	163.5	680.6	45.4	41.8	935.5	93.5	74.8	46.8	288.8
204	3.3	163.1	586.4	45.4	41.8	840.8	84.1	67.3	42.0	259.6
205	3.3	165.0	919.2	45.4	41.8	1176.0	117.6	94.1	58.8	363.1
206	3.3	164.4	809.4	45.4	41.8	1065.5	106.6	85.2	53.3	329.0
207	3.3	163.9	709.1	45.4	41.8	964.6	96.5	77.2	48.2	297.8
208	3.3	163.5	617.9	45.4	41.8	872.8	87.3	69.8	43.6	269.5
209	3.3	164.7	899.4	45.4	41.8	1155.8	115.6	92.5	57.8	356.8
210	3.3	164.1	783.3	45.4	41.8	1039.0	103.9	83.1	52.0	320.8
211	3.3	163.7	678.2	45.4	41.8	933.3	93.3	74.7	46.7	288.1
212	3.3	163.3	582.2	45.4	41.8	836.8	83.7	66.9	41.8	258.3
213	3.3	163.9	771.2	45.4	41.8	1026.5	102.6	82.1	51.3	316.9
214	3.3	163.4	655.5	45.4	41.8	910.2	91.0	72.8	45.5	281.0
215	3.3	163.0	553.0	45.4	41.8	807.2	80.7	64.6	40.4	249.2
216	3.3	165.0	826.9	45.4	41.8	1083.7	108.4	86.7	54.2	334.6
217	3.3	164.4	730.8	45.4	41.8	986.9	98.7	79.0	49.3	304.7
218	3.3	165.3	911.1	45.4	41.8	1168.2	116.8	93.5	58.4	360.7
219	3.3	164.7	801.2	45.4	41.8	1057.6	105.8	84.6	52.9	326.5
220	3.3	164.1	701.0	45.4	41.8	956.7	95.7	76.5	47.8	295.4
221	3.3	163.7	610.1	45.4	41.8	865.1	86.5	69.2	43.3	267.1
222	3.3	164.4	789.8	45.4	41.8	1045.8	104.6	83.7	52.3	322.9
223	3.3	163.8	681.5	45.4	41.8	936.8	93.7	74.9	46.8	289.2
224	3.3	163.4	582.9	45.4	41.8	837.6	83.8	67.0	41.9	258.6
225	3.3	163.6	662.6	45.4	41.8	917.5	91.8	73.4	45.9	283.3
226	3.3	163.2	557.3	45.4	41.8	811.7	81.2	64.9	40.6	250.6
227	3.3	162.8	465.1	45.4	41.8	719.1	71.9	57.5	36.0	222.0
228	3.3	165.3	811.7	45.4	41.8	1068.9	106.9	85.5	53.4	330.0
229	3.3	164.7	716.8	45.4	41.8	973.2	97.3	77.9	48.7	300.5
230	3.3	165.6	909.9	45.4	41.8	1167.4	116.7	93.4	58.4	360.4
231	3.3	164.9	798.8	45.4	41.8	1055.5	105.5	84.4	52.8	325.9
232	3.3	164.3	697.5	45.4	41.8	953.5	95.4	76.3	47.7	294.4
233	3.3	163.8	605.3	45.4	41.8	860.6	86.1	68.8	43.0	265.7
234	3.3	164.1	680.3	45.4	41.8	935.9	93.6	74.9	46.8	288.9
235	3.3	163.6	580.8	45.4	41.8	835.7	83.6	66.9	41.8	258.0
236	3.3	163.1	492.4	45.4	41.8	746.8	74.7	59.7	37.3	230.5
237	3.3	163.3	562.7	45.4	41.8	817.3	81.7	65.4	40.9	252.3
238	3.3	162.9	468.1	45.4	41.8	722.2	72.2	57.8	36.1	223.0
239	3.3	165.6	800.3	45.4	41.8	1057.8	105.8	84.6	52.9	326.6
240	3.3	164.9	705.8	45.4	41.8	962.5	96.3	77.0	48.1	297.2
241	3.3	165.2	790.7	45.4	41.8	1047.8	104.8	83.8	52.4	323.5
242	3.3	164.6	689.3	45.4	41.8	945.6	94.6	75.7	47.3	291.9
243	3.3	164.0	596.1	45.4	41.8	851.7	85.2	68.1	42.6	262.9

Table A-8 (cont.)

#	ACCT 95 [M$]	ACCT 99 [M$]	CAP RET [M$]	O&M [M$]	FUEL [M$]	Capacity [kg/yr]	COF [$/gm]
35 [keV]							
1	212.8	1930.2	289.5	120.5	0.17	7.16E+06	57.30
2	192.2	1743.4	261.5	117.9	0.13	5.82E+06	65.20
3	173.5	1573.5	236.0	114.5	0.11	4.66E+06	75.24
4	217.4	1972.0	295.8	129.3	0.15	6.48E+06	65.59
5	197.5	1791.8	268.8	125.5	0.12	5.34E+06	73.81
6	212.4	1926.9	289.0	115.6	0.17	7.57E+06	53.49
7	191.6	1738.3	260.8	113.5	0.14	6.15E+06	60.85
8	172.8	1567.2	235.1	110.7	0.11	4.93E+06	70.21
9	188.0	1705.0	255.7	103.2	0.17	7.40E+06	48.51
10	167.4	1518.9	227.8	98.6	0.13	5.82E+06	56.09
11	149.2	1353.5	203.0	96.1	0.10	4.49E+06	66.72
12	215.7	1956.4	293.5	125.3	0.15	6.70E+06	62.57
13	195.8	1776.5	266.5	121.8	0.13	5.52E+06	70.40
14	177.7	1611.8	241.8	118.3	0.10	4.49E+06	80.30
15	192.3	1744.4	261.7	107.5	0.16	6.74E+06	54.76
16	172.9	1568.7	235.3	105.5	0.12	5.40E+06	63.14
17	155.2	1408.2	211.2	103.2	0.10	4.25E+06	74.05
18	168.3	1526.2	228.9	93.2	0.15	6.38E+06	50.53
19	149.6	1357.2	203.6	91.0	0.11	4.91E+06	59.98
20	215.1	1950.8	292.6	119.7	0.16	7.14E+06	57.78
21	195.0	1769.2	265.4	116.8	0.14	5.88E+06	65.00
22	176.8	1603.4	240.5	113.7	0.11	4.78E+06	74.09
23	172.4	1563.8	234.6	100.3	0.13	5.75E+06	58.22
24	154.6	1402.2	210.3	98.4	0.10	4.53E+06	68.25
25	150.2	1362.4	204.4	85.2	0.12	5.37E+06	53.90
26	196.5	1782.6	267.4	125.9	0.11	4.90E+06	80.38
27	193.4	1754.1	263.1	112.0	0.14	6.07E+06	61.88
28	175.1	1588.3	238.2	109.3	0.11	4.93E+06	70.49
29	153.9	1395.7	209.4	93.3	0.11	4.79E+06	63.19
30	193.3	1753.7	263.1	122.0	0.11	4.85E+06	79.41
31	172.9	1568.1	235.2	104.5	0.12	5.02E+06	67.74
32	189.6	1720.0	258.0	117.7	0.11	4.70E+06	80.05
30 [keV]							
101	216.3	1962.1	294.3	125.2	0.18	7.96E+06	52.71
102	195.1	1769.3	265.4	120.2	0.15	6.47E+06	59.59
103	175.8	1594.3	239.1	115.6	0.12	5.18E+06	68.45
104	220.6	2000.9	300.1	125.1	0.17	7.21E+06	58.99
105	200.2	1815.6	272.4	121.5	0.14	5.94E+06	66.31
106	181.5	1646.1	246.9	118.3	0.11	4.83E+06	75.63

Table A-8 (cont.)

#	ACCT 95 [M$]	ACCT 99 [M$]	CAP RET [M$]	O&M [M$]	FUEL [M$]	Capacity [kg/yr]	COF [$/gm]
107	216.1	1960.6	294.1	117.3	0.19	8.42E+06	48.90
108	194.7	1765.8	264.9	112.4	0.16	6.84E+06	55.16
109	175.2	1589.2	238.4	107.9	0.13	5.48E+06	63.22
110	157.4	1427.5	214.1	105.4	0.10	4.31E+06	74.17
111	191.6	1737.9	260.7	110.4	0.19	8.24E+06	45.08
112	170.3	1544.8	231.7	105.5	0.15	6.48E+06	52.08
113	151.4	1373.4	206.0	101.0	0.12	4.99E+06	61.56
114	203.9	1850.0	277.5	128.9	0.12	5.25E+06	77.38
115	219.0	1986.3	298.0	120.9	0.17	7.45E+06	56.29
116	198.6	1801.1	270.2	117.7	0.14	6.14E+06	63.25
117	179.9	1631.8	244.8	114.8	0.12	4.99E+06	72.11
118	195.6	1774.5	266.2	105.7	0.17	7.50E+06	49.61
119	175.6	1592.8	238.9	102.5	0.14	6.01E+06	56.88
120	157.3	1427.1	214.1	100.7	0.11	4.72E+06	66.67
121	171.4	1554.6	233.2	99.2	0.16	7.10E+06	46.86
122	152.0	1379.0	206.9	94.7	0.13	5.47E+06	55.20
123	201.1	1824.3	273.7	125.6	0.12	5.28E+06	75.71
124	218.6	1982.7	297.4	115.4	0.18	7.94E+06	52.03
125	197.9	1795.5	269.3	112.8	0.15	6.54E+06	58.44
126	179.1	1624.7	243.7	110.2	0.12	5.32E+06	66.58
127	161.9	1468.9	220.3	107.4	0.10	4.26E+06	76.98
128	175.2	1589.4	238.4	97.5	0.15	6.40E+06	52.50
129	156.8	1422.4	213.4	96.1	0.12	5.03E+06	61.49
130	152.8	1386.3	207.9	89.2	0.14	5.98E+06	49.73
131	135.4	1228.6	184.3	85.2	0.10	4.49E+06	60.03
132	198.9	1804.5	270.7	121.4	0.13	5.44E+06	72.07
133	181.2	1644.0	246.6	117.8	0.10	4.49E+06	81.27
134	196.4	1781.2	267.2	108.1	0.16	6.75E+06	55.66
135	177.5	1610.3	241.6	105.9	0.13	5.48E+06	63.38
136	160.2	1452.9	217.9	103.4	0.10	4.39E+06	73.21
137	156.2	1417.0	212.6	91.0	0.12	5.33E+06	56.98
138	195.7	1775.4	266.3	117.5	0.12	5.39E+06	71.21
139	178.3	1617.1	242.6	114.1	0.10	4.44E+06	80.29
140	175.3	1590.5	238.6	101.2	0.13	5.58E+06	60.94
141	158.1	1434.5	215.2	99.2	0.10	4.47E+06	70.42
142	191.9	1741.0	261.2	113.4	0.12	5.22E+06	71.79
143	174.8	1585.7	237.9	110.1	0.10	4.30E+06	80.94
25 [keV]							
201	220.3	1998.3	299.7	137.5	0.21	8.89E+06	49.21
202	198.3	1798.7	269.8	132.2	0.17	7.23E+06	55.64

Table A-8 (cont.)

#	ACCT 95 [M$]	ACCT 99 [M$]	CAP RET [M$]	O&M [M$]	FUEL [M$]	Capacity [kg/yr]	COF [$/gm]
203	178.4	1617.8	242.7	127.1	0.13	5.79E+06	63.93
204	160.3	1454.2	218.1	122.4	0.11	4.55E+06	74.85
205	224.2	2033.8	305.1	130.6	0.19	8.05E+06	54.15
206	203.1	1842.7	276.4	125.6	0.15	6.63E+06	60.64
207	183.9	1668.1	250.2	120.9	0.12	5.39E+06	68.86
208	166.4	1509.4	226.4	116.5	0.10	4.32E+06	79.46
209	220.4	1998.9	299.8	127.9	0.22	9.40E+06	45.55
210	198.1	1796.9	269.5	122.7	0.18	7.64E+06	51.37
211	177.9	1614.1	242.1	117.8	0.14	6.12E+06	58.87
212	159.5	1447.1	217.1	113.2	0.11	4.81E+06	68.68
213	195.7	1775.2	266.3	120.4	0.21	9.20E+06	42.08
214	173.5	1574.2	236.1	115.2	0.17	7.23E+06	48.59
215	153.9	1396.0	209.4	110.3	0.13	5.57E+06	57.41
216	206.6	1874.1	281.1	128.1	0.14	5.86E+06	69.83
217	188.2	1706.8	256.0	123.6	0.11	4.83E+06	78.62
218	222.7	2020.3	303.0	121.3	0.19	8.31E+06	51.09
219	201.6	1829.1	274.4	118.2	0.16	6.85E+06	57.35
220	182.4	1654.6	248.2	114.9	0.13	5.57E+06	65.24
221	164.9	1496.2	224.4	111.1	0.10	4.46E+06	75.31
222	199.4	1808.6	271.3	114.5	0.19	8.37E+06	46.10
223	178.6	1620.1	243.0	109.7	0.15	6.70E+06	52.64
224	159.7	1448.6	217.3	105.2	0.12	5.27E+06	61.19
225	174.9	1586.7	238.0	107.4	0.18	7.92E+06	43.62
226	154.8	1403.8	210.6	102.7	0.14	6.10E+06	51.35
227	137.1	1243.5	186.5	98.3	0.11	4.59E+06	62.15
228	203.8	1848.5	277.3	124.6	0.14	5.89E+06	68.30
229	185.5	1683.0	252.5	120.3	0.11	4.85E+06	76.88
230	222.6	2018.9	302.8	115.6	0.20	8.86E+06	47.26
231	201.2	1825.3	273.8	113.2	0.17	7.30E+06	53.04
232	181.8	1649.0	247.4	110.5	0.14	5.94E+06	60.32
233	164.1	1488.3	223.2	107.2	0.11	4.75E+06	69.57
234	178.4	1618.5	242.8	102.2	0.17	7.14E+06	48.32
235	159.3	1445.3	216.8	97.9	0.13	5.62E+06	56.02
236	142.4	1291.4	193.7	95.0	0.10	4.33E+06	66.74
237	155.8	1413.4	212.0	95.9	0.15	6.68E+06	46.15
238	137.7	1248.9	187.3	91.6	0.12	5.02E+06	55.65
239	201.7	1829.4	274.4	120.5	0.14	6.07E+06	65.06
240	183.5	1664.6	249.7	116.5	0.12	5.00E+06	73.22
241	199.8	1812.0	271.8	108.6	0.17	7.53E+06	50.56
242	180.3	1635.4	245.3	106.2	0.14	6.12E+06	57.47
243	162.4	1472.9	220.9	103.3	0.11	4.90E+06	66.20

B. PARAMETRIC SYSTEMS CODE

The systems code developed and utilized for design analysis in this research is listed for archival purposes in this appendix. The code was written using Turbo Pascal (Copyright Borland International Incorporated) programming language on IBM PC and IBM AT personal computers. The code prompts the user for design parameters and then calculates the system parameters as indicated in the main body of this thesis.

B.1. Code Listing

```
PROGRAM RESEARCH_MASTERS_THESIS; {user input   version 3.00   13/9/86}

{$I typedef.sys}                    {these files must be}
{$I graphix.sys}                    {included and in this order}
{$I kernel.sys}
{$I windows.sys}
{$I axis.hgh}


LABEL QUIT,JUMP;


TYPE
    DATETIMETYPE = STRING [8];
    REGTYPE      = RECORD
                     ax,bx,cx,dx,bp,si,di,ds,es,flags:  integer
                   END;


CONST

  CXX            :ARRAY [1..5,1..13] OF REAL= ((-21.3777,-25.2041,-7.1013E-2,
      1.9375E-4,4.9247E-6,-3.9837E-8,0.2935,0,0,0,0,0,0),(-15.5119,-35.3187,
      -1.2905E-2,2.6798E-4,-2.9199E-6,1.2748E-8,0.3735,0,0,0,0,0,0),(-15.9938,
      -35.1076,-1.3690E-2,2.7097E-4,-2.9442E-6,1.2841E-8,0.3725,0,0,0,0,0,0),(
      -27.7645,-31.0239,2.7890E-2,-5.5322E-4,3.0294E-6,-2.5233E-9,0.3597
      ,0,0,0,0,0,0),(-14.772,-35.474,-1.90e-2,2.8715E-4,-1.613E-6,9.5084E-10,
      0.3765,0,0,0,0,0,0));  {1--DT, 2--DDT,  3--DD3,  4--D3,  5--TT}
  ENERGY         :ARRAY [1..5] OF REAL=(17.59,4.03,3.27,18.3,11.33);
  Q=2.4;
  MU0=1.2566E-6;
  OWallBlnkt=1;
  OShld=0.5;
  LINECOST=80; {mills/kWeH}
  ENERDTN=14.1;
  ENERD3N=2.45;
  ENERTTN=5.04;
  Efiss=81.5E12;{MJ/kg}
  C=0.75;
  ALPHA=0.1;
  F=0.033;
  KC=0;
```

```
VAR

  PNUCLEAR,KAPA,A,R,R0,T0,BT,ASPECT,VOLUME,CI,EPSLN,IP,BETAC          :REAL;
  QWBS,NFLUX,FM,NTEMPAVE,N0,NAVE,AVETEMP,AVESIGV,NTND,NHE3ND         :REAL;
  NTNDPREV,NTNDTEST,NFLUXTT,WLTT,WLTOT,RCPS,POHMTOTAL,MFISS,PMULT    :REAL;
  PTHERM,NDPREV,NDTEST,NDAVE,NTAVE,NHE3AVE,NHE4ND,NHE4AVE            :REAL;
  FP,POWER,REACTPWR,ALFAN,ALFAT,D,RALFA,PWRTOTAL,PREQ,QPWRAVE        :REAL;
  A2,NFLUXDT,NFLUXD3,SURFACE,WLDT,WLD3,RHe3,BTMAX,MAXBT,PET          :REAL;
  BTMIN,RMAX,RMIN,TEMPMAX,TEMPMIN,AHET,ASPMAX,ASPMIN,Nsup            :REAL;
  NTEMP,N8AR,TEMPBAR,BTM1,THICKNS,FISPROD,RPROT,NPND,POHMMAX         :REAL;
  BTVAL,T0VAL,ASPVAL,RVAL,PEQUIV,IPMAX,PWRMIN,NPAVE,NEAVE            :REAL;
  FMRT,PCD,PAUXAVE,IBS,RDISK,POHMCP,POHMPFC,SQA,SQK,SQKA,majradius   :REAL;
  FCD,FPACK,NTRL,POHMTFC,OPTTRL,WPFCS,WTFCS,POHM,VETRL,I0            :REAL;
  BTINT,RINT,ASPINT,BTREP,ASPREP,RREP,TINT,TREP                      :INTEGER;
  I,J,COUNT,COUNTCOMP,N,OPTEMP                                       :INTEGER;
  FIRST,DTAOUT,UNIMPORT,DTAOUT2,BALANCE,BAL2,DES1OUT                 :TEXT;
  COST,COST2                                                         :TEXT;
  ANS                                                                :CHAR;
  HEADER                                                            :STRING[20];
  SIGVBAR,BTM2,TOP                                  :ARRAY[1..5] OF REAL;



FUNCTION DATE: DATETIMETYPE;
  {Returns Date in Form DD/MM/YY.}
VAR
   REG:        REGTYPE;
   Y,M,D,W:    DATETIMETYPE;
   I:          INTEGER;

BEGIN
   REG.AX:=$2A00;
   INTR($21,REG);
   STR(REG.CX:4,Y);
   DELETE(Y,1,2);
   STR(HI(REG.DX):2,M);
   STR(LO(REG.DX):2,D);
   W := D + '/' + M + '/' + Y;
   FOR I:=1 TO LENGTH(W) DO IF W[I]=' ' THEN W[I]:='0';
   DATE:=W
END;
```

```
FUNCTION TIME: DATETIMETYPE;
  {Returns Current Time in Form HH:MM:SS.}
VAR
   REG:         REGTYPE;
   H,M,S,T,W:   DATETIMETYPE;
   I:           INTEGER;

BEGIN
  REG.AX:=$2C00;
  INTR($21,REG);
  STR(HI(REG.CX):2,H);
  STR(LO(REG.CX):2,M);
  STR(HI(REG.DX):2,S);
  STR(LO(REG.DX):2,T);
  W:=H+':'+M+':'+S+':'+T;
  FOR I:= 1 TO LENGTH(W) DO IF W[I]=' ' THEN W[I]:='0';
  TIME:=W
END;



FUNCTION XYPWR (PWR,NUMBER :REAL) :REAL;

  BEGIN
    XYPWR:=EXP(PWR*LN(NUMBER))
  END; {OF FUNCTION XYPWR}


procedure OneAxisDem;

begin
  ClearScreen;                        {init screen}
  SetColorWhite;
  SetBackground(0);

  DefineHeader(1,'Plasma Model');    {define the window}
  SetHeaderOn;
  DefineWorld(1,-15,(15/1.26),15,(-15/1.26));
  SelectWindow(1);
  SelectWorld(1);

  DrawBorder;                         {draw it}

end;
```

```
procedure PlotPlasma;

var
   x,v1,v2      :real;


begin
InitGraphic;                          {initialize the graphics system}
OneAxisDem;                           {do the demo}
  x:=0;
  drawline(15,0,-15,0);
  drawline(0,15,0,-15);
  for i:=1 to 15 do begin
     drawline(i,0.5,i,-0.5);
     drawline(-i,0.5,-i,-0.5);
     drawline(0.5,i,-0.5,i);
     drawline(0.5,-i,-0.5,-i);
  end;
  drawline(r,-1,r,1);
  drawline(-r,-1,-r,1);
  while x<4*pi+0.01 do begin
     v1:=a*cos(x+d*sin(x));
     v2:=kapa*a*sin(x);
     DrawPoint(r+v1,v2);          {draw the point}
     DrawPoint(-(r+v1),v2);          {draw the point}
     x:=x+0.01;
  end;
LeaveGraphic;                         {leave the graphics system}
end;


PROCEDURE INPUT;

   BEGIN
     WRITELN;
     WRITELN;
     WRITE('ALFA N: ');
     READ(ALFAN);
     WRITE ('                ALFA T: ');
     READ(ALFAT);
     WRITE('             D-Shapeness: ');
     READLN(D);
     WRITELN;
     WRITE('He3 Removal: ');
     READ(RHE3);
     WRITE ('          He4 Removal: ');
```

```
    READ(RALFA);
    WRITE('        Proton Removal: ');
    READLN(RPROT);
    WRITELN;
    WRITE('FIELD on AXIS [T]          MAX: ');
    READ(BTMAX);
    WRITE ('             MIN: ');
    READ(BTMIN);
    WRITE ('         INTERVAL: ');
    READLN(BTVAL);
    WRITE('MAJOR RADIUS [m]           MAX: ');
    READ(RMAX);
    WRITE ('             MIN: ');
    READ(RMIN);
    WRITE ('         INTERVAL: ');
    READLN(RVAL);
    WRITE('ASPECT RATIO           MAX: ');
    READ(ASPMAX);
    WRITE ('             MIN: ');
    READ(ASPMIN);
    WRITE ('         INTERVAL: ');
    READLN(ASPVAL);
    WRITE('TEMPERATURE [keV]          MAX: ');
    READ(TEMPMAX);
    WRITE ('            MIN: ');
    READ(TEMPMIN);
    WRITE ('         INTERVAL: ');
    READLN(TOVAL);
    WRITELN;
    WRITE('MINIMUM ACCEPTABLE POWER: ');
    READLN(PWRMIN);
    WRITE('MAXIMUM ACCEPTABLE PLASMA CURRENT: ');
    READLN(IPMAX);
    WRITELN;WRITELN;
    WRITE('CURRENT DRIVE FACTOR (.15-.25): ');READLN(FCD);
    WRITE('PACKING FACTION: ');READLN(FPACK);
    WRITE('NUMBER OF TF RETURN LEGS: ');READLN(N);
    WRITE('OPERATING TEMPERATURE [C]: ');READLN(OPTEMP);
  END; {OF PROCEDURE INPUT}


PROCEDURE INTEGRAL1;

  CONST
    XX1                              :ARRAY [1..12] OF REAL=(-0.98156,
        -0.90412,-0.76990,-0.58732,-0.36783,-0.12523,0.12523,0.36783,
        0.58732,0.76990,0.90412,0.98156);
```

```
    W1                                  :ARRAY [1..12] OF REAL=(0.04718,
          0.10694,0.16008,0.20317,0.23349,0.24915,0.24915,0.23349,0.20317,
          0.16008,0.10694,0.04718);

VAR
    SUMYNT,SUMYNB,SUMYTB,SUMYVOL,XUL,XLL,AHET,csi,br1,br2,sn1,abr1     :REAL;
    SUMxNT,SUMxNB,SUMxTB,NTEMPFN,NBARFN,SUMxVOL,kasn1,y2a,sqy2a,y2     :REAL;
    X,Y,DVOL,YUL,YLL,TEMP,NSQRD,SUMYBM1,SUMxBM1,kys,ybr1,WIDV       :REAL;
    XAVE,YAVE,SURX                                                  :REAL;
    K,L,m                                                :INTEGER;
    SUMYSF,SIGVFN,SUMYTOP,SUMYBM2          :ARRAY [1..5] OF REAL;
    SUMxSF,SUMxTOP,SUMxBM2                 :ARRAY [1..5] OF REAL;

BEGIN
    SUMxNT:=0;SUMxNB:=0;SUMxTB:=0;NTEMPFN:=0;NBARFN:=0;
    SUMxBM1:=0;SUMxVOL:=0;surx:=0;
    FOR K:=1 TO 5 DO BEGIN
       SUMxSF[K]:=0;SIGVFN[K]:=0;SUMxTOP[K]:=0;SUMxBM2[K]:=0
    END;
    YUL:=A;XUL:=PI;
    YLL:=0;XLL:=0;
    for m:= 1 to 12 do begin
       X:=(XUL+XLL-(XLL-XUL)*XX1[m])/2;
       SUMYNT:=0;SUMYNB:=0;SUMYTB:=0;
       SUMYBM1:=0;SUMYVOL:=0;
       csi:=cos(x);sn1:=sin(x);
       br1:=cos(x+d*sn1);
       br2:=sin(x+d*sn1);
       abr1:=a*br1;kasn1:=kapa*a*sn1;
       ahet:=sqrt(abr1*abr1+kasn1*kasn1);
       FOR K:=1 TO 5 DO BEGIN
          SUMYSF[K]:=0;SUMYTOP[K]:=0;SUMYBM2[K]:=0
       END;
       FOR L:= 1 TO 12 DO BEGIN
          Y:= (YUL+YLL-(YLL-YUL)*XX1[L])/2;
          ybr1:=y*br1;kys:=kapa*y*sn1;
          DVOL:=(R+ybr1)*PI*4*KAPA*(ybr1*csi
                +sn1*Y*br2*(D*csi+1));
          y2:=sqrt(ybr1*ybr1+kys*kys);
          y2a:=y2/ahet;sqy2a:=y2a*y2a;
          TEMP:=TO*(1+ALFAT)*XYPWR(ALFAT,(1-sqy2a));
          NTEMPFN:=XYPWR((ALFAN+ALFAT),(1-sqy2a));
          NBARFN:=XYPWR(ALFAN,(1-sqy2a));
          NSQRD:= XYPWR(2*ALFAN,(1-sqy2a));
          widv:=w1[l]*dvol;
          SUMYNT:= widv*NTEMPFN+SUMYNT;
          SUMYVOL:=widv+SUMYVOL;
```

```
                SUMYNB:= wldv*NBARFN+SUMYNB;
                SUMYTB:=wldv*TEMP+SUMYTB;
                FOR K:= 1 TO 5 DO BEGIN
                   SIGVFN[K]:= EXP(CXX[K,1]*XYPWR(-CXX[K,7],TEMP)+CXX[K,2]
                     +CXX[K,3]*TEMP+CXX[K,4]*temp*TEMP+CXX[K,5]*temp*temp*TEMP
                     +CXX[K,6]*XYPWR(4,TEMP));
                   SUMYTOP[K]:=wldv*SIGVFN[K]*NSQRD+SUMYTOP[K];
                END;
             END;
             yave:=(yul-yll)/2;
             SUMYNT:=SUMYNT*yave;SUMXNT:= SUMYNT*W1[M]+SUMXNT;
             SUMYTB:=SUMYTB*yave;SUMXTB:= SUMYTB*W1[M]+SUMXTB;
             SUMYNB:=SUMYNB*yave;SUMXNB:= SUMYNB*W1[M]+SUMXNB;
             SUMYVOL:=SUMYVOL*yave;SUMXVOL:= SUMYVOL*W1[M]+SUMXVOL;
             SURX:=abs((-abr1*br2*(1+d*cs1)+a*kapa*kapa*sn1*cs1)/sqrt(br1*br1+kapa*kapa*sn1*sn1))*W1[M]+SURX;
             FOR K:= 1 TO 5 DO BEGIN
                SUMYTOP[K]:= SUMYTOP[K]*yave;SUMXTOP[K]:= SUMYTOP[K]*W1[M]+SUMXTOP[K];
             END;
          END;
          xave:=(xul-xll)/2;
          NTEMP:=SUMXNT*xave;
          TEMPBAR:=SUMXTB*xave;
          NBAR:=SUMXNB*xave;
          VOLUME:=SUMXVOL*xave;
          SURFACE:=SURX*4.4*pi*pi*R*XAVE;
          writeln;writeln(r:5:2,'   ',a:5:2,'   ',sqrt((1+kapa*kapa)*a*a/2):7:2,'   ',surx*xave:7:2,'     ',surfa
ce:8:2);
          FOR K:= 1 TO 5 DO BEGIN
             TOP[K]:= SUMXTOP[K]*xave;
          END;
       END; {OF PROCEDURE INTEGRAL1}


       PROCEDURE MAGNET;

          LABEL
             JUMP;

          VAR
             Z,ROHMPFC,GAMMA,LELPS,LTRL,ROHMCP,ROHMDISK,POHMTRL          :REAL;
             POHMDISK,TAUT,TAUR,TAUA,OMEGA,BP0,RHOCU,RHOMASS,BR1,SQI0    :REAL;
             ROHMTRL,RCP0                                                :REAL;
             WPFCO,WTFCO                                                 :INTEGER;

          BEGIN
             RHOCU:=2.45E-10*OPTEMP+1.22E-8;
             SQI0:=I0*I0;
```

```
    WTFCO:=1;
    WPFCO:=1;
    RDISK:=N*WTFCO/2/PI;
    RCPO:=R-1.1*A-0.3;
    IF (RDISK<RCPO) THEN RDISK:=RCPO;
    BR1:=KAPA*A+2*OWBS;
    LELPS:=PI*SQRT((SQA+BR1*BR1)/2);
    LTRL:=2*R+2.2*A+LELPS-2*RDISK;
    ROHMTRL:=1.71E-8*LTRL/FPACK/WTFCO*WTFCO;
    Z:=2*(KAPA+0.1)*A+2*OWBS+2*WTFCO;
    ROHMCP:=RHOCU*Z/FPACK/PI/RCPO*RCPO;
    ROHMDISK:=1.71E-8*(LN(RDISK)-LN(RCPO))/2/PI/WTFCO/FPACK;
    POHMTRL:=SQIO/N/N*ROHMTRL;
    POHMCP:=SQIO*ROHMCP;
    POHMDISK:=SQIO*ROHMDISK;
    POHMTFC:=(POHMTRL*N+POHMCP+POHMDISK)/1e6;
    ROHMPFC:=1.71E-8*6*PI*A/FPACK/WPFCO;
    BR1:=0.3E6*IP;
    POHMPFC:=2*BR1*BR1*ROHMPFC/1e6;
    POHMTOTAL:=POHMTFC+POHMPFC;
    (* IF (POHMTOTAL>POHMMAX) THEN GOTO JUMP; *)
    OPTTRL:=LTRL+RDISK;
    VETRL:=PI*(R+3*A)*(2*(R-RCPO)+8*A+2*(KAPA+0.1)*A+2*OWBS+WTFCO);
    RHOMASS:=1.67e-27*(2*ndave+3*(ntave+nhe3ave)+4*nhe4ave+npave);
    TauA:=SQRT(mu0*RHOMASS)/BT/FM;
    TauR:=mu0*SQA*KAPA/(8.32e-4*xypwr(-1.5,avetemp*1e3));
    TauT:=XYPWR(0.6,TauR)*XYPWR(0.4,TauA);
    GAMMA:=SQRT(TauT/TauR);
    BP0:=MU0*IP*1E6/4/PI/A;
    OMEGA:=1/TauT;
    PCD:=FCD*VETRL*OMEGA*GAMMA*SQRT(XYPWR(4,BT)+XYPWR(4,BP0))/MU0/1e6;
    WRITELN(DES1OUT,COUNTCOMP:3,',',RDISK:10,',',WTFCO:10,',',WPFCO:10,
        ',',POHMTFC:10,       ',',POHMPFC:10,',',PCD:10,',',POHMTOTAL:10,
       ',',Z:10,',',POHMCP/1E6:10);
    FLUSH(DES1OUT);
    JUMP: END;  {OF PROCEDURE MAGNET}


PROCEDURE PWRBALANCE;

VAR

   XE,TE,PTR,PAUX,QPWR                              :ARRAY [1..5] OF REAL;
   ZEFF,K2,XI,PAUX1,PB,D,EATA,PC,PCP,PCDR,BR1,NE20,SQK2          :REAL;
   SQK1                                                          :REAL;
```

```
BEGIN
   PAUXAVE:=0;QPWRAVE:=0;
   BR1:=NEAVE/(NAVE-NEAVE);
   ZEFF:=BR1*BR1;
   NE20:=NEAVE*1E-20;
   sqk2:=2*sqk;
   sqk1:=1+sqk;
   XE[1]:= (4.68*A/(ne20*R*R*Q))*SQRT(sqk2/(sqk1));
   XE[2]:=5.95*XYPWR(1.02,(A*SQRT((sqk1)/2)))
          *XYPWR(-0.9,(ne20))*XYPWR(-1.63,r)*XYPWR(-0.23,ZEFF);
   XE[3]:=0.96*SQRT(sqk2/sqk1)*SQA/IP;
   XE[4]:=3.75*SQK2*SQA/(IP*R*sqk1);
   XE[5]:=625*XYPWR(0.76,BETAC)*XYPWR(1.73,BT)*XYPWR(0.62,(0.1*AVETEMP))
          *XYPWR(3.38,A)*XYPWR(0.71,KAPA)*XYPWR(-2.95,IP)*XYPWR(-2.55,ASPECT);
   K2:=(0.66+1.88*XYPWR(-0.5,ASPECT)-1.54/ASPECT)*(1+1.5/ASPECT*ASPECT);
   XI:=4.12E-22*K2*XYPWR(1.5,ASPECT)*(NAVE-NEAVE)*ZEFF*Q*Q
       *XYPWR(-0.5,(0.1*AVETEMP))/(BT*BT*sqk1);
   PB:=5.35E-43*NEAVE*NEAVE*ZEFF*SQRT(AVETEMP)*VOLUME;
   EATA:=8.32E-4*XYPWR(-1.5,(AVETEMP*1E3));
   D:=2*NEAVE*A*XYPWR(-0.75,(1-BETAC))/SQRT(EATA*XYPWR(3,BT));
   PC:=KC*6.21E-23*NEAVE*AVETEMP*BT*BT*VOLUME*(1+AVETEMP/146);
   PCP:=0.2*CXX[1,13]+CXX[2,13]+0.25*CXX[3,13]+CXX[4,13]+0.11*CXX[5,13];
   PCDR:=IP*IP*EATA*4*R/(SQA*(sqk1));
   PAUX1:=PB+PC-PCP-PCDR;
   WRITE(BAL2,COUNTCOMP:3,',',PB:7:2,',',PCP:7:2,',',PCDR:6:2);
   WRITE(BALANCE,COUNTCOMP:3,',');
   FOR I:=1 TO 5 DO BEGIN
      TE[I]:=6*SQKA/(8*(XE[I]+XI)*(sqk1));
      PTR[I]:=0.5969*betac*FM*BT*fm*bt*volume/te[i];   {1.5*1.602E-22*NTEMPAVE*VOLUME/TE[I]}
      PAUX[I]:=PAUX1+PTR[I];
      QPWR[I]:=PTHERM/PAUX[I];
      WRITE (BAL2,',',TE[I]:6:2,',',PTR[I]:7:2);
      FLUSH(BAL2);
      WRITE(BALANCE,PAUX[I]:7:2,',',QPWR[I]:8:2,',');
      FLUSH(BALANCE);
      IF (PAUX[I]<0) THEN PAUX[I]:=0;
      IF (QPWR[I]<0) THEN QPWR[I]:=9.9999999E8;
      PAUXAVE:=(PAUXAVE+PAUX[I])/5;
      QPWRAVE:=(QPWRAVE+QPWR[I])/5;
   END;
   IF (QPWRAVE>3*9.9999999E8/5) THEN QPWRAVE:=0;
   WRITE(FIRST,PAUXAVE:5:2,' ',QPWRAVE:9:0,' ');
   WRITE(LST,PAUXAVE:5:2,' ',QPWRAVE:9:0,' ');
   WRITELN(BAL2);
   WRITELN(BALANCE);
END; {OF PROCEDURE PWRBALANCE}
```

```
PROCEDURE MERIT;

  VAR
    PNET                        :REAL;

  BEGIN

    PNET:=PAUXAVE-PCD;
    IF (PNET<0) THEN PNET:=0;
    PREQ:=((PNET+30)/0.5)+PCD/0.4;
    FMRT:=(0.40*PEQUIV-PREQ)/1000;
    WRITE (FIRST,FMRT:7:2,' ');
    WRITE (LST,FMRT:6:2,' ');
END;{OF PROCEDURE MERIT}


PROCEDURE COSTANALYSIS;

   CONST
      ACCT20=3.3;
      AVAILABILITY=0.8;
      ACCT23=0.0;
      ACCT24=45.4;

   VAR
      ACCT21T,ACCT22T,ACCT25T,ACCT26,ACCT90,ACCT91,ACCT92,ACCT93     :REAL;
      FUELREQ,PREQCOST,ACCT94,ACCT95,ACCT99,ALONG,PISQ,SQ1,SQ2,PET   :REAL;
      VPLAS,RPLASSQ,RBLNKTSQ,VBLNKT,RSHLDSQ,VSHLD,VRB,VC,VVAC        :REAL;
      CAPRETURN,FWBLIFE,OM,FUELCOST,CAPFACTOR,SELLCOST               :REAL;
      ACCT21,ACCT22             :ARRAY[1..9] OF REAL;
      ACCT25                    :ARRAY[1..6] OF REAL;
      ACCT221                   :ARRAY[1..10] OF REAL;

   BEGIN
      ALONG:=(KAPA+0.1)*A;
      PISQ:=PI*PI;
      RPLASSQ:=((2.2*SQA*2.2)+ALONG*ALONG)/4;
      VPLAS:=PISQ*R*RPLASSQ;
      SQ1:=2.2*A+OWALLBLNKT;
      SQ2:=ALONG+OWALLBLNKT;
      RBLNKTSQ:=(SQ1*SQ1+SQ2*SQ2)/4;
      VBLNKT:=PISQ*R*RBLNKTSQ-VPLAS;
      SQ1:=SQ1+OSHLD;
      SQ2:=SQ2+OSHLD;
      RSHLDSQ:=(SQ1*SQ1+SQ2*SQ2)/4;
      VSHLD:=PISQ*R*RSHLDSQ-VPLAS-VBLNKT;
```

```
SQ2:=SQ2+WTFCS;
VRB:=12*PI*A*R*SQ2;
VC:=PI*Rcps*Rcps*SQ2+18*OPTTRL*WTFCS*WTFCS+12*PI*A*WPFCS*WPFCS;
VVAC:=VSHLD+VBLNKT+VPLAS;
PET:=0.35*PNUCLEAR;
ACCT21[1]:=11.15;
ACCT21[2]:=3E-4*VRB+39.5;
ACCT21[3]:=0;
ACCT21[4]:=7.135*XYPWR(0.3,PET/1000);
ACCT21[5]:=9.16;
ACCT21[6]:=76.5;
ACCT21[7]:=1.81;
ACCT21T:=ACCT21[1]+ACCT21[2]+ACCT21[3]+ACCT21[5]+ACCT21[6]+ACCT21[7];
ACCT21[8]:=0.02*ACCT21T;
ACCT21[9]:=0.15*ACCT21T;
ACCT21T:=ACCT21T+ACCT21[8]+ACCT21[9];
ACCT221[1]:=0.31*VBLNKT*0.05;
ACCT221[2]:=0.105*VSHLD;
ACCT221[3]:=0.584*VC;
ACCT221[4]:=0.0;
ACCT221[5]:=0.112*(0.05*VRB);
ACCT221[6]:=0.0051*VVAC;
ACCT221[7]:=0.028*Ptherm+1.00;
ACCT221[8]:=14.3;
ACCT221[9]:=0.0;
ACCT221[10]:=2.82;
ACCT22[1]:=0;
FOR I:=1 TO 10 DO ACCT22[1]:=ACCT22[1]+ACCT221[I];
ACCT22[2]:=0.069*PTHERM;
ACCT22[3]:=6.7E-4*PTHERM+32.6;
ACCT22[4]:=0.0012*PTHERM;
ACCT22[5]:=0.00965*PTHERM;
ACCT22[6]:=0.010938*PTHERM;
ACCT22[7]:=23.41;
ACCT22T:=ACCT22[1]+ACCT22[2]+ACCT22[3]+ACCT22[5]+ACCT22[6]+ACCT22[7];
ACCT22[8]:=0.02*ACCT22T;
ACCT22[9]:=0.15*ACCT22T;
ACCT22T:=ACCT22T+ACCT22[8]+ACCT22[9];
ACCT25[1]:=15.68;
ACCT25[2]:=12.35;
ACCT25[3]:=6.22;
ACCT25[4]:=1.20;
ACCT25T:=ACCT25[1]+ACCT25[2]+ACCT25[3]+ACCT25[4];
ACCT25[5]:=0.03*ACCT25T;
ACCT25[6]:=0.15*ACCT25T;
ACCT25T:=ACCT25T+ACCT25[5]+ACCT25[6];
```

```
      ACCT26:=0.0142*VBLNKT*0.15; {COST OF U-238 SALT}
      ACCT90:=ACCT20+ACCT21T+ACCT22T+ACCT23+ACCT24+ACCT25T+ACCT26;
      ACCT91:=0.1*ACCT90;
      ACCT92:=0.08*ACCT90;
      ACCT93:=0.05*ACCT90;
      ACCT94:=0;
      ACCT95:=0;
      ACCT99:=ACCT90+ACCT91+ACCT92+ACCT93;
      FOR I:=1 TO 5 DO BEGIN
         ACCT94:=0.251*ACCT99;
         ACCT95:=0.155*ACCT99;
      END;
      ACCT99:=ACCT99+ACCT95+ACCT94;
      CAPRETURN:=0.15*ACCT99;
      FWBLIFE:=12/WLTOT;
      PREQCOST:=LINECOST*PREQ*AVAILABILITY*8760E-6; {M$/yr}
      OM:=ACCT221[1]*AVAILABILITY/FWBLIFE+0.02*ACCT99+PREQCOST;
      FUELREQ:=22E-6*1.05*FISPROD*AVAILABILITY;
      CAPFACTOR:=FISPROD*AVAILABILITY*1000;
      FUELCOST:=(CAPRETURN+OM+FUELREQ)*1.0E6/CAPFACTOR;    {1980$/GRAM PU-239}
      SELLCOST:=0.032*FUELCOST*1E3+0.968*22;   {1980$/kg installed}
      WRITELN(FIRST,' ',FUELCOST:8:3,' ',SELLCOST:8:2);
      WRITELN(LST,' ',FUELCOST:7:2,' ',SELLCOST:8:2);
      WRITELN(COST,ACCT20:6:1,' ',ACCT21T:6:1,' ',ACCT22T:6:1,' ',ACCT23:6:1,
          ' ',ACCT24:6:1,' ',ACCT25T:6:1,' ',ACCT26:6:1,' ',ACCT90:6:1,' ',
          ACCT91:6:1,' ',ACCT92:6:1,' ',ACCT93:6:1,' ',ACCT94:6:1,' ',
          ACCT95:6:1,' ',ACCT99:7:2);
      FLUSH(COST);
      WRITELN(COST2,CAPRETURN:7:2,' ',OM:7:2,' ',
          FUELREQ:7:2,' ',CAPFACTOR:10,' ',FUELCOST:7:3,' ',SELLCOST:7:3);
      FLUSH(COST2);
END; {OF PROCEDURE COST}


PROCEDURE OUTPUT;

  BEGIN
     WRITE (DTAOUT,COUNTCOMP:3,',',R:5:1,',',A:5:1,',',ASPECT:5:1,',',
          KAPA:5:1,',',BT:5:1,',',BETAC:6:3,',',IP:6:2,',',AVETEMP:6:2,',',
          (FISPROD*0.8):10,',',PWRTOTAL:10,',',(NAVE-neave):10,',',PEQUIV:10,',',
          NSUP:7:2,',',VOLUME:7:1,',');
     WRITELN (DTAOUT,NDAVE:10,',',NTAVE:10,',',NHE3AVE:10,',',NHE4AVE:10,','
          ,NPAVE:10,',',NEAVE:10,',',FM:6:3,',',(NFLUX/surface):10);
     FLUSH(DTAOUT);
     WRITE(DTAOUT2,COUNTCOMP:3,',');
     FOR I := 1 TO 5 DO
```

```
        WRITE (DTAOUT2,CXX[I,9]:9,',',CXX[I,13]:10,',');{Fp AND P}
    WRITE (DTAOUT2,WLTOT:7:3,',',WLDT:6:3,',',WLD3:6:3,',',WLTT:6:3,',');
    FOR I:=1 TO 5 DO WRITE (DTAOUT2,CXX[I,8]:10,',');
    WRITELN (DTAOUT2,SURFACE:7:1,',',THICKNS:5:2,',',MAXBT:6:2);
    FLUSH(DTAOUT2);
END;{OF PROCEDURE OUTPUT}



BEGIN  {MAIN PROGRAM}
  clrscr;
  INPUT;
  ASSIGN (FIRST,'FIRSTTS.PRN');
  REWRITE (FIRST);
  ASSIGN (DTAOUT,'TST1.prn');
  REWRITE (DTAOUT);
  ASSIGN (DTAOUT2,'TST2.prn');
  REWRITE (DTAOUT2);
  ASSIGN (BALANCE,'TSBL.PRN');
  REWRITE (BALANCE);
  ASSIGN (BAL2,'TSB2.PRN');
  REWRITE (BAL2);
  ASSIGN (DES1OUT,'D1TS.PRN');
  REWRITE (DES1OUT);
  ASSIGN(COST,'COSTTS.PRN');
  REWRITE(COST);
  ASSIGN(COST2,'COSTSUM.PRN');
  REWRITE(COST2);
  HEADER:=CONCAT(DATE,'    ',TIME);
  WRITELN(FIRST,HEADER);
  WRITELN(DTAOUT,HEADER);
  WRITELN (DTAOUT,ALFAN:6:2,',',ALFAT:6:2,',',D:6:2,','
    ,RALFA:6:2,',',RHE3:6:2,',',rprot:6:2,',',BTMIN:6:2,',',BTMAX:6:2,','
    ,TEMPMIN:7:1,',',TEMPMAX:7:1,',',RMIN:6:2,',',RMAX:6:2,',',PWRMIN:7:1
    ,',',IPMAX:6:1,',',FCD:5:2,',',FPACK:5:2,',',N:4);
  FLUSH(DTAOUT);
  writeln(dtaout);
  WRITELN(DTAOUT);
  WRITELN;
  WRITELN ('Research Phase 2  --- Automatic mode');
  WRITELN;
  WRITELN ('Program Begins ---- Press Q to terminate');
  COUNT:=0;
  COUNTCOMP:=0;
  TINT:=TRUNC((TEMPMAX-TEMPMIN)/TOVAL);
  TO:=TEMPMAX;
```

```
FOR TREP:=1 TO TINT+1 DO BEGIN
  WRITELN(FIRST);
  WRITELN(FIRST);
  WRITELN(FIRST,'T = ',T0:6:1);
  WRITELN(FIRST);
  WRITELN(LST,HEADER);WRITELN(LST);writeln(lst,chr(15));
  WRITELN(LST,'R     ':6,'A     ':6,'B to ':5,'Beta  ':5,'P fus  ':7,
     'P therm  ':8,'Vp   ':7,'Ip   ':5,'Rcps ':6,'IBS ':6,'n flux   ':9,
     'F [kg/yr] ':9,'P cd  ':7,'P aux  ':8,'Q    ':7,'F merit ':7,'Cost  ':7,
     'SELLCOST ':9);
  WRITELN(FIRST,'R     ':6,'A     ':6,'B to  ':6,'Beta  ':5,'P fus  ':8,
     'P THERM  ':9,'Vp   ':7,'Ip   ':5,'Rcps ':5,'IBS ':5,'n flux ':10,
     'F [kg/yr] ':10,'P cd  ':6,'P tfc ':7,'P pfc ':7,'P aux  ':8,
     'Q    ':7,'F merit ':7,'COST ':7,'SELLCOST ':10);
  FLUSH(FIRST);
  WRITELN(COST,'ACCT 20 ':7,'ACCT 21 ':7,'ACCT 22 ':7,'ACCT 23 ':7,
      'ACCT 24 ':7,'ACCT 25 ':7,'ACCT 26 ':7,'ACCT 90 ':7,'ACCT 91 ':7,
      'ACCT 92 ':7,'ACCT 93 ':7,'ACCT 94 ':7,'ACCT 95 ':7,'ACCT 99 ':7);
  WRITELN(COST);FLUSH(COST);
  WRITELN(COST2,'CAP RET ':9,'O&M ':9,'FUEL ':9,'CAPACITY ':10,
      'FUEL COST [$/gal]':18,'SELLCOST [$/kg installed] ':18);
  WRITELN(COST2);FLUSH(COST2);
  WRITELN(DES1OUT,'# ':3,'R disk ':10,'W tfc ':10,'W pfc ':10,'P tfc ':10,
      'P pfc ':10,'P cd ':10,'P total ':10,'Z coil ':10,'P cp ':10);
  WRITELN(DES1OUT);FLUSH(DES1OUT);
  WRITELN(BAL2,'# ':3,'P brem ':9,'P part ':9,'P cd heat ':10,
      'Tau e ':9,'P tr ':10,'Tau e ':9,'P tr ':10,'Tau e ':9,'P tr ':10,
      'Tau e ':9,'P tr ':10,'Tau e ':9,'P tr ':10);
  WRITELN(BAL2);FLUSH(BAL2);
  WRITELN(BALANCE,'# ':3,'P aux ':9,'Q plasma ':10,'P aux ':9,'Q plasma ':10,
      'P aux ':9,'Q plasma ':10,'P aux ':9,'Q plasma ':10,'P aux ':9,
      'Q plasma ':10);
  WRITELN(BALANCE);FLUSH(BALANCE);
  WRITELN(FIRST);
  WRITELN(LST);
  FLUSH(LST);
  BTINT:=TRUNC((BTMAX-BTMIN)/BTVAL);
  ASPINT:=TRUNC((ASPMAX-ASPMIN)/ASPVAL);
  RINT:=TRUNC((RMAX-RMIN)/RVAL);
  WRITELN(TINT,BTINT,ASPINT,RINT);
  BT:=BTMAX;
  FOR BTREP:=1 TO BTINT+1 DO BEGIN
    ASPECT:=ASPMAX;
    FOR ASPREP:=1 TO ASPINT+1 DO BEGIN
      R:= RMAX;
      FOR RREP:=1 TO RINT+1 DO BEGIN
```

```
{CLRSCR; }
IF KEYPRESSED THEN goto quit;
COUNT:=COUNT+1;
WRITE('PASS #',COUNT:4,'     SUCCESSFUL ',COUNTCOMP:4,'       ');
WRITELN('R: ',R:5:2,'    A: ',ASPECT:5:2,'   Bt: ',BT:5:2);
MFISS:=1.33;
PMULT:=1.615E-18;
A:=R/ASPECT;
SQA:=A*A;
A2:=1.1*A;  {PLASMA CHAMBER RADIUS}
THICKNS:=R-A2;
IF THICKNS<0.6 THEN GOTO JUMP;
I0:=2*PI*R*BT/MU0;
RCPS:=SQRT(I0/1500E4)/2/PI;   {SQRT(I0/1500/1E4)}
WRITE('   Rcps ':10,RCPS:7:2);
IF RCPS>1.0 THEN GOTO JUMP;
WTFCS:=SQRT(I0/1500E4/N);
WRITE('   WTFCS ':10,WTFCS:6:3);
IF WTFCS>1.0 THEN GOTO JUMP;
KAPA:=2.277-0.1949*ASPECT;
SQK:=KAPA*KAPA;
SQKA:=SQA*SQK;
MAXBT:=r*bt/THICKNS;
IF MAXBT>14 THEN GOTO JUMP;
PWRTOTAL:=0;
OWBS:=OWALLBLNKT+OSHLD;
IBS:=R-RCPS-A2;
WRITE('   IBS ':10,IBS:6:3);
IF IBS<0.5 THEN GOTO JUMP;
IF (IBS>1.0) THEN BEGIN
   MFISS:=1.1*MFISS;
   PMULT:=1.1*PMULT;
END;
EPSLN:=1/ASPECT;
CI:=1.22 -0.68*EPSLN;
IP:=(5*A*BT/Q)*(CI*EPSLN/SQR(1-EPSLN*EPSLN))*((1+SQK)/2);
IF (IP>IPMAX) THEN GOTO JUMP;
WPFCS:=SQRT(IP/1500E4);
WRITELN('   Wpfcs ':10,WPFCS:6:3);
IF WPFCS>1.0 THEN GOTO JUMP;
FM:=-19.29678-111.6929*ASPECT+406.53*ASPECT*ASPECT-477.5579
    *ASPECT*ASPECT*ASPECT+265.6019*XYPWR(4,ASPECT)-71.9322*XYPWR(5,ASPECT)
    +7.662087*XYPWR(6,ASPECT);
IF (FM<1.00) THEN FM:=1;
BETAC:=F*IP/A/BT/FM;
NTEMPAVE:=BETAC*BT*FM*BT*FM/(2*MU0*1.6022E-16);
```

```
INTEGRAL1;
NO:=NTEMPAVE*VOLUME/(TO*NTEMP*(1+ALFAN)*(1+ALFAT));
NAVE:=NO*(1+ALFAN)*NBAR/VOLUME;
AVETEMP:=TEMPBAR/VOLUME;
FOR I:=1 TO 5 DO BEGIN
   AVESIGV:= EXP(CXX[I,1]*XYPWR(-CXX[I,7],AVETEMP)+CXX[I,2]
      +CXX[I,3]*AVETEMP+CXX[I,4]*AVETEMP*AVETEMP+CXX[I,5]*XYPWR(3,AVETEMP)
      +CXX[I,6]*XYPWR(4,AVETEMP))*1E-6;
   CXX[I,8]:=AVESIGV;
   FP:=TOP[I]*1E-6*VOLUME/(CXX[I,8]*NBAR*NBAR);
   CXX[I,9]:=FP;
END;
NTNDTEST:=CXX[2,8]*CXX[2,9]/2/(CXX[1,8]*CXX[1,9]);
REPEAT
  NTNDPREV:=NTNDTEST;
  NTNDTEST:=CXX[2,8]*CXX[2,9]/(2*CXX[1,8]*CXX[1,9]+NTNDPREV*CXX[5,8]*
          CXX[5,9]);
UNTIL (ABS((NTNDTEST-NTNDPREV)/NTNDTEST)<0.000001);
NTND:=NTNDTEST;
NDPREV:=NAVE/2;
NDTEST:=NDPREV;
REPEAT
   NHE3ND:=CXX[3,8]*CXX[3,9]/2/(CXX[4,8]*CXX[4,9]+RHE3/NDTEST);
   NPND:=(NDTEST*CXX[2,8]*CXX[2,9]/2+NHE3ND*NDTEST*CXX[4,8]*CXX[4,9])/RPROT;
   NHE4ND:=(NHE3ND*NDTEST*CXX[4,8]*CXX[4,9]+NTND*NDTEST*CXX[1,8]
      *CXX[1,9]+NTND*NTND*NDTEST*CXX[5,9]*CXX[5,8]/2)/(RALFA);
   NDPREV:=NDTEST;
   NDTEST:=NAVE/(2+2*(NTND+NPND)+3*(NHE3ND+NHE4ND));
UNTIL (ABS((NDTEST-NDPREV)/NDTEST)<0.000001);
NDAVE:=NDTEST;
CXX[2,11]:=NDAVE;CXX[2,12]:=NDAVE/2;CXX[3,11]:=NDAVE;
CXX[3,12]:=NDAVE/2;CXX[1,12]:=NDAVE;CXX[4,12]:=NDAVE;
NTAVE:=NTND*NDAVE;CXX[1,11]:=NTAVE;
CXX[5,11]:=NTAVE;CXX[5,12]:=NTAVE/2;
NHE3AVE:=NHE3ND*NDAVE;CXX[4,11]:=NHE3AVE;
NPAVE:=NPND*NDAVE;
NEAVE:=(1+NTND+NPND+2*(NHE3ND+NHE4ND))*NDAVE;
NHE4AVE:=NHE4ND*NDAVE;
FOR I:=1 TO 5 DO BEGIN
   POWER:=1.6022E-19*CXX[I,11]*CXX[I,8]*CXX[I,12]*ENERGY[I]*CXX[I,9];
   REACTPWR:=POWER*VOLUME;CXX[I,13]:=REACTPWR;
   PWRTOTAL:=PWRTOTAL+REACTPWR
END;
NFLUXDT:=CXX[1,11]*CXX[1,12]*CXX[1,8]*CXX[1,9];
NFLUXD3:=CXX[3,11]*CXX[3,12]*CXX[3,8]*CXX[3,9];
NFLUXTT:=CXX[5,11]*CXX[5,12]*CXX[5,8]*CXX[5,9]*2;
```

```
        NFLUX:=(NFLUXDT+NFLUXTT+NFLUXD3)*volume;
        FISPROD:=233*1.66E-27*(MFISS*NFLUX)*3.158E7;  {kg Pu/yr}
        PEQUIV:=Efiss*FISPROD*0.8/1E6/(1-C)/(1+ALPHA)/3.158E7;
        PNUCLEAR:=PMULT*NFLUX;
        NSUP:=PEQUIV/PNUCLEAR;
        WLDT:=NFLUXDT*VOLUME*ENERDTN*1.6022E-19/SURFACE;
        WLD3:=NFLUXD3*VOLUME*ENERD3N*1.6022E-19/SURFACE;
        WLTT:=NFLUXTT*VOLUME*ENERTTN*1.6022E-19/SURFACE;
        WLTOT:=WLDT+WLD3+WLTT;
        PTHERM:=PWRTOTAL+PNUCLEAR-WLTOT*SURFACE;
        IF (PTHERM<PWRMIN) THEN GOTO JUMP;
        WRITE(FIRST,COUNTCOMP:3,' ',R:5:2,' ',ASPECT:6:2,' ',Bt:6:2,' ',BetaC:5:3,' '
           ,PWRTOTAL:7:2,' ',PTHERM:8:1,' ',PNUCLEAR:8:1,' ',VOLUME:6:1,' '
           ,Ip:5:1,' ',RCPS:5:2,' ',IBS:5:2,' ',NFLUX:8,' ',
           (FISPROD*0.8/surface):8);
        WRITE(LST,R:4:1,' ',ASPECT:4:1,' ',Bt:4:1,' ',BetaC:6:3,' '
           ,PWRTOTAL:8:1,' ',PTHERM:7:1,' ',VOLUME:6:1,' '
           ,Ip:5:1,' ',RCPS:5:2,' ',IBS:5:2,'  ',NFLUX:8,'  ',(FISPROD*0.8):8);
        MAGNET;
        WRITE(FIRST,WPFCS:5:2,' ',WTFCS:5:2,' ',PCD:8:2,' ',POHMTFC:8:2,' '
             ,POHMPFC:7:2,' ');
        WRITE(LST,PCD:6:2,'  '); {,POHMTFC:8:2,' ',POHMPFC:7:2,' ');}
        COUNTCOMP:=COUNTCOMP+1;
        PWRBALANCE;
        MERIT;
        COSTANALYSIS;
        FLUSH(FIRST);
        FLUSH(LST);
        plotplasma;
        WRITELN ('SUCESSFULLY COMPLETED # ',COUNTCOMP);
        OUTPUT;
        JUMP: writeln;
        R:=R-RVAL;
      END; {R ROUNTINE}
      ASPECT:=ASPECT-ASPVAL;
    END;
    BT:=BT-BTVAL;
  END;        {BT ROUTINE}
  WRITELN(DTAOUT);WRITELN(DTAOUT);WRITELN(DTAOUT);
  WRITELN(DTAOUT2);WRITELN(DTAOUT2);WRITELN(DTAOUT2);
  TO:=TO-TOVAL;
END;    {TO ROUTINE}
QUIT: WRITELN('COMPLETE');
CLOSE (DTAOUT);
CLOSE (DTAOUT2);
CLOSE (BALANCE);
```

```
  CLOSE (BAL2);
  CLOSE(DES1OUT);
  CLOSE(COST);
  CLOSE(COST2);
  CLOSE(FIRST);
END.
```

END

12-86

DTIC